APPLICATION OF A TRACER TECHNIQUE TO STUDY SULFUR DIOXIDE OXIDATION IN CLOUD DROPS AS A FUNCTION OF DROP SIZE

Jill E. Reilly
Jeffrey L. Collett, Jr.

Funding Agency:
National Science Foundation (ATM 9712603)

Colorado State University

DEPARTMENT OF ATMOSPHERIC SCIENCE

PAPER NO. 696

APPLICATION OF A TRACER TECHNIQUE TO STUDY SULFUR DIOXIDE OXIDATION IN CLOUD DROPS AS A FUNCTION OF DROP SIZE

by

Jill E. Reilly
Jeffrey L. Collett, Jr.

Department of Atmospheric Science
Colorado State University
Fort Collins, Colorado 80523

August, 2000

ABSTRACT

APPLICATION OF A TRACER TECHNIQUE TO STUDY SULFUR DIOXIDE OXIDATION IN CLOUD DROPS AS A FUNCTION OF DROP SIZE

This study compared S(IV) oxidation rates predicted using cloud composition in different size cloud drops to the amount of sulfate produced in the cloud as determined by a tracer technique. The tracer technique, developed at SUNY-Albany, quantifies in-cloud sulfate production by comparing pre-cloud aerosol and cloudwater ratios of sulfate to an inert tracer, usually selenium. Measurements were made in two distinctly different atmospheric environments: Whiteface Mountain, NY in July of 1998 and Davis, CA in the winter of 1998/99. The Whiteface Mountain site allowed for the collection of acidic orographic clouds, while alkaline radiation fogs were sampled in Davis. The goal of the project was to gain more insight into the factors governing sulfate production across the drop size spectrum by comparing the results of these two different methods.

The clouds sampled at Whiteface Mountain exhibited a mean pH value of 3.4. Under these acidic conditions S(IV) was oxidized predominantly by hydrogen peroxide. Concentrations of most major inorganic ions, as well as the aqueous phase concentrations of hydrogen peroxide, S(IV) and formaldehyde, were similar for large and small cloud drops. Due to the similarity in drop chemistry, the S(IV) oxidation rates predicted for the different size drops were also similar. At Davis drop composition varied strongly with fog drop size. The average fog pH was 6.3; at times there was as much as a 2 pH unit difference between small and large drops. The oxidation of S(IV) was predicted to be

dominated by ozone, with a significant variation in the rate of sulfate production across the drop size spectrum. The S(IV) oxidation rate for the larger drops was predicted to be up to one hundred times faster than that for the small drops, assuming gas-liquid equilibrium.

The tracer technique results indicate that roughly the same amount of sulfate is produced in both large and small drops at Whiteface Mountain. This agrees with the prediction that the S(IV) oxidation rate is fairly constant across the drop size spectrum at this site. In Davis, however, application of the tracer technique indicated that more sulfate was usually produced in the smaller drops. This finding is in contrast to the faster oxidation rates predicted for larger drops in this alkaline environment.

In order to explain the difference between the predicted and tracer-derived small: large drop oxidation rate ratios, several factors were explored. The most likely explanation is a significant mass transport limitation to the transport of reactants through the fog drops in the aqueous phase, coupled with a strong competing sink for dissolved sulfur dioxide resulting from reaction with formaldehyde to form hydroxymethane sulfonic acid (HMS). Slower mass transport and faster HMS formation in the high pH, large fog drops combined to slow S(IV) oxidation rates in those drops beyond the oxidation rates in the smaller drops, qualitatively consistent with the results from the tracer study.

ACKNOWLEDGMENTS

We are grateful Dr. Sonia M. Kreidenweis and Dr. Kenneth H. Carlson, for providing insightful comments and recommendations for this work. We would also like to recognize D. Eli Shermann and Katharine F. Moore for their extensive contributions to both field campaigns and the subsequent sample analysis. Further support was given by Taehyoung Lee and Mike Hannigan. The cloud chemistry team from the State University of New York – Albany/ New York State Department of Health, including Dr. Liaquat Husain, Oliver Rattigan, Christopher Judd, Mita Das and Vincent Dutkiewicz, were instrumental in the success of this project.

The success of the field projects was due in part to the help of Doug Wolf at the Atmospheric Sciences Research Center (Whiteface, NY) and Dr. Cort Anastasio and Mike Mata (UC Davis).

Funding for this work was provided by the National Science Foundation (ATM-9712603).

TABLE OF CONTENTS:

LIST OF TABLES:

LIST OF FIGURES:

1. Background

1.1 Effects of Sulfate

The atmospheric production of sulfate is an important air quality issue. Sulfate is produced through the oxidation of sulfur oxides, mainly SO_2. Sulfur dioxide is produced anthropogenically through combustion of fossil fuels containing sulfur, and is converted to sulfate through chemical reactions in the atmosphere. The production of sulfate ions is important because of the effects sulfate containing particles can have on the environment, as well as the detrimental health effects the particles can have on humans.

Aerosols of sulfuric acid and other sulfates comprise about 5 to 20 percent of the total suspended particulate matter in urban air (Wark, Warner and Davis, 1998). Outside urban areas this fraction can grow even higher. Sulfate particles therefore make a large contribution to visibility degradation in these areas. Measurements indicate that the peak in the aerosol sulfate distribution is in the size range of 0.2 to 0.9 μm. This is effective for scattering visible light, which has wavelengths of 0.4 to 0.8 μm. Sulfates are therefore responsible for a large amount of visibility extinction, especially in areas downwind of high SO_2 emissions.

Lelieveld and Heintzenberg (1992) also suggest that atmospherically produced sulfate may play an important role in climate cooling. Sulfate formed in clouds is later released as the cloud evaporates. These particles are the ideal size for light scattering and can therefore affect climate forcing. This type of forcing is strongest in the lower troposphere of the Northern Hemisphere, where most SO_2 is released.

Sulfate and sulfuric acid also have strong negative effects on materials and the environment. Sulfuric acid can corrode metals, limestone, marble and also nylon textiles. Acid deposition to the environment can cause loss of plant and animal life (American Chemical Society, 1991). The acidification of lakes and streams in the Adirondacks and New England has resulted in fish losses. Acidic cloud water and other stresses may be responsible for problems in some high elevation red spruce forests in the eastern United States. Long-term changes in soil chemistry are expected for some sensitive environments. Currently the effects of sulfate particles on human health are indistinguishable from those health problems caused by other air pollutants.

1.2 Reactions

The oxidation of sulfur dioxide in the atmosphere can occur in both the gas and aqueous phases. The gas phase conversion involves a reaction with the hydroxyl radical through the following reaction mechanism (Stockwell and Calvert, 1983),

$$SO_2 + OH^{\bullet} + M \rightarrow HOSO_2^{\bullet} + M \qquad (1.1)$$

$$HOSO_2^{\bullet} + O_2 \rightarrow HO_2^{\bullet} + SO_3 \qquad (1.2)$$

$$SO_3 + H_2O + M \rightarrow H_2SO_4 + M \qquad (1.3)$$

Here the sulfate-containing product of the reaction mechanism is sulfuric acid.

This gas phase pathway is not, however, the most common mode of sulfate production in the atmosphere. It is believed that up to 80-90% of all the sulfate produced in the atmosphere is formed in the aqueous phase (Lelieveld and Heintzenberg, 1992). These aqueous phase reactions take place in cloud and fog drops. As the SO_2 enters the drop it partitions into three different forms of dissolved sulfur with oxidation state 4, or

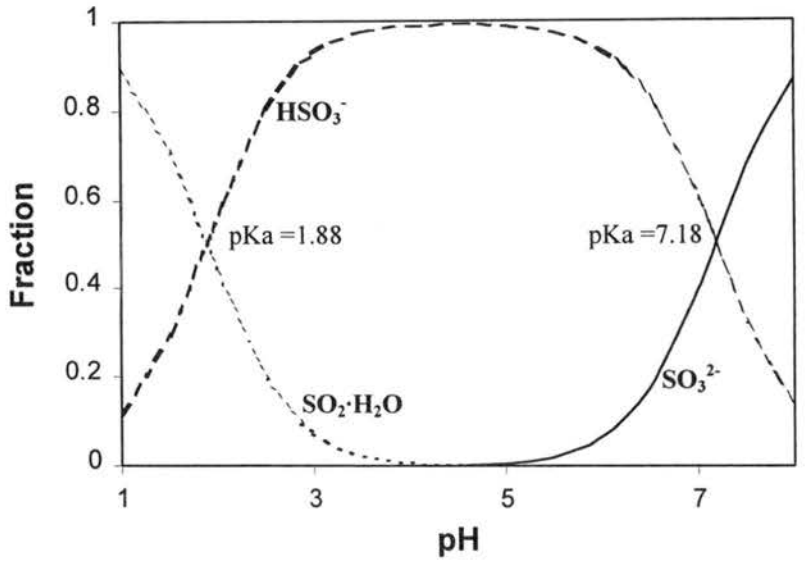

Figure 1.1: S(IV) mole fractions. The mole fraction for each S(IV) species is plotted against pH at 298K. The pKa values are indicated on the plot.

S(IV). These products are hydrated sulfur dioxide ($SO_2 \bullet H_2O$), bisulfite (HSO_3^-), and sulfite (SO_3^{2-}). The mole fractions of each of these species is shown in Figure 1.1 plotted against pH.

Once dissolved into S(IV), SO_2 can be oxidized or complexed readily in the aqueous phase. Some of the more important pathways are the reaction of S(IV) with H_2O_2, O_3, O_2 (catalyzed by Fe(III) and Mn(II)), OH, HNO_2, CH_3OOH, CH_3CO_3H, PAN, HO_2, HCHO and soot. The most prevalent oxidation pathways under typical atmospheric conditions are believed to be the reactions of S(IV) with H_2O_2, O_3 and O_2 (catalyzed by Fe(III) and Mn(II)). There may also be some contribution to the total S(IV) oxidation from reactions with OH, HNO_2 and HO_2. These contributions are, however, likely to be significant only in polluted daytime atmospheres (Hoffman and Calvert, 1985). Another reaction that can be a large sink for S(IV) is its complexation with HCHO to form

hydroxymethanesulfonate (HMS). Complexation of S(IV) and HCHO occurs mainly at high pH values (Rao and Collett, 1995).

1.2.1 S(IV) Oxidation by H_2O_2

The oxidation of S(IV) by hydrogen peroxide in the aqueous phase is the major pathway for the production of sulfate in acidic environments. When gas phase H_2O_2 is present it can readily diffuse into cloud or fog drops due to its high solubility. In the presence of S(IV) the oxidation reaction mechanism proceeds in the following two steps (McArdle and Hoffman, 1983)

$$HSO_3^- + H_2O_2 \leftrightarrow SO_2OOH^- + H_2O \qquad (1.4)$$

$$SO_2OOH^- + H^+ \rightarrow H_2SO_4 \qquad (1.5)$$

The first step is the nucleophilic displacement on the bisulfite ion by hydrogen peroxide to produce peroxymonosulfurous acid. This product then reacts with an available proton to form sulfuric acid. If the pH of the solution is greater than the pKa value (1.88) then the sulfuric acid will dissociate, leaving the sulfate and hydrogen ions in solution.

The second step in the mechanism is clearly dependent on the pH of the solution. The more H^+ ions present, the faster the second step will occur; therefore, this reaction occurs rapidly for low pH values. The overall rate, however, is independent of pH because there is a limited amount of HSO_3^- available at low pH values. So even as the pH drops there is not enough HSO_3^- present for the reaction to proceed at a faster rate. The reaction is then limited by the amount of HSO_3^- present.

In fact the oxidation of S(IV) via the hydrogen peroxide pathway is the only mode of sulfate production found to be effective at low pH values. Calvert et al. (1985) have

shown that gaseous H_2O_2 is present at high enough concentrations in the troposphere to be the major oxidant of S(IV) in the aqueous phase. Oxidation through the peroxide pathway is detectable in clouds through either a decrease in gas phase SO_2 and H_2O_2 or an increase in S(VI) in the cloud or fog drop (Kelly et al., 1989). Other pathways may become more important either at higher pH values, or as the amount of available H_2O_2 is reacted away.

1.2.2 S(IV) Oxidation by O_3

As hydrogen peroxide is depleted, other S(IV) oxidation pathways become more important inside the cloud or fog drop. At higher pH values the reaction of S(IV) with ozone also becomes a major sink for the aqueous phase S(IV). This reaction can be put simply as

$$S(IV) + O_3 \rightarrow S(VI) + O_2 \qquad (1.6)$$

The actual mechanism of the formation of S(VI) via this pathway is far more complicated than what is given above and has been studied by many researchers. For reactions occurring in cloud or fog water it is customary to use the reaction rate derived by Hoffman and Calvert (1985), for the oxidation of S(IV) by ozone in a dilute solution.

There are actually three pathways (one for each type of free S(IV)) by which ozone can react with S(IV) to form sulfate. These three pathways are abbreviated below.

$$O_3 + SO_2 \bullet H_2O \xrightarrow{k_1} S(VI) \qquad (1.7)$$

$$O_3 + HSO_3^- \xrightarrow{k_2} S(VI) \qquad (1.8)$$

$$O_3 + SO_3^{2-} \xrightarrow{k_3} S(VI) \qquad (1.9)$$

The rate constants for these reactions have the following relationship, $k_3 > k_2 > k_1$. In fact the rate constant k_3 is almost 100,000 times faster than k_1. Oxidation of S(IV) by hydrogen peroxide occurs at a much faster rate than oxidation by ozone for low pH values. This is because at lower pH values the partitioning of S(IV) favors higher concentrations of $SO_2 \cdot H_2O$ and HSO_3^-. These are the two slower reacting pathways for S(VI) production. For pH values greater than 5 pH units, the mole fraction of SO_3^{2-} (pKa = 7.18) starts becoming a significant portion of the S(IV) partitioning. Therefore the faster reaction pathway shown in Equation 1.9 begins to contribute to the S(VI) production. As the solution pH approaches the pKa value for sulfite the overall sulfate production via the ozone pathway becomes more rapid than the hydrogen peroxide pathway. At high pH values the ozone pathway will therefore be the dominant mode of sulfate production.

Seidl (1989) studied the effects of pH decreases due to the sulfur oxidation process, on the S(IV)-O_3 reaction. The S(IV)-O_3 reaction is particularly effective only at high pH values, but as the reaction goes on the acidity of the solution increases, thereby decreasing the pH. It seems then that the reaction would work to, in essence, slow itself down as time progresses. In the presence of excess ammonia, however, the sulfuric acid that is produced by the reaction is then neutralized. This keeps the pH of the solution fairly stable and allows the oxidation to proceed. The neutralization of the sulfuric acid can also occur through internal buffering by species already present in the cloud/fog

water (e.g., Collett, et al., 1999). Therefore S(IV) oxidation via the ozone pathway is clearly an important mode of S(VI) production in more alkaline environments.

1.2.3 S(IV) Oxidation by Oxygen (Catalyzed by Fe(III) and Mn(II))

Under certain conditions the oxidation of S(IV) by O_2 catalyzed by Fe(III) and Mn(II) can become a significant source of S(VI) in the atmosphere. This catalyzed reaction is given in a simplified form as

$$S(IV) + \frac{1}{2}O_2 \xrightarrow{MnII,FeIII} S(VI) \qquad (1.10)$$

Both Fe(III) and Mn(II) can act individually as catalysts for the reaction, or they can act together to further speed up the reaction. Hoffman and Jacob (1984) note that while there have been many studies on this catalyzed reaction, there are many discrepancies in the rate laws, reaction rates and pH dependences that have been measured. These differences likely stem from the different laboratory environments used in the studies.

While considerable research has been done on both of the single catalyst reactions, the most important for this study is the iron/manganese synergism. The synergism is relevant when both Fe(III) and Mn(II) are present in the solution containing S(IV). Under most environmental conditions this is the case. Typically in clouds and fog the concentrations of iron are about ten times those of manganese (Martin, 1984). Manganese is still present in a great enough quantity to warrant the use of the rate laws that apply to the synergism.

Rate laws for this iron/manganese synergism oxidation pathway have been determined by Ibusuki and Takeuchi (1987). Using general atmospheric conditions

(micromolar concentrations of Fe(III), Mn(II) and S(IV), and a pH range of 2.6-6.5) they arrived at the following rate laws

$$pH < 4.2$$
$$\frac{-d[S(IV)]}{dt} = k_{c1}[H^+]^{-0.74}[Mn(II)][Fe(III)][S(IV)] \qquad (1.11)$$

$$pH \geq 4.2$$
$$\frac{-d[S(IV)]}{dt} = k_{c2}[H^+]^{0.67}[Mn(II)][Fe(III)][S(IV)] \qquad (1.12)$$

Martin and Good (1991) reexamined this catalyzed reaction and formulated their own rate law. This separate rate law is in good agreement with that of Ibusuki and Takeuchi. The Ibusuki and Takeuchi rate law will be used in the calculations for this study.

1.3 Tracer Theory

The tracer technique was originally developed by Husain and coworkers (1984) as a means of reliably following the long range transport of aerosols, sulfate in particular. This technique related aerosol sulfate to the relative abundance of other trace metals that are also found in accumulation mode aerosols. These accumulation mode aerosol particles tend to act as cloud condensation nuclei. As drops form SO_2 can be absorbed into the aqueous phase and then can be oxidized to S(VI) via the pathways mentioned above. The sulfate produced in the drop is chemically indistinguishable from the sulfate entering the drop through aerosol scavenging. This creation of additional sulfate in the drops changes the relationship of the amount of sulfate in the air to the amount of the trace metals being used to track the aerosol transport. Because the sulfate created in the drop is identical to the sulfate scavenged into the drop, it is difficult to ascertain what amount of sulfate has been transported and what amount was created in the drop.

This motivated the need for a method to determine quantitatively the amount of sulfate being produced in the drop. In order to determine the amount of sulfate produced in the drops, Husain (1989) developed a method using Se to determine the amount of sulfate scavenged into the drops. Selenium is a trace element that can also be found in accumulation mode aerosols. The method was expanded to include two other trace species, As and Sb.

These elements are generally released into the atmosphere as gaseous by-products of high temperature combustion processes. The elements then go through gas to particle conversion processes, emerging as Aitken mode particles which can then coagulate into larger, accumulation mode, particles.

There is no source of Se, As or Sb to cloud drops other than aerosol scavenging. Sulfate, on the other hand, can be either scavenged into the drop, or formed inside the cloud or fog drop. SO_4^{2-} and the trace elements are all found on aerosol particles that are mostly, if not totally, soluble. Aerosol ratios of SO_4/Se, As, and Sb often remain unchanged over periods of several hours. Given these parameters, the elements Se, As, and Sb can be used as tracers to quantitatively determine the amount of SO_4 scavenged by the cloud or fog drop. Then the total amount of both the sulfate and the tracer found in the aqueous phase can be measured in the collected cloud or fog water. The amount of sulfate produced in the cloud can then be determined by difference.

Husain (1989) gives the total amount of sulfate in the drop as

$$[SO_4]_{cw} = \alpha/L\,[SO_4]_{aa} + [SO_{4in}]_{cw} \qquad (1.13)$$

For the above equation, α represents the scavenging coefficient of aerosol SO_4 and L denotes the liquid water content of the cloud. $[SO_{4in}]$ is the concentration of sulfate, in

μ**M**, formed in the cloud or fog drop by the oxidation of SO_2. The subscript "aa" denotes ambient aerosol. So the first term on the right hand side of the equation represents the amount of aerosol sulfate scavenged into the drop. The subscript "cw" indicates a cloud water concentration.

Because the total amount of the tracer element found in the drop has arrived there via aerosol scavenging, the concentration of Se, As or Sb found in the drop can be given simply as

$$[Se]_{cw} = \beta/L\,[Se]_{aa} \qquad (1.14)$$

The scavenging coefficient of the trace element is represented by β.

In order to solve for SO_{4in}, Equation 1.13 must be rearranged as

$$[SO_{4in}]_{cw} = [SO_{4in}]_{cw} - \alpha/L\,[SO_4]_{aa} \qquad (1.15)$$

The next step is to divide through by $[Se]_{cw}$, to give

$$[SO_{4in}/Se]_{cw} = [SO_{4in}/Se]_{cw} - (\alpha/L\,[SO_4]_{aa})/[Se]_{cw} \qquad (1.16)$$

Then Equation 1.14 is used to substitute into the last term on the right hand side of Equation 1.16,

$$[SO_{4in}/Se]_{cw} = [SO_{4in}/Se]_{cw} - (\alpha/\beta\,[SO_4/Se]_{aa}) \qquad (1.17)$$

Finally SO_{4in} can be isolated by multiplying through by $[Se]_{cw}$,

$$[SO_{4in}]_{cw} = ([SO_4/Se]_{cw} - \alpha/\beta[SO_4/Se]_{aa})[Se]_{cw} \qquad (1.18)$$

Using Equation 1.18, if α/β is known, the amount of sulfate produced in the cloud or fog drop can be determined by measuring the concentrations of Se and SO_4 both in the pre-cloud ambient aerosol and in the cloud water itself.

This technique has been tested by Husain and co-workers at Whiteface Mountain on more than twenty clouds (Husain et al., 1991). The cloud water samples were taken at

the mountain summit, an elevation of 1.5 km. The out of cloud aerosol samples were taken at a site lower on the mountain, at roughly 0.6 km, as well as at the summit site.

A comparison between the aerosol samples taken at both locations indicate that the concentrations measured at the summit site were about half or less of those measured at the lower site. The relationships between the measured concentrations of SO_4 and the tracer elements did, however, remain constant within experimental uncertainty. This indicates that the 0.6 km site provides a good representation of pre-cloud aerosol. The ratios between the two sites are not comparable, however, when an inversion exists between them. The inversion layer can be identified through chemical or meteorological data and SO_4in measurements made during those times should be disregarded.

Data collected during these previous Whiteface studies shows the ratio of $\alpha/\beta=1$ for sulfate and all three tracers. The values of SO_4in determined using each of the three tracers (Se, As and Sb) all showed reasonably good agreement, within 10-20% (Burkhard et al., 1995). These previous tracer studies also showed that the technique could be applied to clouds or fog with pH values ranging from 2.4 to 6.

For the current study the tracer technique was employed at both Whiteface Mountain, NY and Davis, CA. The set up at Whiteface was the same as in the previous studies. The Davis site is slightly different in that fog was sampled instead of clouds, and it was a new site for the tracer technique.

1.4 Chemical Composition and SO_2 Oxidation as a Function of Cloud Drop Size

Recent field studies by Collett and coworkers suggest chemical heterogeneity among cloud drop populations can lead to differential oxidation across the drop size

spectrum. Several different types of cloud collectors have been used in more than a dozen locations in field studies conducted throughout the United States. Drops have been collected both in bulk and in different size fractions.

Throughout each of these varied sampling environments at least some degree of chemical heterogeneity related to the cloud drop size was found (Collett et al., 1994; Rao and Collett, 1998; Bator and Collett, 1997, Xu et al., 1999, Collett et al., 1999). Cloud and fog pH, inorganic ion concentrations and trace metals concentrations were found to differ between small and large drops. Bulk cloud water samples exhibited concentrations of the aforementioned species that fell between the values measured for the large and small drop fractions.

In many earlier cloud chemistry studies all drops within the same cloud were assumed to have the same chemical composition. Work by Collett et al. (1994) showed, however, that this was not the case and that variations in drop composition could have a significant influence on the rate of production of sulfate in clouds. Their study included a variety of different types of samples, including frontal clouds, coastal stratus clouds and radiation fogs. The samples were collected in environments that ranged from heavily polluted to pristine.

Collett et al. (1994) found that the differences between large and small cloud drop acidities could be as large as two pH units. Pristine environments such as Angora Peak, Oregon (along the Pacific coast) showed little difference in pH values between large and small drops. Some environments that were heavily polluted, like the central valley in California, showed greater differences in acidity between the two size fractions. Significant differences in pH across the drop size spectrum can be seen for pH values

ranging from less than three to more than seven. The smaller drops tended to be more acidic than larger drops in most locations.

Further chemical analysis of these samples (Bator and Collett, 1997) also shows that the small drops tend to have higher concentrations of accumulation mode species like sulfate, ammonium, and nitrate, and large drops tend to be enriched in coarse mode species such as sodium, chloride and calcium. The accumulation mode particles tend be more acidic, thereby lowering the pH of the small drops in which they are found. The coarse mode particles generally make more alkaline contributions to the drops that contain them. This provides some insight into the aforementioned pH differences among the drops.

Rao and Collett (1998) found that the concentrations of the trace metals iron and manganese also vary with cloud and fog drop size. For most of the locations from which samples were taken for this study, significantly higher concentrations of total iron and total manganese were found in the larger drop fraction. Small drops were, however, enriched with these metals at two locations: Bakersfield, CA and Angora Peak, OR. The anomaly at the Bakersfield site may be an artifact of local industrial sources, while the difference at the Angora site is likely due the pristine nature of the environment. The study also showed that the speciation of iron appeared to vary with drop size. This can be important, as the autooxidation pathway for sulfate production relies on the presence of Fe(III).

Because these studies found that the sample acidity and the concentration of trace metals vary with drop size, they imply that the rate of aqueous phase sulfate production might also vary with drop size. These variations are expected to be most important in

environments where the oxidation of S(IV) is dominated by either the ozone pathway or the metal catalyzed autooxidation pathway. There is little expected variation for areas where sulfate production is dominated by the peroxide pathway. The rate of the peroxide pathway should be independent of drop size because measurements indicate no drop size dependence on the distribution of H_2O_2 in the drops, and there is only a slight pH dependence for the H_2O_2-S(IV) oxidation pathway. Drop size related differences in chemical composition may become a factor for samples dominated by the peroxide pathway when H_2O_2 is available in a limited supply. This can occur in daytime clouds when the production of hydrogen peroxide is dominated by aqueous phase photochemistry, which varies with drop size. The other two pathways may dominate the in cloud production of sulfate when the pH values are high (typically above about 4 -5 pH units) and the concentration of hydrogen peroxide in the drop is low.

Collett, et al. (1994) found that the variations in acidity across the drop size spectrum indicate that the predictions of the rate of S(IV) oxidation that are based on bulk (uniform) cloud drop compositions are inaccurate for certain environments. Calculations indicate that large drops are capable of sustaining much faster S(IV) oxidation rates than small drops from the same cloud, when sulfate production is dominated by either the ozone or autooxidation pathway. This is generally due to the more alkaline nature of the large drops, as both the ozone and catalyzed autooxidation pathways are extremely dependent on pH. The rate of sulfate production in the large drop fraction may be ten or more times the rate calculated for the small drop fraction sample.

The rapid production of sulfate in the large drop seems to suggest that the drop will acidify itself and therefore act to lower the oxidation rate. This does not always

seem to be the case as temporal studies show that the composition and pH differences between the small and large drops are maintained over time. This could be due to a significant amount of buffering in the alkaline drops (Collett et al., 1999). This buffering can take the form of drop uptake of gaseous ammonia, or internal buffering, by the protonation of bases in the drop solution. The presence of substantial buffering indicates that large drops should be able to sustain the rapid sulfate production rate.

Due to the non-linear characteristics of the sulfate production pathways with respect to drop composition, an oxidation rate calculated from the average fog composition is smaller than the rate established using a liquid water content weighted average of the two drop size fractions (Gurciullo and Pandis, 1997). The enhancement in the S(IV) oxidation rate seen when large and small drop compositions are used is often 25 – 100% greater than the values predicted from the bulk method.

Collett et al (1994) found that variations in the acidity of cloud and fog drops as a function of the drop size can significantly enhance sulfate production via the ozone pathway. The amount of enhancement was quantified by using a quantity known as the enhancement factor. This is calculated as a ratio of the liquid water weighted rate average for the two distinct drop compositions divided by the rate calculated using the average drop composition. For the 1994 Collett et al. study, 67% of the samples were found to experience up to 20% enhancement (enhancement factors of 1 – 1.2). Roughly 26% of the samples experienced from 20% to 100% enhancement, and the remainder of the samples experienced more than 100% enhancement. They found samples with at least 50% enhancement at almost every sampling site, except those totally dominated by S(IV) oxidation via the hydrogen peroxide pathway.

Results from Rao and Collett (1997) for the metals catalyzed autooxidation pathway are not as simple as those for ozone. For the ozone pathway, chemical heterogeneity among the drops always results in oxidation rate enhancement, whereas for the metals catalyzed pathway oxidation rate suppression is also possible. Oxidation rate suppression for the autooxidation pathway occurs when higher than average Fe(III) and Mn(II) concentrations are found in drops that are more acidic than average. If, however, higher than average trace metal concentrations are associated with more alkaline drops, the autooxidation pathway shows greater enhancement than the ozone pathway would from the pH difference alone.

Typically S(IV) oxidation via the catalyzed autooxidation pathway does not play a large role in the overall production of sulfate in clouds and fog (Rao and Collett, 1997). The average contribution of this pathway is generally about 10% of the total S(IV) oxidation, although in certain cases the autooxidation pathway was calculated to contribute about 30% of the total S(IV) oxidation. The enhancement seen for this pathway will, of course, be most important when the rate of the catalyzed autooxidation pathway is close to, or greater than the rates of the other two S(IV) oxidation pathways.

In actual clouds and fog there are more than just two drop sizes, therefore more than just two distinct chemical compositions are likely to exist. The pH values of the drops are likely to vary across the entire drop size spectrum, as well as from drop to drop within similar size ranges. This suggests that oxidation rate enhancement estimates from the two stage cloud sampler measurements represent only the lower bound of the actual effect due to drop size dependent chemistry.

1.5 Study Goal

The results from the studies mentioned above indicate that sulfate production rates should vary with drop size in environments where aqueous phase S(IV) oxidation takes place predominantly via the ozone and metal catalyzed autooxidation pathways, and should be independent of size when oxidation is dominated by the hydrogen peroxide pathway. In order to test this hypothesis, the techniques and experience from both SUNY and CSU were combined for this study. The two groups worked together to collect data at two sampling locations. From there the groups worked individually to analyze the samples recovered from the field projects. The results from these analyses were then brought together for a comparison.

The goal of this study was to compare predictions of drop size-dependent S(IV) oxidation rates with quantities of sulfate determined to be produced in large and small cloud/fog drops through the application of the tracer technique. In order to accomplish this two sampling sites were chosen, each with a different dominant S(IV) oxidation pathway. The site at Whiteface Mountain, NY was chosen as the control site, where the S(IV) oxidation should be dominated by the hydrogen peroxide pathway. The second site was Davis, CA, chosen as a site likely to exhibit S(IV) oxidation dominated by the ozone pathway. Strong variations in pH across the drop size spectrum in Davis fogs were expected to produce S(IV) oxidation rates that also varied with drop size.

The selection of these two sites, as well as the use of a two-stage cloud sampler, allowed for the determination of SO_4in and the calculation of sulfate production rates for small and large drops in two different environments. A comparison of these results indicates whether each of the approaches is working as expected.

2. Experiment

The fieldwork for this study was carried out in July of 1998 at Whiteface Mountain, NY and then in the winter of 1998/99 at Davis, CA. Cloud collectors, along with a myriad of other instruments were set up at both sites to obtain the information necessary to achieve the study goals. Laboratory work was done following the field campaigns at both Colorado State University (CSU) and the State University of New York – Albany (SUNY).

2.1 Sites

2.1.1 Whiteface Mountain, NY

The Whiteface Mountain (44.39°N, 73.86°W) sampling site is located in the Adirondacks of upstate New York. From previous studies at this site approximately 70% of the cloud water was found to have pH < 4 and only about 6% of the samples have pH > 4.5. This is therefore a very acidic environment and the predominant pathway for sulfate production is likely to be oxidation of S(IV) by H_2O_2. Aqueous phase chemistry suggests that since oxidation of S(IV) is dominated by the peroxide pathway there should be little variation in the oxidation rate across the drop size spectrum. This site should provide a good control case for the comparison of the cloud chemistry predicted rates and the tracer determined amount of sulfate produced.

The cloud collection at Whiteface was done at the mountain's summit (Figure 2.1). The collectors were mounted on the roof of a small building at an elevation of

Figure 2.1: Field setup at the summit of Whiteface Mountain, NY. Note that the collectors are covered for storage while not sampling.

approximately 1.5km. In order to get the required data for the tracer portion of the study a second site was needed to collect aerosol below the cloud level. This site was located just above the base of the mountain at an elevation of 0.6 km. Measurements of aerosols, trace gases and meteorological parameters were made at both sites on the mountain.

2.1.2 Davis, CA

The second site is located in Davis, California (38.32°N, 121.47°W) at the northern end of the San Joaquin valley. This area is known for its radiation fogs, prevalent in the winter months. The median pH measured in previous studies by Collett et al. (1999) of the San Joaquin valley was 6.49. There were also significant differences in pH between large and small cloud drops of up to one pH unit found in these studies. The high pH values measured favor the production of sulfate through the ozone or metal

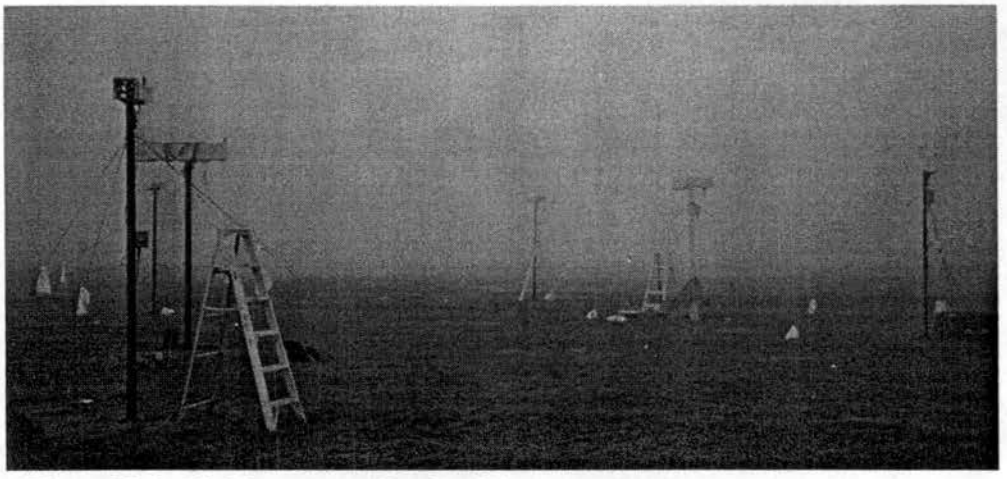

Figure 2.2: Field setup at Davis, CA.

catalyzed oxygen pathways. This indicates that the fog chemical heterogeneity with respect to drop size characteristic of the region could alter production of sulfate when compared to expected production rates based on average drop compositions.

At the Davis site fog was sampled by collectors mounted on poles roughly 3 meters above the ground in an open field (Figure 2.2). All measurements, including trace gas and meteorological parameters, were made at or near the location where the radiation fogs were being sampled. High volume aerosol samplers were used for collection both before and after the fog events.

2.2 Sampling

2.2.1 Cloud/Fog Samplers

The two primary cloud collectors used on the campaign were the Caltech Active Strand Cloudwater Collector version 2 (CASCC2) and the size-fractionated Caltech Active Strand Cloudwater Collector (sf-CASCC). The same collectors were used at both the Whiteface Mountain site and the Davis California site.

The CASCC2 (Demoz et al., 1996) is an active cloudwater collector that uses a fan to draw the cloud drops through its body and impact them on Teflon strands (Figure 2.3). The 508 micron diameter strands have a 50% cut diameter of 3.5 microns for collection of drops. The flow rate of the CASCC2 is 5800 liters/minute. Collected drops are then drawn down by gravity and aerodynamic drag into a trough and collected in a polyethelyne sample bottle at the end of a short length of Teflon tubing.

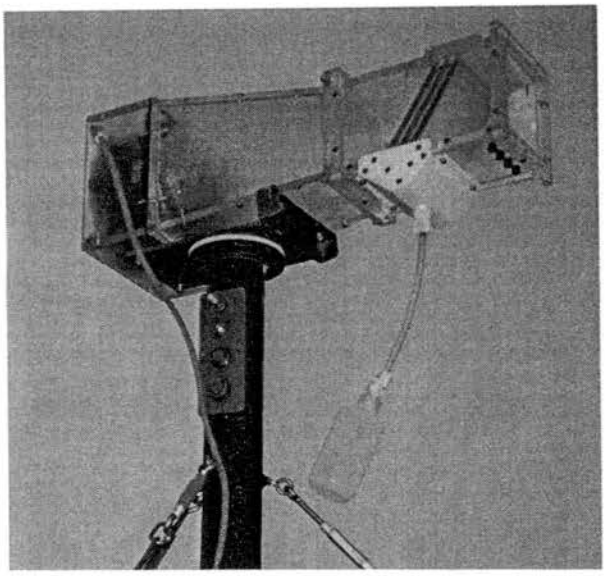

Figure 2.3: Caltech Active Strand Cloud Collector Version 2 (CASCC2).

The size-fractionated CASCC (Munger et al., 1989; Demoz et al., 1996) separates the drop distribution into two different size bins. Recent modeling of this collector suggests that the 50% cut diameter is actually at 17 μm and not 23 μm as previously thought. So, the drops collected in the first stage are mainly those with diameters greater than 17 μm, and the second stage mainly collects drops with diameters between 4 μm and 17 μm. Again inertial impaction is used to collect the drops. The cloud is drawn into the collector by a fan and first encounters a bank of Teflon rods. The larger drops are

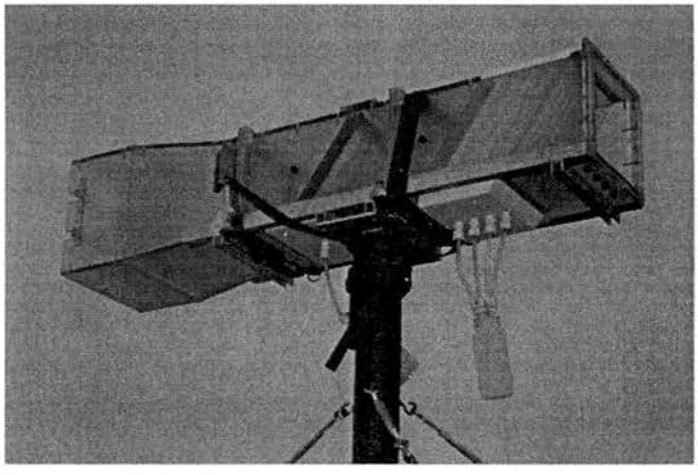

Figure 2.4: Size Fractionated Caltech Active Strand Cloud Collector (sf-CASCC).

impacted onto these rods and collected in a trough as in the CASCC2. The remaining drops continue through the collector to a cartridge of Teflon strands. These strands collect the remaining drops with diameters larger than 4 microns. The flow rate of the sf-CASCC is 19,000 liters per minute.

2.2.2 Instruments for Other Measurements

Other measurements that will support the data obtained from the processing of the cloud collector samples include measurements of liquid water content, drop size distribution and meteorological parameters. The Gerber Scientific Particulate Volume Monitor (model PVM-100) was used in both Whiteface and Davis to provide continuous measurements of liquid water content. A Particle Measurements Systems CSASP-100-HV cloud probe was used to make measurements of the cloud drop size distribution. Data from this instrument are only available for the Whiteface campaign. Meteorological data including temperature, pressure, relative humidity, wind speed and wind direction were recorded using a standard weather station. These three instruments (PVM, CSASP, and the weather station) were collocated with the cloud collectors. In addition, meteorological data were also recorded at the 0.6 km site at Whiteface.

Other measurements necessary for this study are the concentrations of the trace gases hydrogen peroxide, sulfur dioxide and ozone. These values were obtained from a mixture of continuous monitoring sites and instruments set up specifically for this study. The hydrogen peroxide concentrations were measured by continuous analyzers using a flourometric technique (Lazrus et al., 1985). Thermo Environmental Instruments Model 43S pulsed fluorescence analyzers were used to measure sulfur dioxide concentrations.

Ozone concentrations and supplemental SO_2 measurements were obtained from state-operated monitoring sites for both the Whiteface and Davis sites. At Whiteface, trace gas measurements were made both at the summit site and the 0.6 km base site, while at Davis all measurements were made at the fog sampling site.

2.2.3 SUNY aerosol measurements

In order to obtain the data necessary to make the tracer calculations high volume aerosol samples were taken of both in-cloud and out-of-cloud air. These samples were collected at two-hour intervals. Although shorter intervals are desired for better time-resolved data, two hours are needed to assure that there is enough aerosol loading to enable accurate sulfate/tracer ratios to be calculated.

For the Whiteface field campaign two different high volume sampler set-ups were used. Aerosol at the summit was collected on 20 x 25 cm Whatman 41 filters using standard high volume pumps operating in a sampling box and inlet designed to minimize the collection of cloud drops and precipitation (Husain, 1989). At the lower sampling site aerosol samples were collected with modified high volume samplers on 15 x 15 cm Whatman 41 filters as described by Burkhard et al. (1995).

2.3 Cloud/Fog Sample Preservation & Analysis

2.3.1 On-Site Activities

Once sufficient sample volumes were collected on both size fractions of the sf-CASCC and on the CASCC2 the sample bottles were removed and replaced with a new

Table 2.1: Aliquot priority and preservation: The species aliquots are listed in the order of their priority for each sample. The volume of each aliquot is listed in the second column. The amount and type of the preservative solution added to each aliquot is indicated on the right.

Aliquot	Volume	9.7% HNO3 Solution	S(IV) Preservative Solution	Catalase Solution	Conditioning Reagent	Fluorescent Reagent	HCHO Preservative Solution
PH	40 µl						
IC	500 µl						
Metals: LARGE SMALL	1 ml 100 µl	100 µl 10 µl					
H2O2: LARGE SMALL	1 ml 100 µl				200 µl 20 µl	200 µl 20 µl	
S(IV): LARGE SMALL	1 ml 100 µl		100 µl 10 µl	100 µl 10 µl			
HCHO: LARGE SMALL	1 ml 100 µl						100 µl 10 µl

set of bottles. The sample length was typically one hour, but at times it did vary corresponding to the amount of liquid water in the cloud/fog. The same bottles were then weighed to find the volume collected by each sampler or size fraction. If sufficient volumes were available most cloud water samples would then be aliquotted for pH measurement and preservation for later analysis of S(IV), formaldehyde, hydrogen peroxide, inorganic ions, total iron and total manganese. SUNY was also given an aliquot for trace metal analysis (Se, As, and Sb).

The highest priority aliquot was for the pH measurement. Therefore, for nearly every sample collected there is a pH measurement. An Orion 250A portable pH meter attached to a microelectrode (Microelectrodes Inc. Model MI-710) was used to make

these measurements. The probe was calibrated using buffers of pH 4 and pH 7. The pH measurements were generally made within 10 minutes of the sample retrieval.

The other aliquots were made as sample volume allowed. There was priority given to aliquots for inorganic ion and trace metal analysis. Again the aliquot preservation was made in a timely fashion and generally completed within 20 minutes of the sample retrieval. Table 2.1 summarizes the priority and preservation procedures for each type of aliquot.

2.3.2 Laboratory Analysis

The inorganic ion analysis was done using two Dionex DX500 series ion chromatographs. Major anion (Cl^-, NO_3^-, and SO_4^{2-}) concentrations were quantified using an AS4A column and a self-regenerating anion suppressor. A CS12 separator column and a self-regenerating cation suppressor were used to find concentrations of major cations (Na^+, K^+, NH_4^+, Ca^{2+}, and Mg^{2+}). Inorganic ion analysis was also done by SUNY for the Whiteface cloudwater samples. Concentrations of major ions in the aerosols collected by the high volume samplers were also measured by SUNY. A 10.13 cm^2 portion of each filter underwent ultrasonic extraction in 25 ml of double-deionized water at 85-90 degrees Celsius for two hours. The extract was then analyzed by ion chromatography.

SUNY was also responsible for the trace metal analysis in the cloud water and on the high volume aerosol filters. The cloud water samples were analyzed using a Fisons ICP-Mass Spectrometer, which allows for the concentrations of all five elements (Se, As, Sb, Fe and Mn) to be simultaneously determined, minimizing the sample volume required

for this measurement. Analysis for the trace metals Mn and Fe in cloudwater was also done at CSU using a Varian model 640Z Zeeman-corrected atomic absorption spectrophotometer with a Varian GTA-96 graphite furnace. The preservation of these two trace metals was done by adding 9.7% HNO_3 to the sample aliquot. Established instrumental neutron activation analysis (INAA) techniques (Dutkiewicz et al., 1987) were used to measure the concentrations of trace metals from the aerosol filters.

The hydrogen peroxide cloud water concentration was measured using a fluorescence spectrophotometer. Hydrogen peroxide in the cloud or fog water was preserved by the addition of p-hydroxyphenylacetic acid (POHPA) to form a stable dimer. For every molecule of peroxide, one molecular dimer is formed. The concentration of the dimer can then be determined. This method measures total peroxide (both hydrogen peroxide and organic peroxide), but because organic peroxide typically represents less than 1% of the total peroxides in solution the values are representative of the hydrogen peroxide concentration (Lazrus et al., 1985). These measurements were made using a Shimadzu RF-1501 spectrofluorophotometer.

Samples to be used for formaldehyde analysis were preserved in the field using bisulfite. The bisulfite reacts with the formaldehyde to form the complex known as hydroxymethanesulfonate (HMS). In the lab the sample is then mixed with 2,4-pentanedione and ammonia to form a yellow product. This product can then be measured using absorbance (Dong and Dasgupta, 1987). This method measures total formaldehyde, which is defined here as free formaldehyde and HMS that existed in the sample prior to preservation. The analysis was done using a Hach DR/4000 spectrophotometer.

Total S(IV) analysis was also done using the Hach DR/4000 spectrophotometer. Because S(IV) is readily converted to sulfate in the aqueous phase, prompt preservation is important. This is done with a buffered solution containing formaldehyde, thereby forming HMS with all available S(IV). To analyze the samples a strong base is added to decompose the HMS into S(IV) and formaldehyde. Then acidic pararosaniline is added to form a purple compound with the now free S(IV) and HCHO. This can then be measured using the spectrophotometer to find concentrations of total S(IV), which includes free S(IV) and any HMS present before the preservation of the sample (Dasgupta et al., 1980).

2.3.3 Quality Assurance and Control

Several different types of quality control measures were taken throughout both field campaigns and during the chemical analysis of the samples to ensure that the samples collected were not contaminated and were accurately and precisely analyzed. These included washing the cloud collectors after each event, taking blanks, measuring sample replicates and duplicates, along with careful instrument calculations. These measures were intended to maintain the integrity of each cloud or fog water sample.

2.3.3.1 Collector Cleaning and Blanks

Following the initial equipment set up at each location the cloud collectors were cleaned with deionized water and blanks were taken for later analysis. This type of collector cleaning followed each cloud or fog interception event as well. The collectors' rods and strands were first drenched with copious amounts of deionized (DI) water.

After particularly dirty events these functional parts of the collectors were scrubbed using Kimwipes and Triton-X100, and then doused with DI water again. One of the final steps of the cleaning procedure includes spraying DI water directly into the collector using clean spray bottles. The water drops from these bottles follow the same paths as the samples collected, as they are caught on the rods or strands and follow the natural flow of the collector, arriving in the sample collection bottles. The collector blank sample is taken after this spray down of the collector. Blank samples were also taken from the carboys used to carry the DI water to the sampling site, as well as direct blanks from the spray bottles themselves. After blanks were taken, the collectors were covered with clean plastic bags to prevent contamination.

A limitation to this approach is that soluble gases may be captured by the sprayed water and can cause an artifically high collector blank. Aerosol particles can also contribute to the blank's chemical loading, but the collection of these particles is far less efficient than that of the soluble gases. Note also that as the sampler collects the cloud or fog drops, it is in essence cleaning itself with the sample. Therefore at the start of each event the collectors were run for a brief time (between 10 to 30 minutes), and the sample collected from this pre-run was not used. This technique should reduce possible contamination of the first sample and remove any residual DI water left from the previous cleaning.

2.3.3.2 Determination of Uncertainties and Detection Limits

Different uncertainties and detection limits were calculated for each species

measured throughout both field campaigns. Also because the field projects took place five months apart from each other, the laboratory measurements for most species were done at distinctly different times. Therefore, in most cases there are two different relative standard deviations (RSD) and minimum detection limits (MDL) associated with each species, one for the Whiteface Mountain samples and the other for the Davis samples.

Analytical uncertainties are calculated and reported as RSD in percent. The RSD was calculated using replicate analysis pairs when a large enough population (more than ten) of these existed. If it was not possible to use sample replicates, then analytical standard replicates were used. The formula for the calculation of the species relative standard deviation is shown in Equation 2.1.

$$RSD = \frac{\left[\left(\frac{1}{M}\right) \bullet \sum_{j=1}^{M} \left(\sigma_j^{'}\right)^2\right]^{\frac{1}{2}}}{\bar{x}} \bullet 100\% \qquad (2.1)$$

The value for σ'_j is calculated as in Equation 2.2.

$$\sigma_j^{'} = \frac{|x_1 - x_2|}{\sqrt{2}} \qquad (2.2)$$

For the above equations, M represents the number of pairs of replicates used, σ'_j is the standard deviation of each replicate pair and x bar is the average of all replicates.

To calculate the minimum detection limits for each species as many blanks as possible were used. If there was little to no variability in the blank measurements (e.g., all were reported as zero), then the MDL values were calculated using replicates of the standard with the lowest concentration. The equation used to calculate the MDL is shown as Equation 2.3.

$$MDL = \bar{x}_b + t \cdot s_b \cdot \sqrt{\frac{N_b + N_s}{N_b \cdot N_s}} \qquad (2.3)$$

For the previous equation, t is the t value given at the 95% confidence level for the appropriate number of degrees of freedom, s_b is the blank standard deviation, N_b is the number of blanks, N_s is the number of samples and x_b bar is the mean value of all the blanks.

Table 2.2: Statistical analysis for species measured using the ion chromatograph.

Minimum Detection Limit (in µN)(95% CL)								
	Sodium	Ammonium	Potassium	Magnesium	Calcium	Chloride	Nitrate	Sulfate
Whiteface Mnt.	1.64	0.67	0.41	3.35	4.11	0.24	0.63	0.98
Davis, CA	0.83	1.03	0.64	4.61	6.88	2.23	1.30	1.24
Relative Standard Deviation (concentration units in µN)								
	Sodium	Ammonium	Potassium	Magnesium	Calcium	Chloride	Nitrate	Sulfate
Whiteface Mountain								
	<10 µN	<10 µN	<10 µN	<10 µN	<10 µN	<10 µN	<10 µN	< 22 µN
RSD	*8.5%*	*24.9%*	*13.5%*	*31.4%*	*10.3%*	*7.0%*	*11.6%*	*11.0%*
count	80	9	82	62	17	19	5	6
min	-0.34	0.00	0.00	1.66	1.15	0.00	0.00	0.00
max	9.82	4.60	9.95	16.73	11.83	10.70	1.48	21.72
mean	3.01	0.73	4.00	4.65	6.67	5.14	1.02	5.35
	>10 µN	>10 µN	>10 µN	>10 µN	>10 µN	>10 µN	>10 µN	> 22 µN
RSD	*5.2%*	*2.9%*	*3.7%*	*2.2%*	*4.6%*	*4.2%*	*2.2%*	*0.9%*
count	6	79	6	24	67	41	54	48
min	12.94	13.30	10.48	10.33	10.06	10.35	11.35	26.40
max	298.91	1124.39	15.16	99.10	442.46	88.63	1341.66	1509.76
mean	134.79	239.29	12.89	39.75	66.70	31.49	326.27	612.29
Davis, CA								
	<10 µN	<10 µN	<10 µN	<10 µN	< 20 µN	<10 µN	< 20 µN	< 20 µN
RSD	*4.52%*	*42.81%*	*8.94%*	*31.67%*	*17.19%*	*8.01%*	*12.5%*	*5.3%*
count	69	15	65	90	83	56	12	34
min	-0.49	-0.34	-0.01	-0.09	-1.26	0.00	0.00	0.00
max	9.93	3.68	10.81	12.94	27.86	9.87	16.49	19.22
mean	3.51	0.79	4.06	3.37	9.21	3.60	2.22	6.60
	>10 µN	3000µN> x >10µN	>10 µN	>10 µN	> 20 µN	>10 µN	> 20 µN	> 20 µN
RSD	*2.5%*	*4.4%*	*19.7%*	*7.7%*	*6.1%*	*4.1%*	*1.1%*	*3.9%*
count	29	76	31	8	14	68	83	90
min	10.32	102.23	10.00	10.01	21.06	10.00	52.6	20.43
max	702.25	2977.89	50.34	34.08	67.82	497.70	9587.7	1791.2
mean	50.88	841.60	19.97	18.80	37.19	65.01	1088.2	257.5

For the inorganic ion analysis the ion chromatograph is calibrated before each run. After every ninth sample, a calibration standard was rerun to ensure that the IC was still well calibrated. NIST-traceable standards were also used to check the accuracy of the instrument calibration. There were two RSD values calculated for each species from each field campaign. The RSDs are split up into high and low concentration values. Both the MDL and the chromatogram peak threshold value were calculated for each inorganic species. Here only the minimum detection limit will be reported as both values are comparable. The ion chromatograph statistics are reported in Table 2.2.

Iron and manganese samples from both campaigns were run together using the GFAAS. Once preserved the metals are stable and therefore the results are not greatly compromised by delaying the analysis. Note that the deionized water used in the field to clean collectors was contaminated with Fe for some Whiteface samples. Therefore the collector blanks are corrected for this by subtracting off the Fe concentration from the deionized water blank. The statistics from the metals analysis are reported in Table 2.3.

Table 2.3: Metals statistics: Compiled from both Whiteface Mountain and Davis, CA.

Metals Statistics		
	MDL 95% CL	**RSD**
Fe	4.44 μg/l	11.05%
Mn	0.16 μg/l	3.56%

Aqueous phase hydrogen peroxide measurements were done separately for each campaign. The Shimadzu RF-1501 spectrofluorophotometer was calibrated using up to ten standards. A standard repetition took place every tenth measurement while the

sample concentrations were being determined. The statistics from these measurements are found in Table 2.4.

Table 2.4: H_2O_2 statistics

Hydrogen Peroxide Statistics					
	MDL 95% CL	RSD	Max	Min	Average
Whiteface Mountain	0.21 μM	2.04%	78.5 μM	0.0 μM	16.2 μM
Davis, CA	0.06 μM	9.25%	30.2 μM	0.0 μM	7.65 μM

The measurements of the formaldehyde and S(IV) concentrations were done similarly to those for hydrogen peroxide. The instrument was calibrated at the beginning of each run and individual standards were repeated about every tenth measurement. The statistical results from these two aqueous phase species can be found in Tables 2.5 and 2.6.

Table 2.5: HCHO statistics

Formaldehyde Statistics					
	MDL 95% CL	RSD	Max	Min	Average
Whiteface Mountain	1.39 μM	4.04%	21.11 μM	5.75 μM	9.04 μM
Davis, CA	2.29 μM	7.70%	143.2 μM	0.51 μM	57.45 μM

Table 2.6: S(IV) statistics. Large vol and small vol refers to the amount of sample used to make the S(IV) measurement.

S(IV) Statistics							
		MDL 95% CL	RSD (reps)	RSD (stnrds)	Max	Min	Average
Whiteface Mnt.	Large Vol	3.06 μM	73.80%	25.70%	7.03 μM	-0.1 μM	2.08 μM
	Small Vol	4.88 μM		52.10%			
Davis, CA	Both	2.41 μM	91.80%	12.50%	14.31 μM	-0.1 μM	4.25 μM

3. Results and Discussion

3.1 Sample Composition and Predicted S(IV) Oxidation

3.1.1 Whiteface Mountain (Event Summary and Results of Chemical Analysis)

Throughout July of 1998 there were a total of six cloud interception events at Whiteface Mountain. These events took place at various times during the day and night and lasted anywhere from two to twelve hours. Table 3.1 shows an event summary for the Whiteface field campaign. Note that meteorological and liquid water content data are unavailable for the first event. The samples were generally collected at hourly intervals, except when a high liquid water content dictated more frequent sample collection. In these cases the samples were collected at half hour intervals.

Of primary interest in these breakdowns are the pH values given for each type of sample. There is very little difference between the pH values for each of the fractions in the sf-CASCC. These sf-CASCC values are also consistent with the pH values found for the cloudwater collected by the bulk CASCC2 sampler. The average relative standard deviation for the three measurements is 1.14%. The relative standard deviation of the instrument is roughly 2% of the measurement; so, in several cases there is no statistical difference among the measurements for each sample time.

The pH of the samples will play an important role in the rate and dominant pathway of S(IV) oxidation. For the environmental conditions seen at Whiteface, the pH distribution over the drop size spectrum appears quite homogeneous, as determined by

Table 3.1 Whiteface Mountain event summary: Liquid water content, temperature and pressure are all averaged over the event. (*) indicates values that were approximated.

Event 1: July04, 1998 7/4/98 – 7/5/98 9:45pm 7:00am			**Event 2: July07, 1998** 7/7/98 – 7/8/98 12:30pm 12:50am		
LWC (mg/m^3)	Temperature (°C)	Pressure (mb)	LWC (mg/m^3)	Temperature (°C)	Pressure (mb)
N/A	14.5*	850.4*	420	12.1	854.5
	Number of Samples	Average pH (Max pH – Min pH)		Number of Samples	Average pH (Max pH – Min pH)
CASCC2	10	4.34 (4.6-3.9)	CASCC2	19	3.33 (3.6 – 2.9)
Large - sf	10	4.34 (4.7-3.9)	Large - sf	19	3.34 (3.6 – 2.9)
Small - sf	10	4.29 (4.6-3.8)	Small - sf	19	3.37 (3.8 – 2.9)
Event 3: July16, 1998 7/16/98 – 7/16/98 7:25am 11:30am			**Event 4: July17, 1998** 7/17/98 – 7/17/98 1:30am 11:00am		
LWC (mg/m^3)	Temperature (°C)	Pressure (mb)	LWC (mg/m^3)	Temperature (°C)	Pressure (mb)
332	17.1	849.6	511	15.6	849.4
	Number of Samples	Average pH (Max pH – Min pH)		Number of Samples	Average pH (Max pH – Min pH)
CASCC2	8	2.93 (3.1 – 2.8)	CASCC2	8	3.16 (3.3 – 3.0)
Large - sf	8	2.96 (3.0 – 2.8)	Large –sf	10	3.14 (3.3 – 3.0)
Small - sf	8	2.89 (3.0 – 2.7)	Small - sf	10	3.17 (3.3 – 3.0)
Event 5: July20, 1998 7/20/98 – 7/20/98 9:00am 1:00pm			**Event 6: July22, 1998** 7/22/98 – 7/22/98 2:00am 4:00am		
LWC (mg/m^3)	Temperature (°C)	Pressure (mb)	LWC (mg/m^3)	Temperature (°C)	Pressure (mb)
454	15.0	844.6	323	16.8	847.8
	Number of Samples	Average pH (Max pH – Min pH)		Number of Samples	Average pH (Max pH – Min pH)
CASCC2	8	3.26 (3.6 – 3.0)	CASCC2	4	3.56 (3.8 – 3.3)
Large - sf	8	3.25 (3.6 – 3.0)	Large - sf	4	3.57 (3.8 – 3.4)
Small - sf	8	3.25 (3.6 – 3.0)	Small - sf	4	3.54 (3.8 – 3.4)

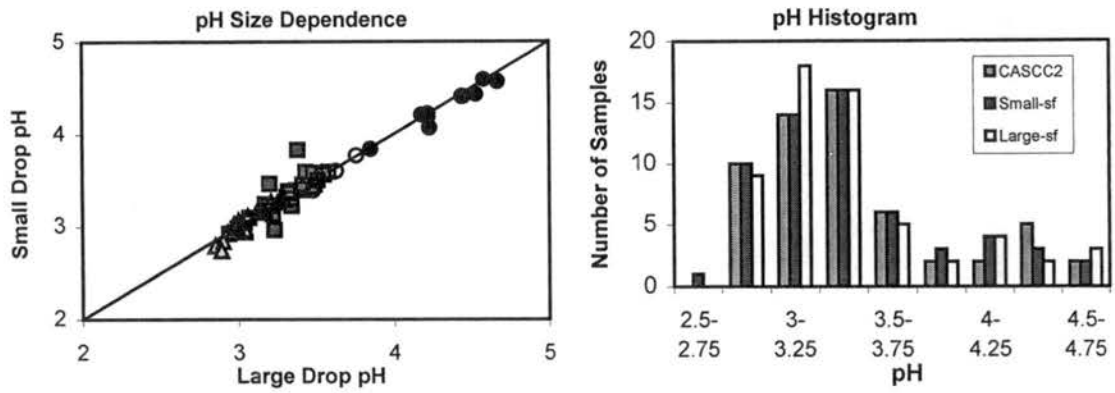

Figure 3.1 Whiteface Mountain pH size dependence and histogram: The first plot above is the pH size dependence, the different types of symbols represent different events. The second plot is a histogram showing the frequency, in number of samples, of each pH range labeled on the x-axis for the CASCC2, and the large and small drop size fractions of the sf-CASCC.

using two-stage observations. This can be seen in Figure 3.1, where the large drop pH is plotted against the small drop pH of the same sample. All points fall close to, if not on, the one to one line that runs diagonally through the center of the plot.

The second plot in Figure 3.1 shows a frequency distribution of pH values for the Whiteface samples. The peak frequencies occur between the values of 3 to 3.5 pH units. The expected pH value for drops in a pristine environment that are in equilibrium with the carbon dioxide in the atmosphere is 5.6. Naturally occurring acids can sometimes depress the background pH to a value near 5 pH units. None of the sample pH values measured during the Whiteface campaign even approach this neutral environmental value. This indicates that the clouds sampled at this location were quite acidic, as expected.

The results of the chemical analysis of additional cloudwater species for the Whiteface Mountain samples show a fairly homogeneous distribution across the drop size

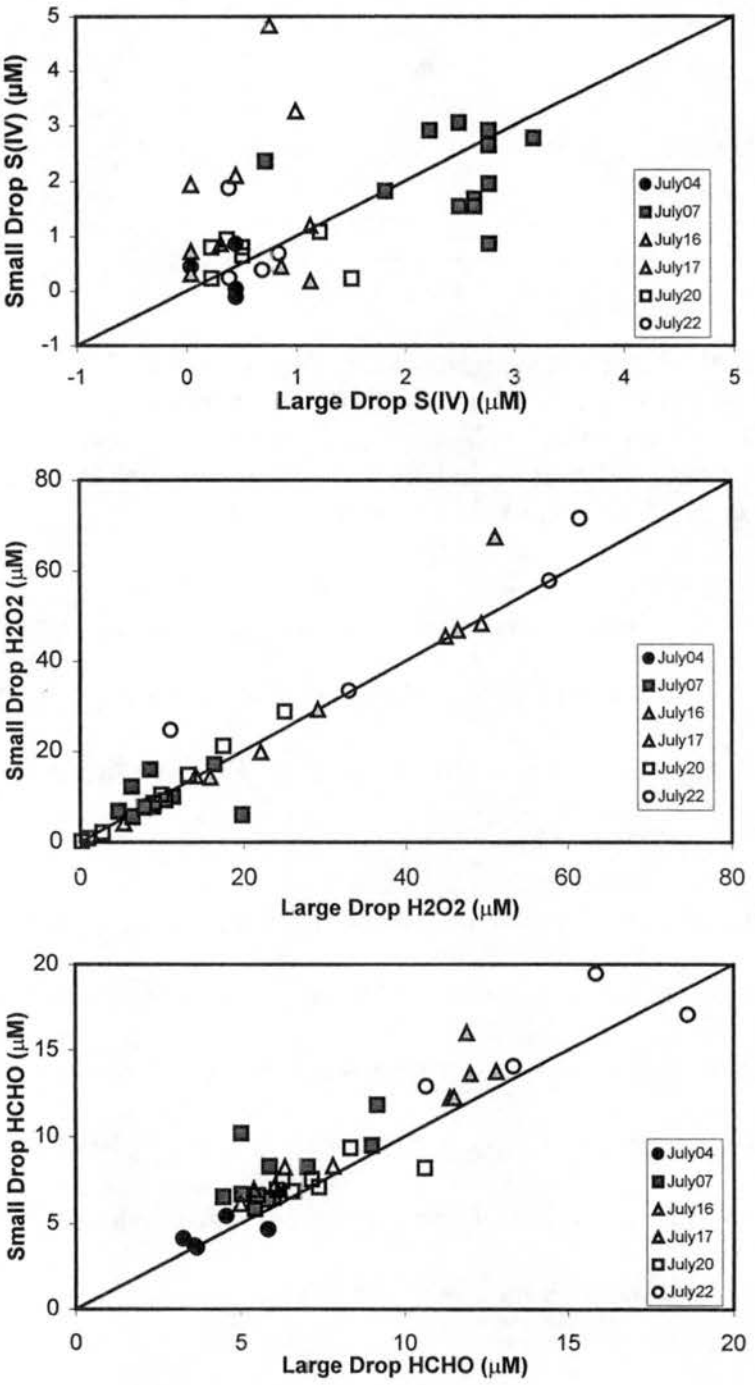

Figure 3.2 Whiteface Mountain size dependence for aqueous S(IV), hydrogen peroxide and formaldehyde. Small drop concentrations are plotted on the y-axis and large drop concentrations are on the x-axis.

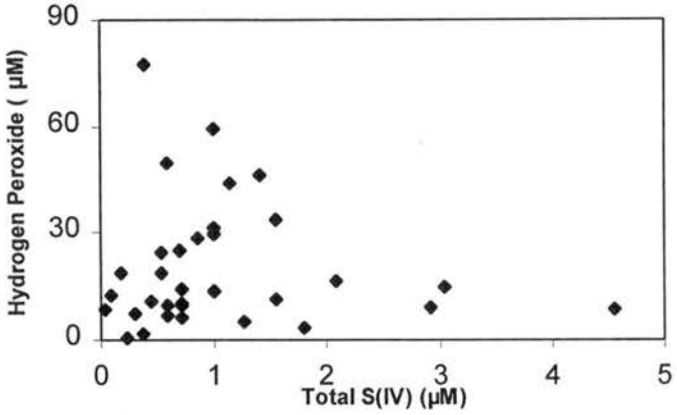

Figure 3.3: Whiteface hydrogen peroxide concentration vs. total S(IV) concentration.

spectrum. Figure 3.2 shows plots relating the concentrations in the two different size fractions of the sf-CASCC of total sulfur (IV), hydrogen peroxide and total formaldehyde, all in the aqueous phase. Total S(IV) measurement includes free S(IV) as well as S(IV) complexed with formaldehyde as HMS, and any other aldehyde complexes that S(IV) may form. Similarly total HCHO includes free HCHO and HMS. These plots show a fairly straightforward one to one relationship for most of the species. The most scatter occurs in the S(IV) measurements (probably reflecting their low concentrations), while the formaldehyde results are slightly skewed towards the smaller drops.

These plots also provide some insight into what is going on inside the cloud drops. The concentrations of H_2O_2, combined with the low pH values indicate that the peroxide pathway is likely to be the dominant mode of S(IV) oxidation in this environment. This becomes more evident when the concentrations of S(IV) and H_2O_2 are compared. The characteristic time for the

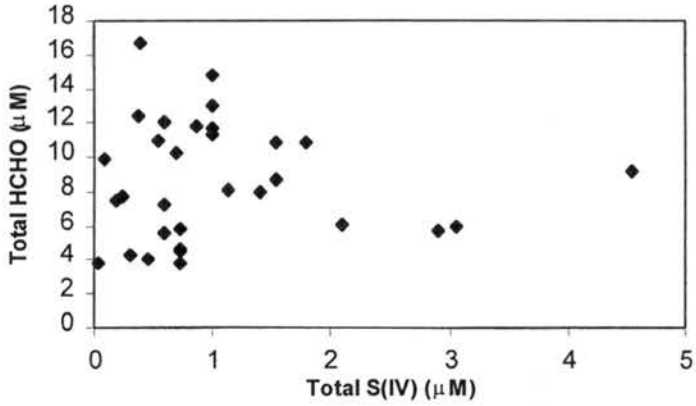

Figure 3.4: Whiteface Mountain formaldehyde vs. total S(IV).

oxidation of S(IV) via the hydrogen peroxide pathway is fast, on the order of a few seconds. Because of this rapid reaction it is not likely that the two species will coexist. There is an obvious negative correlation between S(IV) and hydrogen peroxide seen in the sample concentrations (Figure 3.3). The figure shows that when the concentration of S(IV) or peroxide is high, the concentration of the other species tends to be low.

Similar results can be seen when the formaldehyde concentration is plotted against the total S(IV) concentration (Figure 3.4). It is more difficult to compare these concentrations, however, since both measurements will include any HMS present in the sample. The rate of this complexation is not likely to be competitive with the rate of

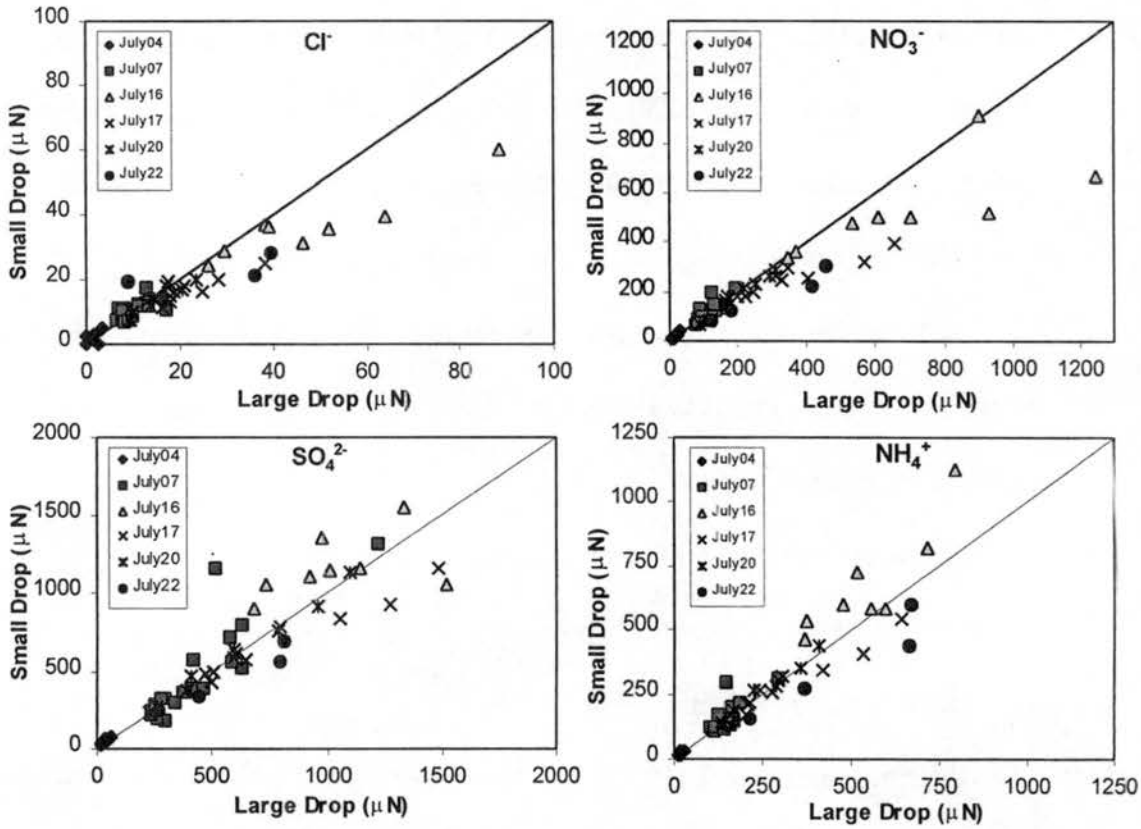

Figure 3.5 Whiteface Mountain size dependence relationships for inorganic ions: chloride, nitrate, sulfate and ammonium.

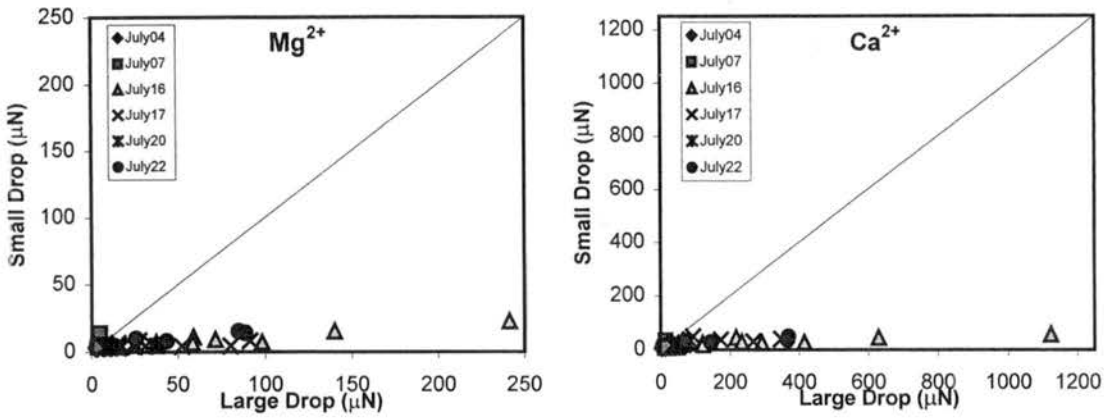

Figure 3.6 Whiteface Mountain divalent cations: magnesium and calcium

sulfate production at low pH values, like those seen in the Whiteface samples (Rao and Collett, 1995).

Figure 3.5 shows the scatter plots for some of the ionic species found in the cloud water. Again large and small drop concentrations are similar for most species. There does, however, exist some modest amount of size dependence for individual samples and events. Note that there is some slight enhancement in the concentrations of chloride and nitrate in the large drops. Time resolved data show that ammonium and sulfate seem to track each other, showing small or large drop enhancement for the same periods. The divalent cations, Ca^{2+} and Mg^{2+}, are the only species that show any significant deviation from this trend of homogeneity (Figure 3.6). These species are enhanced in the large size fraction. Also enhanced in the large size fraction are the metals, Fe and Mn (Figure 3.7).

The reason that several species are more predominantly found in the large size fraction is likely because they are derived from crustal materials that form coarse mode aerosols. Large particles tend to form larger drops (e.g., Twohy et al., 1989).

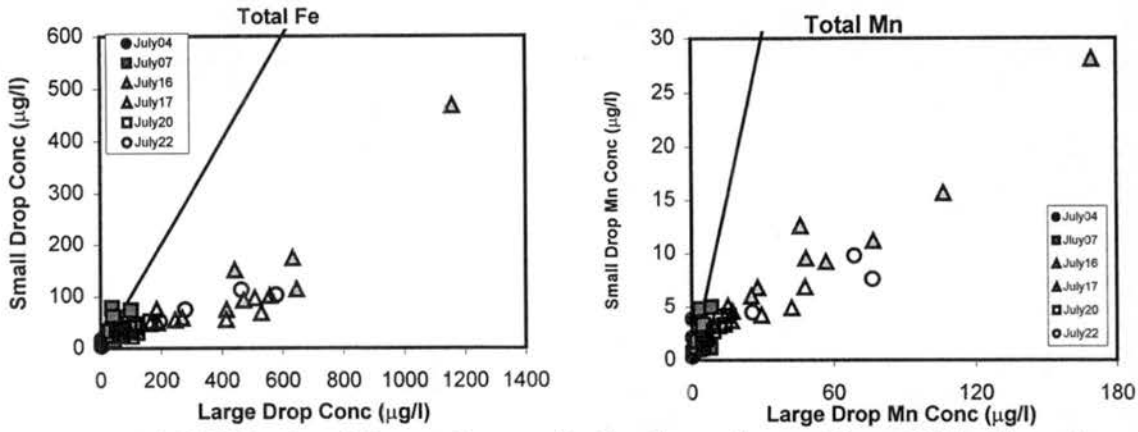

Figure 3.7 Whiteface Mountain metals size dependence: Fe and Mn. Note the one to one line is also plotted.

3.1.2 Davis (Event Summary and Results of Chemical Analyses)

The Davis field campaign took place in late December and early January of the winter of 1998-1999. During this time there were a total of six fog collection events. These events took place predominantly from the middle of the night through mid morning, lasting anywhere from seven to fourteen hours. The event summary is given in Table 3.2. The table shows that the temperatures were much colder than at Whiteface, hovering just a few degrees above zero. These cold temperatures will tend to slow down reaction rates and increase trace gas solubilities. Also the liquid water content was much lower than observed at Whiteface. Not only was there less liquid water, but the size distribution of the drops heavily favored the larger drop sizes.

The pH values for the Davis samples are much higher than those seen at Whiteface. There is also a noticeable difference in pH (approximately 0.4 pH units) between the different drop sizes as seen in the one to one plot in Figure 3.8. A pH value frequency plot is also shown. For the Davis samples the peak pH values are between 6.2

Table 3.2 Davis, CA event summary: The values for liquid water content (LWC), temperature and pressure are averages over the entire event.

Event 1: December18, 1998 12/18/98 – 12/18/98 3:22am 11:20am			**Event 2: January04, 1999** 1/4/99 – 1/5/99 8:08pm 10:00am		
LWC (mg/m^3)	Temperature (°C)	Pressure (mb)	LWC (mg/m^3)	Temperature (°C)	Pressure (mb)
185	4.9	1013.9	79	2.8	1027.6
	Number of Samples	Average pH (Max pH – Min pH)		Number of Samples	Average pH (Max pH – Min pH)
CASCC2	9	6.09 (6.5 – 5.5)	CASCC2	13	6.49 (6.6 – 5.3)
Large - sf	9	6.34 (6.7 – 5.9)	Large - sf	13	6.53 (6.8 – 6.0)
Small - sf	8	5.94 (6.4 – 5.5)	Small - sf	12	6.24 (6.5 – 6.0)
Event 3: January09, 1999 1/9/99 – 1/9/99 3:00am 10:36am			**Event 4: January10, 1999** 1/10/99 – 1/10/99 2:45am 10:00am		
LWC (mg/m^3)	Temperature (°C)	Pressure (mb)	LWC (mg/m^3)	Temperature (°C)	Pressure (mb)
52	2.9	1027.3	49	2.8	1023.6
	Number of Samples	Average pH (Max pH – Min pH)		Number of Samples	Average pH (Max pH – Min pH)
CASCC2	8	6.66 (6.8 – 6.6)	CASCC2	6	6.18 (6.6 – 5.6)
Large - sf	8	6.74 (6.9 – 6.4)	Large –sf	6	6.33 (6.6 – 5.7)
Small - sf	8	6.32 (6.6 – 6.0)	Small - sf	6	5.82 (6.3 – 5.5)
Event 5: January10b, 1999 1/10/99 – 1/11/99 10:50pm 9:42am			**Event 6: January11, 1999** 1/11/99 – 1/12/99 11:00pm 10:00am		
LWC (mg/m^3)	Temperature (°C)	Pressure (mb)	LWC (mg/m^3)	Temperature (°C)	Pressure (mb)
57	2.4	1019.2	60	2.9	1019.2
	Number of Samples	Average pH (Max pH – Min pH)		Number of Samples	Average pH (Max pH – Min pH)
CASCC2	8	6.06 (6.7 – 5.5)	CASCC2	8	6.24 (6.4 – 6.1)
Large - sf	8	6.27 (6.9 – 5,7)	Large - sf	8	6.34 (6.5 – 6.0)
Small - sf	8	5.92 (6.4 – 5.6)	Small - sf	8	5.92 (6.4 – 5.6)

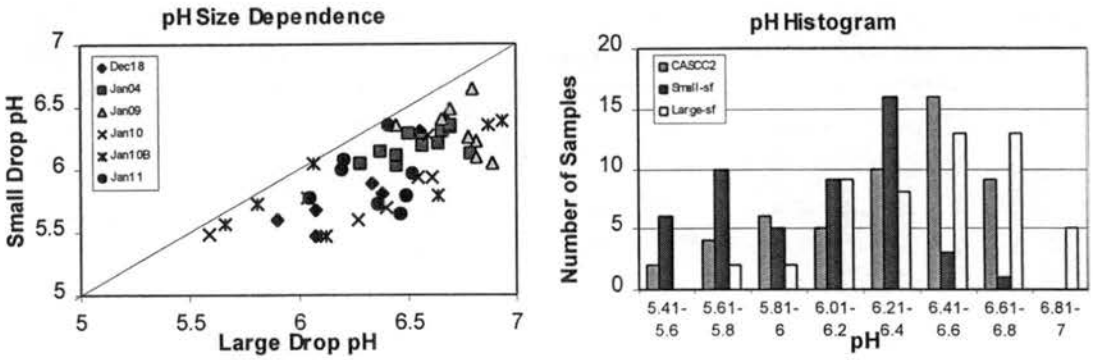

Figure 3.8 Davis, CA pH size dependence and histogram: The first plot is the small drop pH plotted against the large drop pH. The one to one line crosses diagonally through the graph. The second plot shows the frequency in number of samples that each pH range was measured for the CASCC2 and both fractions of the sf-CASCC.

and 6.6 pH units. This indicates that the fog water was more alkaline than the previously mentioned environmentally neutral pH value of 5.6. This, coupled with lower aqueous phase H_2O_2 concentrations, indicates that sulfate production is likely to be dominated by either the ozone or catalyzed oxygen pathway.

Drop size dependent plots for aqueous S(IV), H_2O_2 and HCHO are shown in Figure 3.9. Only a few peroxide aliquots were made during the Davis field campaign, as the peroxide pathway has not previously been an important mode of S(IV) oxidation in this region and gaseous H_2O_2 measurements were made . Plots of aqueous sulfur (IV) and formaldehyde show that these species are present in higher concentrations in the smaller drop fraction of the sf-CASCC. This chemical heterogeneity with respect to drop size has been seen in previous San Joaquin valley drop chemistry studies (e.g. Collett et al., 1994; Rao and Collett, 1995; Bator and Collett, 1997; Collett et al., 1999).

The inorganic ions show an even stronger trend towards higher concentrations in the small drop fraction (Figure 3.10). Again this is similar to results from the past studies

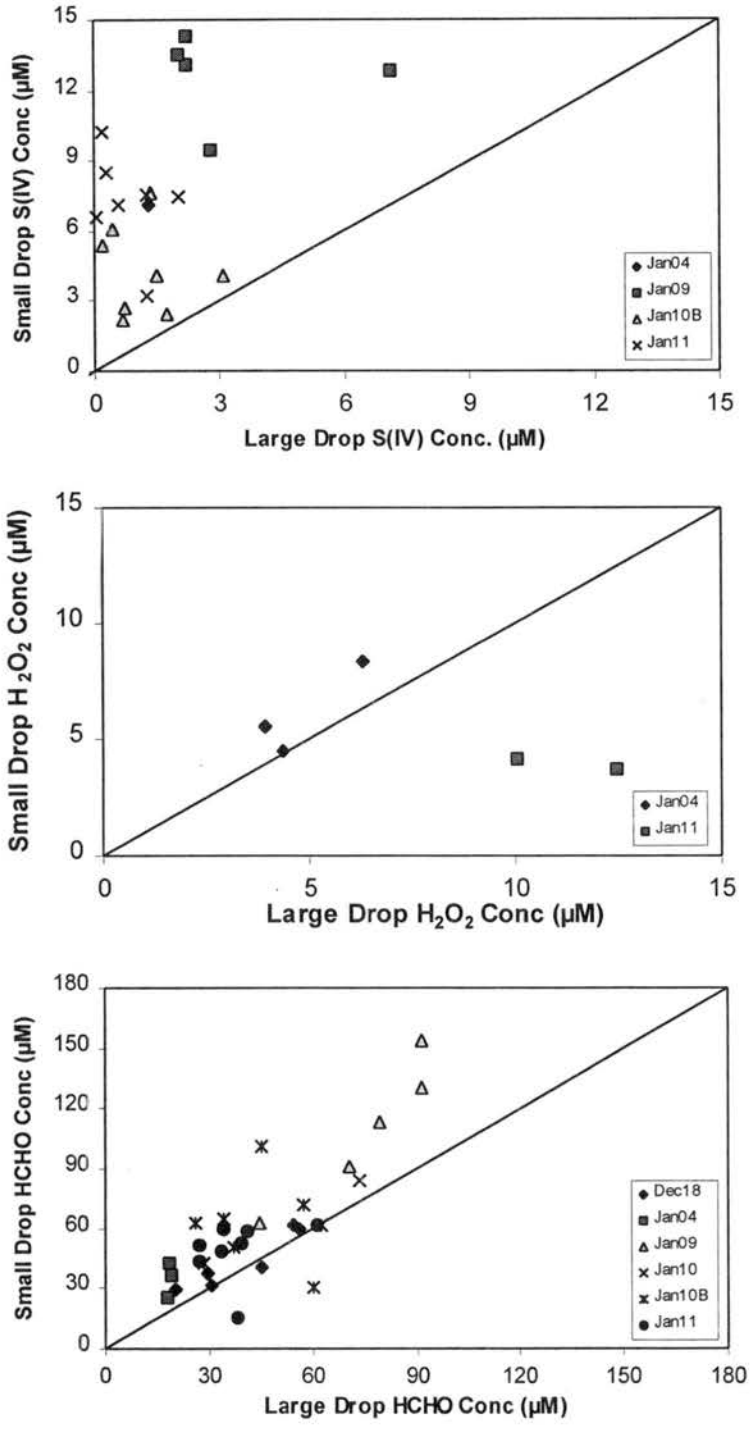

Figure 3.9 Davis, CA size dependence relationships for S(IV), hydrogen peroxide and formaldehyde. Small drop concentrations are plotted on the y-axis and large drop concentrations are on the x-axis.

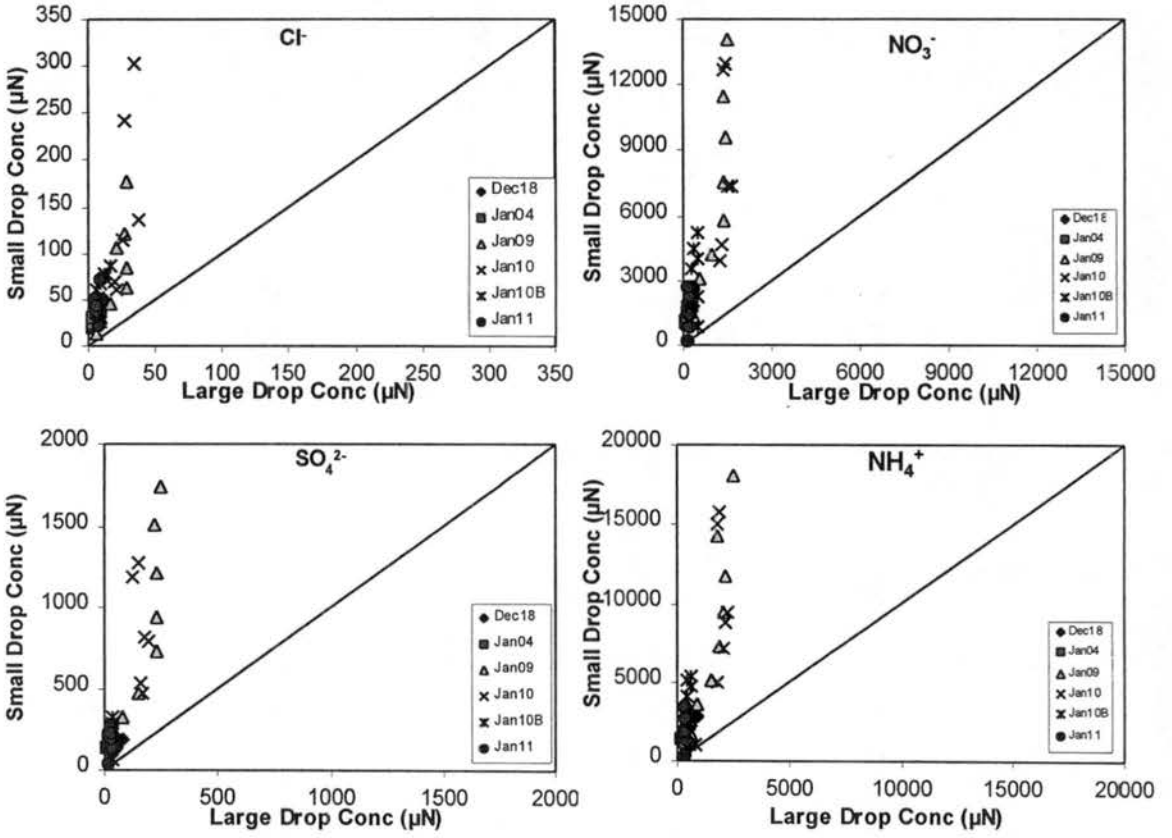

Figure 3.10 Davis, CA size dependence relationships for inorganic ions: chloride, nitrate, sulfate and ammonium.

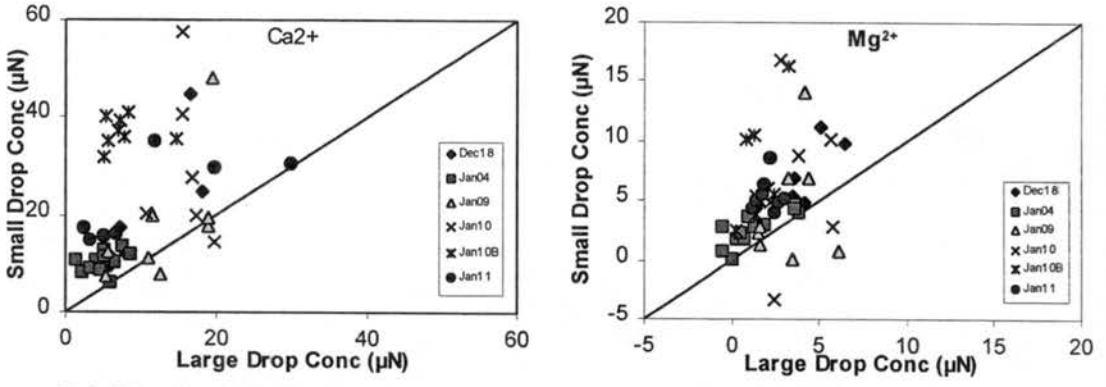

Figure 3.11 Davis, CA divalent cations: calcium and magnesium.

of the area. Even the divalent cations are found to have higher small drop concentrations (Figure 3.11), which is opposite of what was found for the Whiteface data. The concentration difference between large and small drops for the divalent cations is not as strong as for the other inorganic ions.

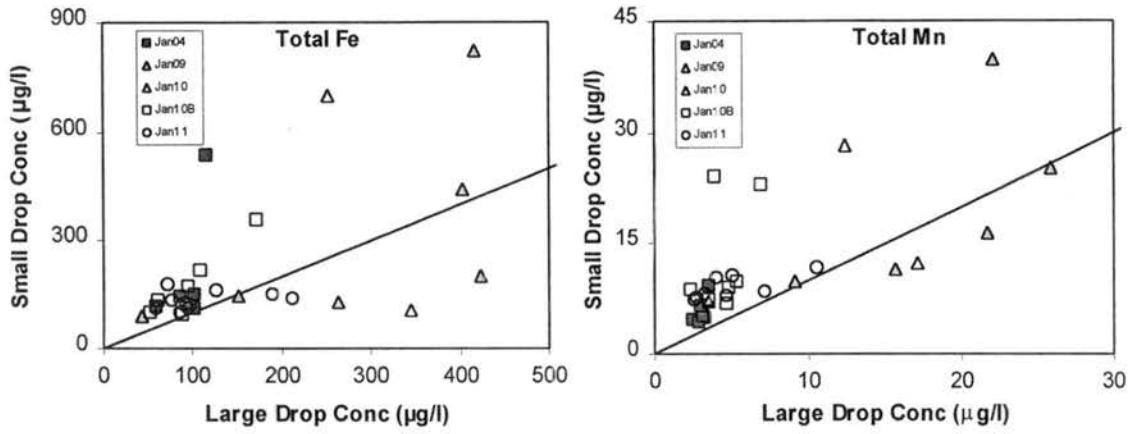

Figure 3.12 Davis, CA metals size dependence: iron and manganese. The one to one lines have been added.

Even the trace metals analyzed in the Davis samples sometimes appear to be enriched in the small drop fraction (Figure 3.12). This again is different from the trend seen in the metals concentrations for the Whiteface samples. The spread of the data points on the plots is similar to that seen for the divalent cations.

3.2 Oxidation Rate Calculations

In order to calculate the rate of sulfate production the reactions that need to be considered are the ionization of dissolved SO_2 in the drop and the reaction rates of each of the main oxidation pathways. Therefore the rates of each of the individual reactions need to be considered. Equations 1-7 in Table 3.3 show that different reactions occur for each of the three different forms of S(IV). Therefore it is relevant to examine first the how SO_2 dissolves in the cloud or fog drop.

The partitioning of S(IV) into $SO_2 \bullet H_2O$, HSO_3^- and SO_3^{2-} depends on the aqueous solution acidity (Figure 1.1). These three species are known as free S(IV), as

Table 3.3: S(IV) reactions and rates. Sources: (1 – 4) Hoffman and Calvert (1985); (5) Ibusuki and Takeuchi (1987); (6) & (7) Boyce and Hoffman (1984).

Reaction		Activation Energy (kJ/mole)	k($M^{-n}s^{-1}$) 5°C	10°C	25°C
(1)	$HSO_3^- + H_2O_2 \rightarrow H_2SO_4^{2-} + H_2O$	39.5	2.37E7	3.20E7	7.45E7
(2)	$SO_2 \bullet H_2O + O_3 \rightarrow SO_4^{2-} + O_2 + 2H^+$		2.40E4	2.40E4	2.40E4
(3)	$HSO_3^- + O_3 \rightarrow SO_4^{2-} + O_2 + H^+$	46	9.73E4	1.38E5	3.70E5
(4)	$SO_3^{2-} + O_3 \rightarrow SO_4^{2-} + O_2$	43.9	4.19E8	5.86E8	1.50E9
(5)	$S(IV) + 1/2O_2(Fe^{3+}, Mn^{2+}) \rightarrow S(VI)$	70.1	@pH<4.2 4.86E6 @pH≥4.2 3.28E12	@pH<4.2 8.30E6 @pH≥4.2 5.60E12	@pH<4.2 3.72E7 @pH≥4.2 2.51E13
(6)	$HSO_3^- + HCHO \rightarrow HMS$	24.7	2.42E2	3.30E2	7.90E2
(7)	$SO_3^{2-} + HCHO \rightarrow HMS$	20	1.62E7	1.82E7	2.50E7

they are not complexed with any other species and are capable of taking part in reactions. From the equations in Table 3.4 and assuming Henry's Law equilibrium the concentrations of these three species can be given as

$$[SO_2 \bullet H_2O] = H_{SO_2} p_{SO_2} \tag{3.1}$$

$$[HSO_3^-] = \frac{H_{SO_2} K_{S1} p_{SO_2}}{[H^+]} \tag{3.2}$$

$$[SO_3^{2-}] = \frac{H_{SO_2} K_{S1} K_{S2} p_{SO_2}}{[H^+]^2} \tag{3.3}$$

$$[S(IV)] = H_{SO_2} p_{SO_2} \left[1 + \frac{K_{S1}}{[H^+]} + \frac{K_{S1} K_{S2}}{[H^+]^2} \right] \tag{3.4}$$

Table 3.4: SO_2 in water. Source: Seinfeld and Pandis, 1998.

Absorption of SO_2 in Water
$SO_2(g) + H_2O \leftrightarrow SO_2 \cdot H_2O$
$SO_2 \cdot H_2O \leftrightarrow H^+ + HSO_3^-$
$HSO_3^- \leftrightarrow H^+ + SO_3^{2-}$

Here S(IV) is defined as the sum of dissolved sulfur dioxide, sulfite and bisulfite. Knowing these values, the mole fraction of each species in solution can be calculated. Standard notation dictates that the mole fraction for hydrated sulfur dioxide is labeled as α_0, bisulfite as α_1, and sulfite as α_2. The mole fractions are

$$\alpha_0 = \left(1 + \frac{K_{S1}}{[H^+]} + \frac{K_{S1}K_{S2}}{[H^+]^2}\right)^{-1} \tag{3.5}$$

$$\alpha_1 = \left(1 + \frac{[H^+]}{K_{S1}} + \frac{K_{S2}}{[H^+]}\right)^{-1} \tag{3.6}$$

$$\alpha_2 = \left(1 + \frac{[H^+]}{K_{S2}} + \frac{[H^+]^2}{K_{S1}K_{S2}}\right)^{-1} \tag{3.7}$$

The partitioning of S(IV) will help dictate which sulfate production pathway will be dominant.

The oxidation of S(IV) through the hydrogen peroxide pathway predominantly involves bisulfite (Seinfeld and Pandis, 1998). Hoffman and Calvert (1985) give the rate expression for the destruction of S(IV) by reaction with H_2O_2 as

$$-\frac{d[S(IV)]}{dt} = \frac{k_{H_2O_2}[H^+][H_2O_2][HSO_3^-]}{1+K[H^+]} \qquad (3.8)$$

If Henry's Law equilibrium with the gas phase is assumed the rate can be given as

$$-\frac{d[S(IV)]}{dt} = \frac{k_{H_2O_2}}{1+K[H^+]}\left(\alpha_1 H_{SO_2} p_{SO_2} H_{H_2O_2} p_{H_2O_2}\right) \qquad (3.9)$$

Here the mole fraction coefficient for bisulfite has been used. The above equation allows the rate of sulfate production via the peroxide pathway to be calculated using the gas phase concentrations of SO_2 and H_2O_2, along with the drop pH.

The production of sulfate through reaction with ozone can occur with any of the three aqueous phase free S(IV) species. This reaction rate is given by Hoffman and Calvert (1985) as

$$-\frac{d[S(IV)]}{dt} = \left(k_0[SO_2 \bullet H_2O] + k_1[HSO_3^-] + k_2[SO_3^{2-}]\right)[O_3] \qquad (3.10)$$

Using the previously defined mole fractions and Henry's law equilibrium the expression can be reduced to

$$-\frac{d[S(IV)]}{dt} = (\alpha_0 k_0 + \alpha_1 k_1 + \alpha_2 k_2) H_{SO_2} p_{SO_2} H_{O_3} p_{O_3} \qquad (3.11)$$

Again, by knowing the gas phase concentrations of SO_2 and O_3 along with the sample pH, the ozone reaction rate can be determined if gas/liquid equilibrium is assumed.

The autooxidation pathway catalyzed by Fe(III) and Mn(II) can occur through two different mechanisms, depending on the drop pH. Ibusuki and Takeuchi (1987) give rates for these pathways as

For $2.6 \leq pH \leq 4.2$

$$-\frac{d[S(IV)]}{dt} = k_{M1}[H^+]^{-0.74}[Fe(III)][Mn(II)][S(IV)] \qquad (3.12)$$

For $4.2 < pH \leq 6.5$

$$-\frac{d[S(IV)]}{dt} = k_{M2}[H^+]^{0.67}[Fe(III)][Mn(II)][S(IV)] \qquad (3.13)$$

For these two equations [S(IV)] is determined using the effective Henry's Law coefficient, H^*, as

$$[S(IV)] = H^*_{S(IV)} p_{SO_2} = \left(H_{SO_2}\left[1 + \frac{K_{s1}}{[H^+]} + \frac{K_{s1}K_{s2}}{[H^+]^2}\right]\right) p_{SO_2} \qquad (3.14)$$

Therefore gas phase SO_2 concentrations can still be used in the calculation. The values for total Fe and total Mn are obtained from fog sample analysis. In order to get concentrations for Fe(III) and Mn(II) some assumptions were made about the total metals compositions. Fe(III) was assumed to compose 25% of the total Fe measured in the sample, and all the Mn measured was assumed to be in the form of Mn(II). The speciation of iron is dependent on the pH of the sample. Previous work (Rao and Collett, 1998) suggests that 25% Fe(III) and 100% Mn(II) are reasonable assumptions.

3.2.1 Whiteface Mountain Predicted S(IV) Oxidation

As mentioned previously, the oxidation of S(IV) at Whiteface Mountain is typically dominated by the hydrogen peroxide pathway. In order to test this assumption for the current study, sulfate production rates were calculated for each of the three oxidation paths mentioned in the preceding section. The calculated rates for the large and small fractions of the sf-CASCC were then compared; this comparison was intended to

determine what, if any, effect size resolved cloud drop chemistry should exert on S(IV) oxidation in this environment.

In order to calculate the rates of sulfate production, gas phase concentrations of SO_2, O_3 and H_2O_2 are required. The average concentrations of these gases during the cloud sampling events were, SO_2 = 1.24 ppbv, O_3 =50 ppbv, and H_2O_2 = 0.16 ppbv. Histograms of the concentrations of these three gases during the cloud interception events at Whiteface Mountain are located in Figure 3.13. Note that the ozone concentration appears to be very high, while the concentrations of hydrogen peroxide and sulfur dioxide are rather low. Low H_2O_2 concentrations may reflect consumption by the S(IV) oxidation reaction.

Oxidation calculations suggest that the hydrogen peroxide pathway is responsible for nearly 100% of the aqueous phase sulfate production at Whiteface Mountain. For most samples the H_2O_2 pathway is more than one hundred times faster than both the ozone and metal catalyzed pathways. Table 3.5 shows the dominant (fastest) oxidation pathway for each Whiteface sample.

Also shown in this table is a value known as the enhancement factor. The enhancement factor is the ratio of the oxidation rate of the total drop population calculated using size resolved data divided by the total oxidation rate calculated using the average fog composition. The average oxidation rate is calculated by volume weighting the small and large drop rates. In the average composition method, the oxidation rate is predicted using the weighted average H^+ and trace metal concentrations from the large and small fractions. These values are approximately representative of those that would be

measured if the cloud drop sizes had been sampled together instead of collected in separate fractions. This "bulk" rate should therefore be similar to the rate calculated using the data from the CASCC2 collector. Once these two numbers are determined for

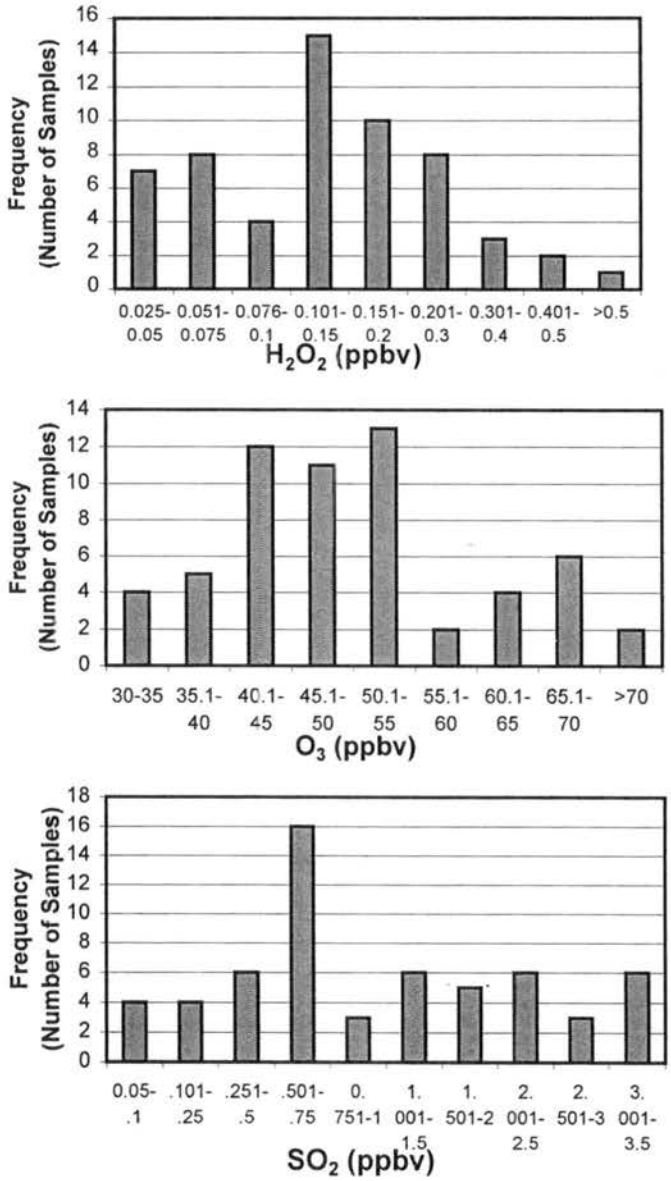

Figure 3.13: Whiteface Mountain trace gas concentration histograms: H_2O_2, O_3 and SO_2.

Table 3.5: Whiteface Mountain oxidation breakdown

Sample	pH CASCC2	PH Small	pH Large	% Peroxide	% Metals	% Ozone	Enhancement Factor
July4 01	4.61	4.57	4.67	82.6%	0.02%	17.39%	1.00
July4 02	4.46	4.43	4.53	88.4%	0.02%	11.59%	1.00
July4 03	4.28	4.22	4.22	96.6%	0.02%	3.37%	1.00
July4 04	3.86	3.84	3.85	99.1%	0.01%	0.91%	1.00
July4 05	4.28	4.07	4.23	97.0%	0.00%	2.95%	1.00
July4 06	4.45	4.41	4.45	88.9%	0.04%	11.04%	1.00
July4 01	4.19	4.21	4.18	96.5%	0.02%	3.50%	1.00
July4 07	4.22	4.19	4.22	96.3%	0.03%	3.69%	1.00
July4 08	4.46	4.41	4.44	92.4%	0.01%	7.62%	1.00
July4 09	4.59	4.59	4.58	89.2%	0.01%	10.74%	1.00
July7 01	3.51	3.59	3.43	99.9%	0.05%	0.04%	1.00
July7 02	3.55	3.58	3.48	99.9%	0.02%	0.04%	1.00
July7 03	3.56	3.58	3.54	99.9%	0.02%	0.07%	1.00
July7 04	3.55	3.56	3.55	99.9%	0.01%	0.09%	1.00
July7 05	3.46	3.45	3.49	99.9%	0.02%	0.07%	1.00
July7 06	3.33	3.32	3.31	99.9%	0.03%	0.04%	1.00
July7 07	3.44	3.39	3.41	99.9%	0.01%	0.06%	1.00
July7 08	3.45	3.43	3.47	99.9%	0.01%	0.06%	1.00
July7 09	3.38	3.39	3.37	99.9%	0.01%	0.05%	1.00
July7 10	3.44	3.45	3.41	99.9%	0.01%	0.06%	1.00
July7 11	3.39	3.83	3.38	99.9%	0.01%	0.07%	1.00
July7 12	3.2	3.22	3.34	99.9%	0.01%	0.06%	1.00
July7 13	3.2	3.13	3.22	99.9%	0.02%	0.03%	1.00
July7 14	2.95	2.96	3.23	100%	0.01%	0.03%	1.00
July7 15	2.92	2.92	2.94	100%	0.01%	0.02%	1.00
July7 16	3.28	3.24	3.17	99.9%	0.01%	0.07%	1.00
July7 17	3.23	3.22	3.2	99.9%	0.01%	0.08%	1.00
July7 18	3.33	3.38	3.32	99.9%	0.01%	0.11%	1.00
July7 19	3.07	3.46	3.2	99.9%	0.00%	0.06%	1.00
July16 01	2.88	2.79	2.85	99.9%	0.10%	0.01%	1.00
July16 02	3	2.94	3.04	99.7%	0.24%	0.02%	1.00
July16 03	3.05	2.99	3.04	99.8%	0.13%	0.02%	1.00
July16 04	2.98	2.96	3.04	99.7%	0.30%	0.02%	1.00
July16 05	2.96	2.93	2.93	99.7%	0.29%	0.01%	1.00
July16 06	2.95	2.94	2.96	99.5%	0.53%	0.01%	1.00
July16 07	2.84	2.84	2.9	99.4%	0.61%	0.01%	1.00
July16 08	2.77	2.74	2.89	98.6%	1.40%	0.01%	1.01

Table 3.5 cont.: Whiteface Mountain oxidation breakdown

Sample	pH CASCC2	PH Small	pH Large	% Peroxide	% Metals	% Ozone	Enhancement Factor
July17 01	3.01	3.02	2.97	n/a	n/a	n/a	n/a
July17 02	3.05	3.06	3	99.7%	0.29%	0.02%	1.00
July17 03	3.09	3.1	3.06	99.7%	0.23%	0.02%	1.00
July17 04		3.18	3.16	99.8%	0.15%	0.03%	1.00
July17 05	3.17	3.19	3.13	99.9%	0.07%	0.02%	1.00
July17 06	3.18	3.17	3.16	99.9%	0.08%	0.02%	1.00
July17 07	3.16	3.15	3.13	99.9%	0.08%	0.03%	1.00
July17 08		3.27	3.21	99.9%	0.05%	0.05%	1.00
July17 09	3.27	3.26	3.25	99.9%	0.03%	0.05%	1.00
July17 10	3.32	3.29	3.29	99.9%	0.03%	0.04%	1.00
July20 01	3.61	3.59	3.58	99.7%	0.14%	0.19%	1.00
July20 02	3.5	3.5	3.51	99.8%	0.05%	0.12%	1.00
July20 03	3.37	3.36	3.33	99.9%	0.03%	0.06%	1.00
July20 04	3.36	3.3	3.34	99.9%	0.04%	0.05%	1.00
July20 05	3.16	3.17	3.17	100%	0.02%	0.02%	1.00
July20 06	3.1	3.09	3.07	100%	0.02%	0.02%	1.00
July20 07	3.05	3.04	3.04	100%	0.03%	0.02%	1.00
July20 08	2.96	2.98	2.994	99.7%	0.25%	0.09%	1.00
July22 01	3.32	3.41	3.41	99.3%	0.68%	0.02%	1.00
July22 02	3.48	3.39	3.48	98.4%	1.58%	0.03%	1.01
July22 03	3.68	3.6	3.63	99.3%	0.66%	0.06%	1.00
July22 04	3.78	3.77	3.76	99.4%	0.52%	0.13%	1.00

each sample period the enhancement factor can then be found by dividing the average rate by the "bulk" rate.

This number is useful in determining if drop heterogeneity enhances or suppresses aqueous sulfate production across the drop size spectrum. Factors greater than one indicate that the rate of sulfate production was found to be greater, or enhanced, by the drop heterogeneity. A factor of less than one, which is rare but can occur for the catalyzed autooxidation pathway, indicates that the drop heterogeneity reduces the rate of

sulfate production. An enhancement factor of one indicates that there is no difference between the size resolved and bulk rates under the sample conditions.

The results from Whiteface Mountain show enhancement factors of one for all samples. This is a typical result for regions where the oxidation of S(IV) is dominated by the hydrogen peroxide pathway. Even the ratio of large to small drop S(IV) oxidation rates are close to one, indicating that there is little difference in the rates for the two size fractions. Therefore Whiteface Mountain works well as a control site for this study in that sulfate production is not predicted to be a function of drop size.

3.2.2 Davis Predicted S(IV) Oxidation

The environment at Davis is very different from that of Whiteface Mountain. The fogs sampled in California tended to be more alkaline and showed much greater chemical heterogeneity with respect to drop size. These two factors tend to promote oxidation enhancement factors greater than one and sulfate production dominated by the ozone oxidation pathway.

Trace gas measurements of SO_2, O_3 and H_2O_2 were also made in Davis. The average in-fog concentrations were: $SO_2 = 0.37$ ppbv, $O_3 = 4.42$ ppbv and $H_2O_2 = 0.23$ ppbv. The lower ozone concentration indicates that it is being consumed by a chemical reaction. San Joaquin Valley ozone is frequently low during winter stagnation episodes, especially at night, due to low photochemical activity and chemical destruction by reaction with NO. The trace gas histograms (Figure 3.14) also indicate that ozone is present in lower gas phase concentrations than at Whiteface.

Results from the oxidation rate calculations for the Davis samples suggest that aqueous sulfate production in this area is dominated by the ozone oxidation pathway. Table 3.6 gives a breakdown of the oxidation calculation results for each sample. Note that for the first two events S(IV) oxidation via the hydrogen peroxide pathway plays a significant role in the overall oxidation rate. This is particularly true for the smaller drops, which tend to have lower pH values, favoring oxidation via the peroxide pathway.

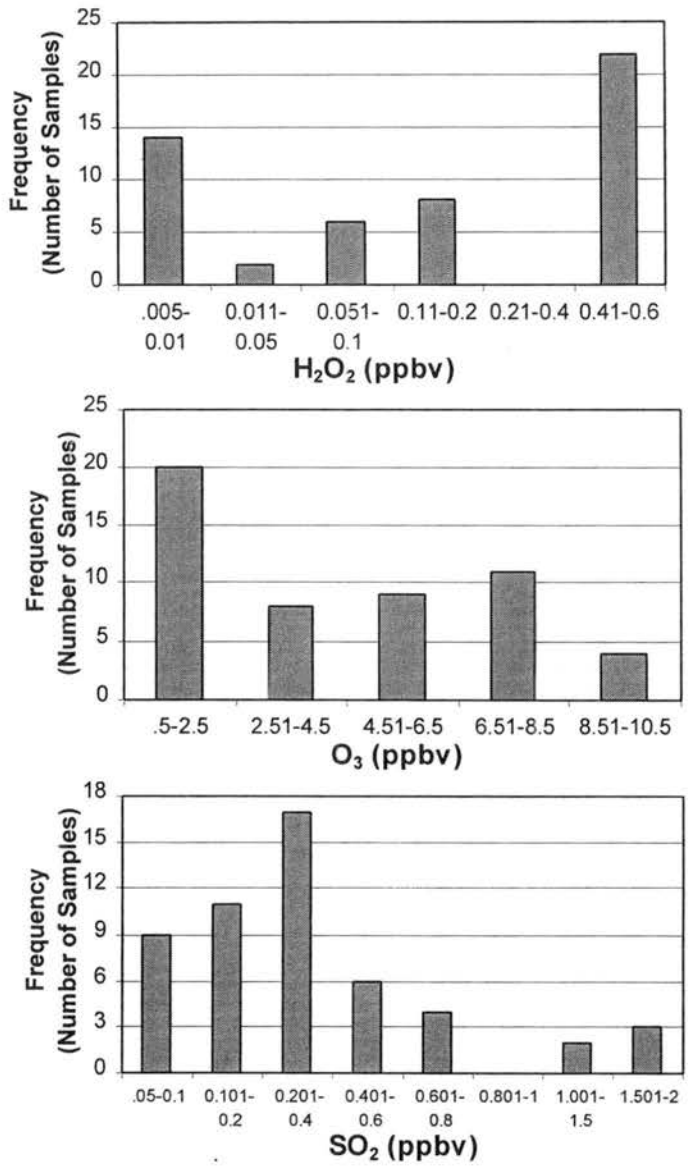

Figure 3.14 Davis trace gas histograms: H_2O_2, O_3, and SO_2.

The remainder of the samples, however, shows the dominance of the ozone oxidation pathway. Figure 3.15 shows the percentage of time that each of the different oxidation pathways was predicted to be dominant for samples from each collector. The first set of plots is for the December 18th event, and it clearly shows the important role played by the hydrogen peroxide oxidation pathway for that event, especially for the small drop fraction. The second set of plots show the percentage of time each pathway was dominant throughout the entire field project. These plots suggest that ozone is indeed the most dominant oxidation pathway for the Davis fogs. For the entire Davis campaign, the ozone oxidation pathway is calculated to be responsible for about 82% of the total aqueous S(IV) oxidation.

Also of note is the strong drop size dependence of these predicted rates. To quantify the difference between the oxidation rates for the large and small drop fractions the ratio of the two is used. For the Davis samples the ratio of large to small drop oxidation rates is almost always greater than one and can be as large as 47. This indicates that the S(IV) oxidation reaction is predicted to occur at a much greater rate in the larger drops than in the smaller ones. Upon examination of the ozone oxidation pathway rate laws it is apparent that the larger drops have faster rates due to the higher pH values of the large drop fraction samples.

The enhancement factor also reflects this effect of drop size related chemical heterogeneity. Figure 3.16 shows plots of both the enhancement factors for each sample time throughout the campaign as well as a frequency distribution of the enhancement factors. There is a peak between enhancement factor values of one and 1.2. The plot

Table 3.6: Davis oxidation breakdown

Sample	pH CASCC2	pH Small	pH Large	% Peroxide	% Metals	% Ozone	Enhancement Factor
Dec18 01	5.52		6.03	n/a	n/a	n/a	n/a
Dec18 02	5.9	5.68	6.08	66.80%	0.82%	32.38%	1.09
Dec18 03	5.78	5.6	5.9	76.20%	n/a	23.80%	1.07
Dec18 04	5.9	5.47	6.08	82.32%	n/a	17.68%	1.29
Dec18 05	6.18	5.88	6.34	57.89%	n/a	42.11%	1.21
Dec18 06	6.26	5.8	6.38	36.34%	n/a	63.66%	1.38
Dec18 07	6.48	6.31	6.56	19.56%	n/a	80.44%	1.08
Dec18 08	6.4	6.39	6.68	11.45%	n/a	88.55%	1.10
Dec18 09	6.42	6.36	6.69	7.59%	n/a	92.41%	1.20
Jan04 01	6.45		6.55	n/a	n/a	n/a	1.00
Jan04 02	6.4	6.45	6.05	64.02%	0.25%	35.72%	1.12
Jan04 03	6.63	6.31	6.66	4.33%	0.02%	95.65%	1.13
Jan04 04	6.48	6.29	6.56	9.72%	0.02%	90.26%	1.08
Jan04 05	6.5	6.11	6.45	42.02%	0.11%	57.87%	1.11
Jan04 06	6.6	6.24	6.57	29.47%	n/a	70.53%	1.08
Jan04 07	6.59	6.21	6.64	23.20%	0.08%	76.72%	1.11
Jan04 08	6.53	6.2	6.57	29.43%	0.09%	70.48%	1.08
Jan04 09	6.4	6.13	6.79	9.27%	n/a	90.73%	1.35
Jan04 10	6.32	6.15	6.37	35.32%	n/a	64.68%	1.07
Jan04 11	6.32	6.05	6.28	61.55%	n/a	38.45%	1.05
Jan04 12	6.54	6.34	6.7	19.47%	n/a	80.53%	1.18
Jan04 13	6.55	6.36	6.7	8.57%	n/a	91.43%	1.14
Jan09 01	6.7	6.48	6.7	0.10%	0.01%	99.89%	1.01
Jan09 02	6.7	6.64	6.8	0.05%	0.01%	99.94%	1.03
Jan09 03	6.66	6.41	6.66	0.08%	0.09%	99.83%	1.15
Jan09 04	6.65	6.35	6.45	0.24%	0.59%	99.17%	1.03
Jan09 05	6.59	6.23	6.82	0.05%	0.36%	99.59%	2.64
Jan09 06	6.57	6.26	6.78	0.03%	0.33%	99.64%	1.34
Jan09 07	6.75	6.1	6.82	0.02%	0.23%	99.75%	1.26
Jan09 08	6.68	6.05	6.89	0.01%	n/a	99.99%	1.53
Jan10 01	6.51	6.27	6.59	0.09%	0.39%	99.53%	1.13
Jan10 02	6.55	5.94	6.61	0.06%	0.19%	99.75%	1.08
Jan10 03	6.5	5.93	6.55	0.07%	0.19%	99.74%	1.22
Jan10 04	5.64	5.69	5.69	3.97%	1.98%	94.05%	1.00
Jan10 05	5.94	5.59	6.27	0.24%	0.18%	99.57%	1.11
Jan10 06	5.94	5.48	6.27	0.26%	0.21%	99.53%	1.17

Table 3.6 continued: Davis oxidation breakdown

Sample	pH CASCC2	pH Small	pH Large	% Peroxide	% Metals	% Ozone	Enhancement Factor
Jan10B 01	5.98	6.05	6.07	17.29%	0.27%	82.44%	1.00
Jan10B 02	5.65	5.72	5.81	30.91%	0.25%	68.84%	1.01
Jan10B 03	5.51	5.56	5.66	42.17%	0.31%	57.52%	1.01
Jan10B 04	5.76	5.47	6.12	10.80%	0.12%	89.08%	1.60
Jan10B 05	5.84	5.78	6.04	11.84%	0.05%	88.11%	1.08
Jan10B 06	6.38	5.79	6.64	1.63%	0.01%	98.36%	2.29
Jan10B 07	6.68	6.36	6.87	0.59%	0.02%	99.39%	1.46
Jan10B 08	6.69	6.39	6.94	0.25%	0.02%	99.72%	1.62
Jan11 01	6.06	6.35	6.41	5.73%	0.18%	94.09%	1.00
Jan11 02	6.2	6.08	6.21	21.29%	0.54%	78.17%	1.02
Jan11 03	6.31	6	6.2	6.53%	0.05%	93.42%	1.03
Jan11 04	6.07	5.77	6.05	7.76%	0.13%	92.12%	1.07
Jan11 05	6.18	5.73	6.36	4.65%	0.05%	95.30%	1.35
Jan11 06	6.44	5.79	6.49	3.00%	0.18%	96.82%	1.46
Jan11 07	6.3	5.64	6.47	1.95%	0.16%	97.89%	2.30
Jan11 08	6.38	5.97	6.52	1.09%	0.17%	98.74%	1.55

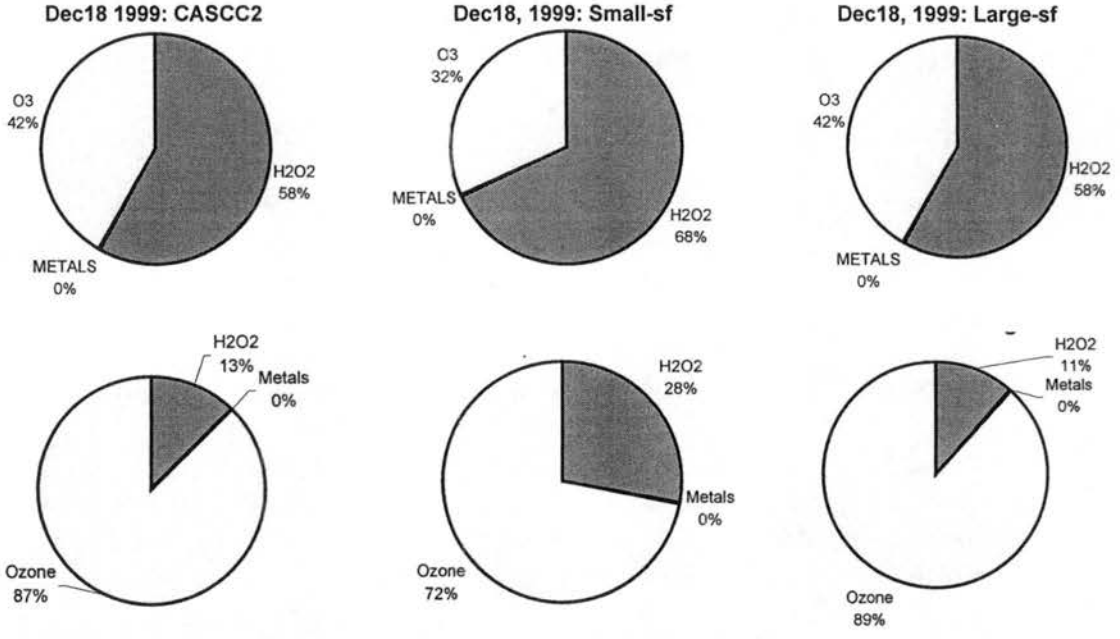

Figure 3.15: Percentage of time each oxidation pathway is dominant for the first Davis fog event (top) and for all the Davis events (bottom). Results are shown for the bulk fog composition and for the large and small fog drop fractions.

indicates that a vast majority of the samples show at least some enhancement due to the drop size-dependence of the Davis fog composition.

The results from Davis are therefore strikingly different from those observed at Whiteface Mountain. Not only was the S(IV) oxidation dominated by a completely different pathway (ozone at Davis vs. hydrogen peroxide at Whiteface), but also there was significant chemical heterogeneity seen in the two drop sizes. While there was no appreciable enhancement predicted in the Whiteface samples, nearly all the Davis samples are predicted to show at least some S(IV) oxidation enhancement resulting from the fog drop chemical heterogeneity.

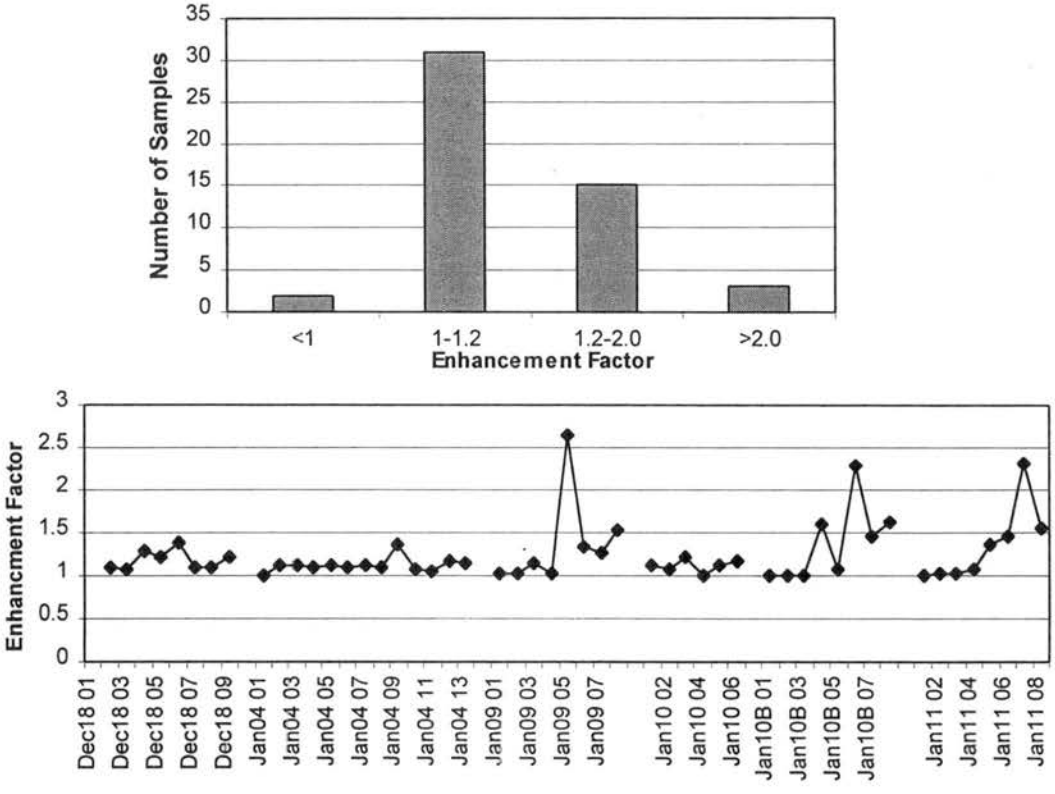

Figure 3.16: Davis enhancement factors. The first plot is a frequency plot of the enhancement factor. The second plot shows the amount of enhancement for each sample period.

3.3 Tracer Results

All results from the tracer technique have been supplied by Dr.Husain's group at SUNY Albany/NYSDOH. Using their own aerosol measurements, along with samples from the CSU cloudwater collectors, they computed the amount of sulfate produced in the cloud or fog.

Using the previously described tracer method the aerosol concentrations of selenium and sulfate were compared to those found in the cloudwater. Operating under the principle that both of these aerosols have the same scavenging coefficient, the ratio of SO_4/ Se from pre cloud air can be compared to the same ratio in the cloud or fog water to find the amount of sulfate (SO_4in) produced in the aqueous phase. These SO_4in calculations were done in the same way for both the Whiteface and Davis samples except for samples where the "lowest bulk ratio" was used in Davis. The "lowest bulk ratio", referring to the lowest ratio observed in the bulk fog samples, was used when the aerosol ratios of SO_4/ Se were larger than the fog water ratios.

3.3.1 Determined SO_4in for Whiteface Mountain

The amount of sulfate produced in-cloud was calculated for all but the first Whiteface Mountain event. The actual values of SO_4in determined by this technique are displayed in Table 3.7. Values in the table that are represented by n/a are not available due to an insufficient amount of cloud water. The table shows values for the CASCC2 as well as both the large and small fraction of the sf-CASCC, for all but the first event. For most samples these three values of SO_4in are fairly close to each other, with their relative standard deviations being less than 20% on average for each sample time.

Table 3.7: Whiteface Mountain determined SO_4in.

Sample	CASCC2	Large	Small	L/S	Sample	CASCC2	Large	Small	L/S
July7 01	16.27	20.46	11.73	1.75	July17 01	94.10	95.13	118.68	0.80
July7 02	15.83	18.07	13.31	1.36	July17 02	68.25	84.50	82.23	1.03
July7 03	16.42	16.99	15.12	1.12	July17 03	99.49	66.88	121.52	0.55
July7 04	17.81	17.82	17.22	1.04	July17 04	n/a	66.84	91.30	0.73
July7 05	22.03	18.77	22.05	0.85	July17 05	52.32	44.25	52.10	0.85
July7 06	31.30	32.87	30.87	1.06	July17 06	40.38	40.50	48.39	0.84
July7 07	22.50	23.53	27.71	0.85	July17 07	40.88	41.25	42.13	0.98
July7 08	98.11	52.36	63.01	0.83	July17 08	n/a	n/a	44.70	n/a
July7 09	51.25	66.63	61.23	1.09	July17 09	34.50	35.00	50.78	0.69
July7 10	47.86	57.06	48.91	1.17	July17 10	32.13	32.63	n/a	n/a
July7 11	68.97	65.09	66.97	0.97					
July7 12	135.49	131.09	145.74	0.90	July20 01	15.64	13.44	15.85	0.85
July7 13	137.51	140.68	143.32	0.98	July20 02	18.67	17.40	18.35	0.95
July7 14	218.72	151.71	225.06	0.67	July20 03	32.35	34.80	33.61	1.04
July7 15	213.28	294.88	246.07	1.20	July20 04	48.68	41.10	35.37	1.16
July7 16	40.53	55.01	45.17	1.22	July20 05	53.26	41.76	40.67	1.03
July7 17	n/a	51.50	48.03	1.07	July20 06	61.41	52.14	80.60	0.65
July7 18	n/a	50.70	52.23	0.97	July20 07	86.45	66.67	96.82	0.69
July7 19	n/a	n/a	252.03	0.00	July20 08	127.04	72.72	127.58	0.57
July16 01	85.76	66.64	208.69	0.32	July22 01	51.12	54.14	47.37	1.14
July16 02	106.76	74.48	168.45	0.44	July22 02	37.49	53.26	37.42	1.42
July16 03	101.13	79.33	142.36	0.56	July22 03	23.68	31.03	22.69	1.37
July16 04	84.74	61.22	120.75	0.51	July22 04	14.90	68.83	14.79	4.65
July16 05	81.14	66.95	101.86	0.66					
July16 06	142.94	81.78	144.51	0.57	**All units are μM except for the L/S ratios.**				
July16 07	175.50	82.62	310.16	0.27					

These values are plotted in Figure 3.17 for each sample time. There appears to be no specific trend in the sulfate produced in the clouds. Three of the events (July 7, July 16, July20) show the amount of sulfate produced increasing throughout the event, while the other two (July 17, July 22) show the amount decreasing. This plot also shows the ratio of the amount of sulfate produced in the large drop fraction to the amount produced in the small drop fraction. This ratio has some obvious scatter, but is for the most part centered near one.

SUNY investigators report that the uncertainty in the SO_4in values depends on the fraction of cloud water SO_4^{2-} contributed by SO_4^{2-}in (SO_4in %). The uncertainty is expressed by the power law function

$$Relative\ Error = 2902.7(SO_4in\%)^{-1.2735} \qquad (3.15)$$

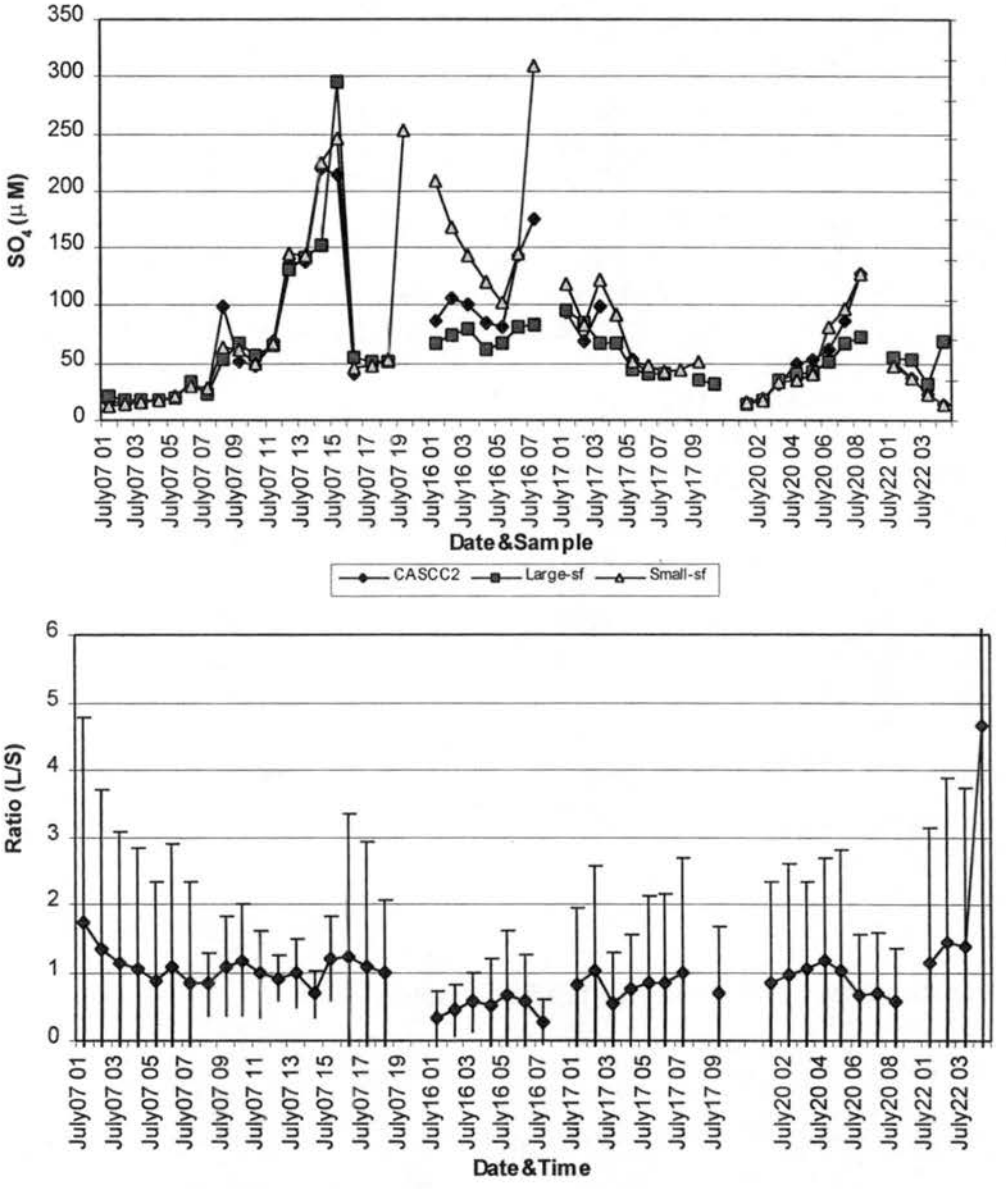

Figure 3.17: Whiteface Mountain SO_4in plots. The first plot shows the determined amount of sulfate produced in the cloud for the CASCC2 and both fractions of the sf-CASCC for each sample period. The second plot shows the ratio of large to small drop SO_4in.

Once the relative error in each measurement is obtained using equation 3.15, the error in the large to small ratios can be determined through error propagation using the following equation (Bevington and Robinson, 1992)

$$\sigma_{Ratio} = \left[Ratio^2 * \left(\frac{\sigma^2_{\text{Large}SO4in}}{(\text{Large}SO4in)^2} + \frac{\sigma^2_{\text{Small}SO4in}}{(\text{Small}SO4in)^2} \right) \right]^{\frac{1}{2}} \qquad (3.16)$$

The values obtained from this error analysis were used to create the error bars for the tracer ratios in the second plot from Figure 3.17.

The power law relationship from Equation 3.15 indicates that the smaller the percent of SO_4in, the larger the error. In fact for values of 30% or less, the error in the SO_4in determination sharply increases from about 40%. Table 3.8 shows the percentage of SO_4in for each collector or size fraction, as well as the computed uncertainty for the SO_4in measurement. The final columns of the table show the ratio of large to small size fraction SO_4in, and the uncertainty in that value. Note that in many cases the SO_4in percentages are below 20%, creating a large uncertainty in the estimates.

3.3.2 Determined SO_4in for Davis

Tracer data for the Davis field campaign are available for the fog events are those starting on of December 18th, January 4th and the first event of January 10th. For the remaining events the ratio of SO_4/Se was smaller in the size fractioned CASCC samples than in the pre-fog aerosol samples. This seems to indicate that sulfate was actually being destroyed in the fog, which is not the case. The reason for this larger pre fog aerosol ratio may have to do with the timing of the aerosol samples. Air masses present

Table 3.8: Whiteface Mountain SO_4in percentages and uncertainties.

	SO4in Percent			Percent Error in SO4in			Ratio and Uncertainty	
Sample	CASCC2	Small-sf	Large-sf	CASCC2	Small-sf	Large-sf	Ratio (L/S)	Uncertainty
July07 01	12.0	12.0	12.0	122.6	122.6	122.6	1.75	173%
July07 02	12.0	12.0	12.0	122.6	122.6	122.6	1.36	173%
July07 03	12.0	12.0	12.0	122.6	122.6	122.6	1.12	173%
July07 04	12.0	12.0	12.0	122.6	122.6	122.6	1.04	173%
July07 05	12.0	12.0	12.0	122.6	122.6	122.6	0.85	173%
July07 06	12.0	12.0	12.0	122.6	122.6	122.6	1.06	173%
July07 07	12.0	12.0	12.0	122.6	122.6	122.6	0.85	173%
July07 08	48.0	29.2	29.0	39.8	39.5	39.8	0.83	56%
July07 09	21.2	25.1	26.0	45.8	47.8	45.8	1.09	66%
July07 10	22.4	23.9	24.8	48.5	50.9	48.5	1.17	70%
July07 11	26.3	26.3	25.6	46.7	45.2	46.7	0.97	65%
July07 12	32.4	36.0	44.3	23.2	30.2	23.2	0.90	38%
July07 13	31.8	28.1	34.7	31.7	41.5	31.7	0.98	52%
July07 14	26.2	28.1	40.1	26.3	41.5	26.3	0.67	49%
July07 15	24.8	28.2	35.0	31.4	41.3	31.4	1.20	52%
July07 16	12.0	12.0	12.0	122.6	122.6	122.6	1.22	173%
July07 17		12.0	12.0	122.6	122.6	122.6	1.07	173%
July07 18		18.8	15.3	89.9	69.2	89.9	0.97	113%
July07 19		44.3			23.2			
July16 01	16.9	29.1	12.3	118.6	39.7	118.6	0.32	125%
July16 02	22.2	29.6	17.9	73.6	38.9	73.6	0.44	83%
July16 03	22.7	28.4	19.2	67.4	41.0	67.4	0.56	79%
July16 04	14.7	20.0	12.0	122.6	64.0	122.6	0.51	138%
July16 05	14.0	16.9	12.0	122.6	79.1	122.6	0.66	146%
July16 06	22.3	23.4	13.1	109.6	52.4	109.6	0.57	121%
July16 07	19.8	33.2	12.0	122.6	33.6	122.6	0.27	127%
July17 01	13.7	18.4	12.0	122.6	71.2	122.6	0.80	142%
July17 02	12.0	15.6	12.0	122.6	88.0	122.6	1.03	151%
July17 03	18.9	24.5	12.0	122.6	49.5	122.6	0.55	132%
July17 04		20.7	15.0	92.6	61.1	92.6	0.73	111%
July17 05	15.0	16.1	12.0	122.6	84.1	122.6	0.85	149%
July17 06	12.0	14.4	12.0	122.6	97.3	122.6	0.84	157%
July17 07	12.0	12.0	12.0	122.6	122.6	122.6	0.98	173%
July17 08		18.0			73.0			
July17 09	12.0	17.9	12.0	122.6	73.6	122.6	0.69	143%
July17 10	12.0		12.0	122.6		122.6		
July20 01	12.0	12.0	12.0	122.6	122.6	122.6	0.85	173%
July20 02	12.0	12.0	12.0	122.6	122.6	122.6	0.95	173%
July20 03	15.5	15.5	15.6	88.1	88.5	88.1	1.04	125%
July20 04	19.5	13.4	17.4	76.2	106.6	76.2	1.16	131%
July20 05	13.9	12.0	12.0	122.6	122.6	122.6	1.03	173%
July20 06	13.9	18.7	12.0	122.6	69.9	122.6	0.65	141%
July20 07	16.6	19.1	12.8	112.4	67.9	112.4	0.69	131%
July20 08	18.9	20.2	12.1	121.4	63.0	121.4	0.57	137%

Table 3.8 cont.: Whiteface Mountain SO_4in percentages and uncertainties.

	SO4in Percent			Percent Error in SO4in			Ratio and Uncertainty	
Sample	CASCC2	Small-sf	Large-sf	CASCC2	Small-sf	Large-sf	Ratio (L/S)	Uncertainty
July22 01	12.0	12.0	12.0	122.6	122.6	122.6	1.14	173%
July22 02	12.0	12.0	12.0	122.6	122.6	122.6	1.42	173%
July22 03	12.0	12.0	12.0	122.6	122.6	122.6	1.37	173%
July22 04	12.0	12.0	45.9	22.2	122.6	22.2	4.65	125%

long before the fog starts may not be the same air mass present when the fog is formed, so if the aerosol samples are started too long before the fog is formed irrelevant data may be collected. Calculations for these events can be done using the lowest bulk ratio of SO_4/Se from the CASCC2 in place of the pre-fog ratio, but this method is somewhat questionable. Therefore the tracer results from the January 9th, the second event on the 10th and the event on the 11th are likely to be less accurate than the tracer results from the other three events.

The tracer results for the Davis fog events are shown in Table 3.9. Again values are not available for all samples due to an insufficient amount of fog water collected. This is a problem particularly in the small fraction of the sf-CASCC due to the fact that the fog drop distribution heavily favored larger drops for many events. The data are also plotted in Figure 3.18. As with the Whiteface data, it is difficult to see any notable trends from the plot. The December event and first January event results suggest that the amount of sulfate produced in the fog increases throughout the event. The January 10th event, however, shows an increase in in-fog sulfate production followed by a sharp decrease as the event progresses.

The ratio of the amount of in-fog sulfate produced in the large fraction to the amount produced in the small fraction is also shown in both the table and the second plot

Table 3.9: Davis determined SO_4in.

Sample	CASCC	Large	Small	L/S	Sample	CASCC	Large	Small	L/S
Dec18 01	n/a	17.3	n/a	n/a	Jan10 01	47.7	26.2	60.3	0.43
Dec18 02	3.5	3.7	12.7	0.29	Jan10 02	38.7	17.8	n/a	n/a
Dec18 03	1.5	1.7	8.7	0.20	Jan10 03	49.9	21.7	275.9	0.08
Dec18 04	1.1	0.6	11.4	0.06	Jan10 04	91.5	25.5	n/a	n/a
Dec18 05	1.5	0.9	8.0	0.11	Jan10 05	39.0	16.7	n/a	n/a
Dec18 06	1.6	1.2	7.1	0.17	Jan10 06	25.0	10.8	n/a	n/a
Dec18 07	7.2	8.2	6.1	1.34					
Dec18 08	16.6	14.6	10.9	1.34	Jan10B 01	11.8	6.8	n/a	n/a
Dec18 09	n/a	27.9	38.5	0.72	Jan10B 02	10.7	5.9	24.6	0.24
					Jan10B 03	4.6	2.6	37.2	0.07
Jan04 01	1.8	1.1	n/a	n/a	Jan10B 04	5.0	3.9	29.7	0.13
Jan04 02	2.0	1.3	12.9	0.10	Jan10B 05	4.0	5.3	16.8	0.32
Jan04 03	1.9	1.2	9.9	0.12	Jan10B 06	4.5	4.4	14.1	0.31
Jan04 04	2.2	1.3	9.2	0.14	Jan10B 07	3.6	3.1	12.4	0.25
Jan04 05	4.7	2.7	8.3	0.33	Jan10B 08	11.1	5.9	17.0	0.35
Jan04 06	5.1	2.7	8.6	0.32					
Jan04 07	4.4	1.5	19.9	0.08	Jan11 01	9.0	5.2	13.3	0.39
Jan04 08	6.3	4.4	23.9	0.18	Jan11 02	15.6	8.8	35.1	0.25
Jan04 09	7.1	5.3	35.2	0.15	Jan11 03	12.0	6.9	48.3	0.14
Jan04 10	8.1	5.9	31.5	0.19	Jan11 04	4.0	3.1	44.5	0.07
Jan04 11	7.2	5.4	23.1	0.24	Jan11 05	2.2	1.0	25.3	0.04
Jan04 12	7.5	6.0	30.7	0.19	Jan11 06	2.9	2.6	30.6	0.08
Jan04 13	9.6	6.1	26.9	0.23	Jan11 07	8.0	5.6	21.9	0.26
					Jan11 08	14.7	11.1	37.4	0.30
Jan09 01	5.1	2.9	8.7	0.34					
Jan09 02	10.4	6.6	19.5	0.34					
Jan09 03	16.7	9.3	31.8	0.29					
Jan09 04	26.6	20.6	58.4	0.35					
Jan09 05	30.7	24.5	56.4	0.43	**Units are in μM except for L/S ratios.**				
Jan09 06	40.4	29.8	535.0	0.06					
Jan09 07	35.1	32.6	n/a	n/a					
Jan09 08	52.6	20.7		n/a					

in Figure 3.18. This ratio rarely achieves values greater than one and for the most part is well below one. Therefore the tracer results from Davis indicate that more in-fog sulfate is produced in the small drop fraction than in the large drop fraction for the majority of samples.

The error bars for the tracer determined SO_4in values were calculated in the same manner as those for the Whiteface results. The uncertainties for the large to small SO_4in ratios are sometimes smaller for the Davis results. This is due to an increased percentage of aqueous sulfate being produced in the fog. These data are shown in Table 3.10.

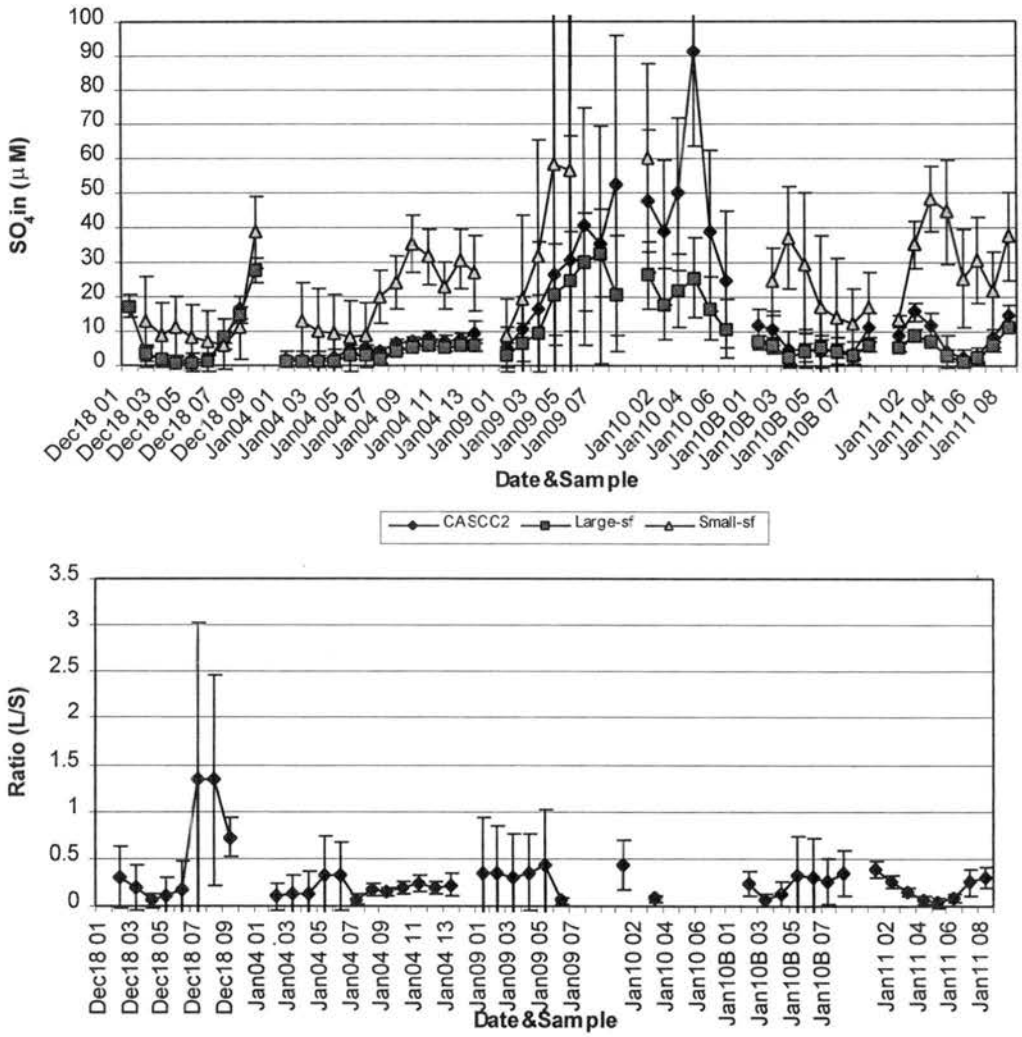

Figure 3.18: Davis SO_4in plots. The first plot shows the amount of SO_4in calculated for the CASCC2 and both fractions of the sf-CASCC for the Davis events, error bars are included. SO_4in for two small-sf samples are outliers, see Table 3.9. The second plot is of the ratio of SO_4in for the large and small drop fractions of the sf-CASCC. Note some of the uncertainties in the second plot are contained within the size of the data points.

Table 3.10: Davis SO_4in percentages and uncertainties.

	SO4in Percent			Percent Error in SO4in			Ratio and Uncertainty	
Sample	CASCC2	Small-sf	Large-sf	CASCC2	Small-sf	Large-sf	Ratio (L/S)	Uncertainty
Dec18 01			54.78			17.73		
Dec18 02	18.43	13.68	29.81	70.99	103.74	38.48	0.29	111%
Dec18 03	12.50	13.38	21.20	116.38	106.75	59.38	0.20	122%
Dec18 04	12.50	17.96	12.00	116.38	73.34	122.59	0.06	143%
Dec18 05	12.50	12.00	12.00	116.38	122.59	122.59	0.11	173%
Dec18 06	12.50	12.00	12.78	116.38	122.59	113.14	0.17	167%
Dec18 07	35.38	12.00	46.92	30.94	122.59	21.59	1.34	124%
Dec18 08	49.80	16.39	59.05	20.02	82.45	16.11	1.34	84%
Dec18 09		40.39	71.62		26.14	12.60	0.72	29%
Jan04 01	12.50		12.00	116.38		122.59		
Jan04 02	12.50	15.45	14.03	116.38	88.86	100.50	0.10	134%
Jan04 03	12.50	12.00	12.00	116.38	122.59	122.59	0.12	173%
Jan04 04	12.50	12.00	12.00	116.38	122.59	122.59	0.14	173%
Jan04 05	36.08	12.00	36.98	30.17	122.59	29.24	0.33	126%
Jan04 06	55.92	13.18	45.57	17.27	108.83	22.41	0.32	111%
Jan04 07	47.77	29.63	25.83	21.11	38.77	46.18	0.08	60%
Jan04 08	55.15	34.30	61.06	17.58	32.18	15.44	0.18	36%
Jan04 09	51.40	43.52	56.04	19.22	23.76	17.22	0.15	29%
Jan04 10	44.37	42.05	45.52	23.19	24.83	22.45	0.19	33%
Jan04 11	43.97	37.65	46.32	23.45	28.58	21.95	0.24	36%
Jan04 12	40.64	38.81	48.75	25.93	27.50	20.57	0.19	34%
Jan04 13	34.26	28.42	37.81	32.23	40.89	28.42	0.23	50%
Jan09 01	12.50	12.00	12.00	116.38	122.59	122.59	0.34	173%
Jan09 02	15.32	12.00	16.04	89.83	122.59	84.70	0.34	149%
Jan09 03	12.50	13.51	12.00	116.38	105.37	122.59	0.29	162%
Jan09 04	12.50	15.97	18.17	116.38	85.19	72.29	0.35	112%
Jan09 05	12.50	12.00	21.56	116.38	122.59	58.11	0.43	136%
Jan09 06	15.91	88.03	25.50	85.61	9.69	46.93	0.06	48%
Jan09 07	14.30		29.85	98.02		38.24		
Jan09 08	16.34		16.59	82.75		81.14		
Jan10 01	27.09	26.03	31.33	43.47	45.72	36.11	0.43	58%
Jan10 02	22.86		21.83	53.96		57.23		
Jan10 03	26.74	67.49	24.61	44.20	13.59	49.12	0.08	51%
Jan10 04	35.82		26.61	30.45		44.45		
Jan10 05	21.17		22.36	59.49		55.49		
Jan10 06	16.83		16.99	79.72		78.72		
Jan10B 01	29.42		34.71	39.13		31.69		
Jan10B 02	25.96	29.20	30.82	45.88	39.51	36.88	0.24	54%
Jan10B 03	12.50	28.99	16.23	116.38	39.87	83.44	0.07	92%
Jan10B 04	12.50	18.80	19.42	116.38	69.20	66.42	0.13	96%
Jan10B 05	12.50	12.00	28.53	116.38	122.59	40.68	0.32	129%
Jan10B 06	16.16	12.00	27.87	83.93	122.59	41.92	0.31	130%

Table 3.10 continued: Davis SO_4in percentages and uncertainties.

	SO4in Percent			Percent Error in SO4in			Ratio and Uncertainty	
Sample	CASCC2	Small-sf	Large-sf	CASCC2	Small-sf	Large-sf	Ratio (L/S)	Uncertainty
Jan10B 07	15.80	16.78	25.10	86.38	79.99	47.89	0.25	93%
Jan10B 08	30.87	21.03	32.44	36.81	60.02	34.55	0.35	69%
Jan11 01	46.93	75.04	51.19	21.59	11.87	19.33	0.39	23%
Jan11 02	54.01	51.96	56.62	18.05	18.96	17.00	0.25	25%
Jan11 03	37.47	51.36	45.97	28.75	19.25	22.16	0.14	29%
Jan11 04	12.50	33.12	22.03	116.38	33.65	56.56	0.07	66%
Jan11 05	12.50	22.29	12.00	116.38	55.72	122.59	0.04	135%
Jan11 06	15.80	28.40	26.89	86.35	40.93	43.87	0.08	60%
Jan11 07	33.87	24.03	44.49	32.70	50.63	23.11	0.26	56%
Jan11 08	47.35	32.99	71.88	21.35	33.82	12.54	0.30	36%

3.4 Comparison of Tracer Results with Predicted Rates

The S(IV) oxidation results predicted using aqueous phase chemistry are reported in the form of oxidation rates, in units of **M**/s. The results from the tracer portion of the study are determined as the amount of sulfate produced in the cloud or fog, with units **μM**. In order to convert the predicted rates to the predictions of the amount of sulfate produced, a great deal more would need to be known about the history of the sampled fog/cloud drops. The ratios of the predicted rates in the large and small drops can, however, be compared with the ratios of the sulfate produced in these drop size fractions as determined using the tracer technique. Although it is unreasonable to expect quantitative agreement between these ratios, qualitative agreement is expected if there is an accurate understanding of the process determining aqueous sulfate production.

3.4.1 Whiteface Mountain Ratio Comparison

Both the predicted rates and the tracer determined in-cloud sulfate show similar trends for the events at Whiteface Mountain. As shown in the previous sections the

homogeneous nature of the cloud chemistry, even for different drop sizes, yields similar results for the samples obtained from the CASCC2, and both fractions of the sf-CASCC for the two methods. This homogeneity is reflected in the predicted and tracer-determined oxidation ratios.

The results from Whiteface show relatively good agreement between the two methods (Figure 3.19). The ratios both hover near one, with more spread occurring for the tracer determined values. The error bars reflect the uncertainty in the tracer ratios. The predicted rate ratios are almost always within the error of the tracer ratios.

The agreement is not always good however; at times the determined ratios can be as much as 185% different from the predicted ratio. This difference between the two occurs most severely during the July 16th event, where the predicted ratio remains close to one as the tracer determined ratio drops to about 0.35. For this event even the error in the tracer-determined rates is not enough to cover the difference for some samples. On the whole however, the results match well.

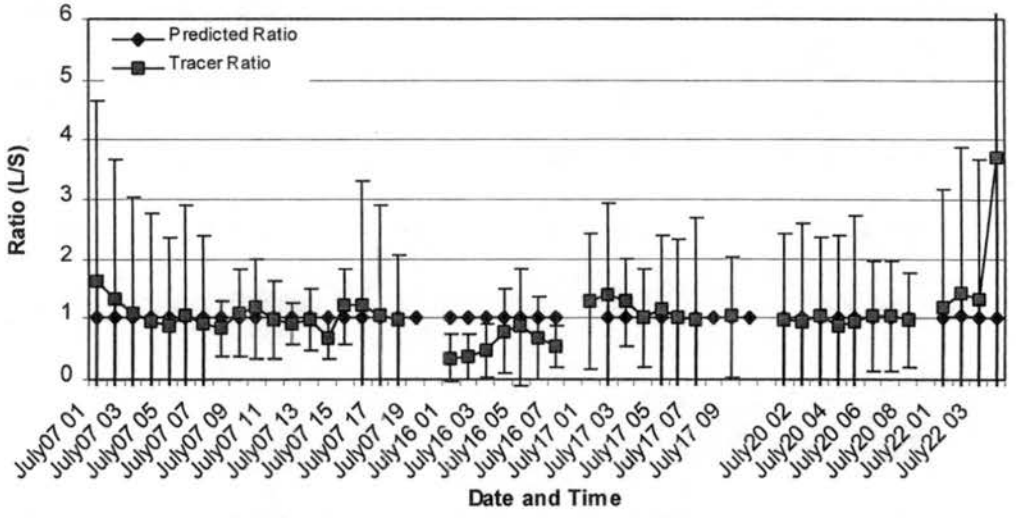

Figure 3.19: Whiteface Mountain ratio comparison. Both the ratios for the predicted oxidation rates and the determined sulfate production are plotted. The error bars are associated with the tracer-determined results.

3.4.2 Davis Ratio Comparison

The predicted rates for the Davis events all suggest more sulfate should be produced in the larger drops than in the smaller drops. From the tracer determined method an opposite trend is observed. These results indicate that more sulfate is produced in the smaller drops with many samples having ratios of less than 0.35.

There is obviously a large difference in these results. Figure 3.20 shows the ratios for both methods plotted on a log scale. The error analysis values for the tracer ratios are also incorporated into the plot. The tracer ratio is dramatically different from the predicted rate ratio, as seen in the plot. The error bars are smaller for the Davis ratios than for the Whiteface ratios and do not come close to most of the predicted rate ratios. At times the ratios even show opposite trends. The causes of this discrepancy require further investigation.

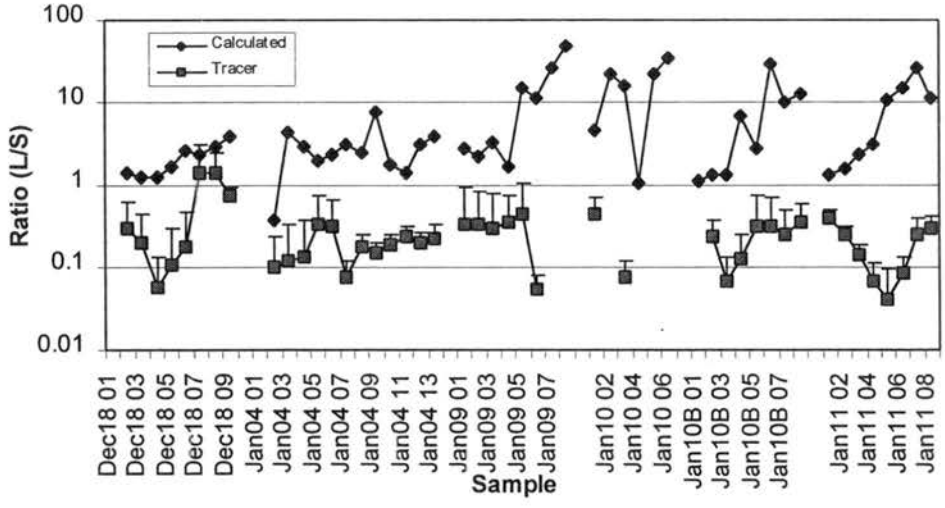

Figure 3.20: Davis ratio comparison. The ratios of the S(IV) oxidation rates are plotted along with the ratios from the tracer study for the Davis events. Error bars are only shown in the positive direction to avoid negative values on the log plot.

3.4.2.1 Analysis of the Difference in the Davis Results

The differences between the ratios could stem from either imperfections in the tracer study assumptions or incorrect assumptions in the oxidation rate calculations. The tracer calculations are based on the assumption that both selenium and sulfate are scavenged in the same way for all particle sizes. The simplified rate calculations have neglected possible effects of finite rates of mass transport and competing reactions.

3.4.2.1.1 Differential Scavenging

The aerosols sampled for the tracer portion of the study were collected by high volume bulk samplers. The aerosol ratios of SO_4/Se are then compared to the fog water ratios. The fog water is collected in two size fractions by the sf-CASCC. The different drop size can arise from not only differential growth of drops, but also the formation of different size drops on different size particles that act as cloud condensation nuclei (CCN). Variability in the ratio of SO_4/Se for different size ranges of aerosol particles, therefore, might give rise to variations in the SO_4/Se ratio the across the fog drop size spectrum.

A difference in the aerosol ratio could explain the discrepancy seen in the results from the comparison of the two different methods above, especially if there is more selenium present in larger particles. Using the bulk aerosol ratio would then cause an underprediction of the amount of sulfate produced in the larger fog drops since larger particles are expected to act as CCN for the larger drops collected by the sf-CASCC. This would produce an artificially small SO_4/Se fog water ratio for the large drops when

compared to that bulk aerosol ratio. Thereby it would artificially appear as though less sulfate is being produced in the larger fog drops and more in the small drops.

For selenium to be preferentially present in the larger, coarse particle mode, it would likely come from a crustal or soil source. It is estimated that between one half and two-thirds of the selenium emitted into the atmosphere worldwide is produced through natural processes (Mosher and Duce, 1987). The anthropogenic portion of selenium emissions is predominantly from combustion. In either case it is usually released as a gas and rapidly converted into secondary particles. This indicates that most selenium should be present, for the most part, in the Aitken and possibly the accumulation modes.

While much of the atmospheric selenium is derived from marine sources, a possible continental natural selenium source is soil. This is however thought to be smallest of the continental sources (Cahill and Eldred, 1998). A previous study done in the eastern portion of the San Joaquin valley indicated that soil is not a significant source of particulate selenium in areas other than those with highly enriched soil.

The size distribution of selenium can be investigated using additional size resolved aerosol data collected at Davis. For portions of the Davis field campaign an eight stage aerosol impactor was run. The sampler is the Micro Orifice Uniform Deposition Impactor (MOUDI) and it was run both before and after some Davis fog events. The data from the MOUDI was not intended to be used in this study and therefore the bulk aerosol sampler and the MOUDI did not have synchronized runtimes. Several of the MOUDI runs however did coincide with the sample times for the bulk aerosol collector, enough so that both were indeed sampling the same air mass. The data for these times are therefore comparable.

Again because the MOUDI filters were not intended to be used for the purpose of creating SO_4/Se ratios the following data should be viewed cautiously. The Zylon PTFE membrane filters (Gelman) were removed from the MOUDI within an hour after sampling and then frozen. The filters were later extracted in the lab at CSU with ethanol and deionized water for ion chromatograph analysis. The sulfate data were obtained from this analysis. Sulfate concentrations were rather low and therefore a large uncertainty is attached to these measurements. The sample acidification and subsequent metals analysis (Se) were done several months later at SUNY. Metals were not preserved in the sample over the storage time, so this measurement has a larger amount of uncertainty associated with it.

This indicates that the MOUDI data should not be taken as quantitative proof of anything, but the results may suggest relationships between the size distributions of selenium and sulfate. This comparison will indicate how well a bulk ratio of SO_4/Se represents the entire aerosol size spectrum. There were a total of five MOUDI samples taken, all but one of those occurred either immediately before or after a fog event, at similar times to when the high volume bulk aerosol collectors were sampling.

Examination of the results of these chemical analyses shows that the size distributions for sulfate and selenium track each other extremely well. Plots of the MOUDI data are shown in Figure 3.21. The run times for the five MOUDI samples are: 1/7/99 16:02 to 1/7/99 22:55, 1/8/99 16:00 to 1/9/99 02:30, 1/9/99 11:10 to 1/10/99 02:21,1/10/99 10:33 to 1/10/99 22:28, and 1/11/99 10:00 to 1/11/99 19:12. The event on January 9th and both of the January 10th events occurred between the last 4 sets of filter samples. The plots show the percentage of the total amount of SO_4^{2-} and Se on each

stage. The numbers on the x-axis indicate the 50% cut diameters for the stages. The distributions of sulfate and selenium are obviously very closely related. This indicates that differential scavenging is not likely to be the cause of the difference seen in the comparison of the predicted large to small drop oxidation ratio with the tracer determined

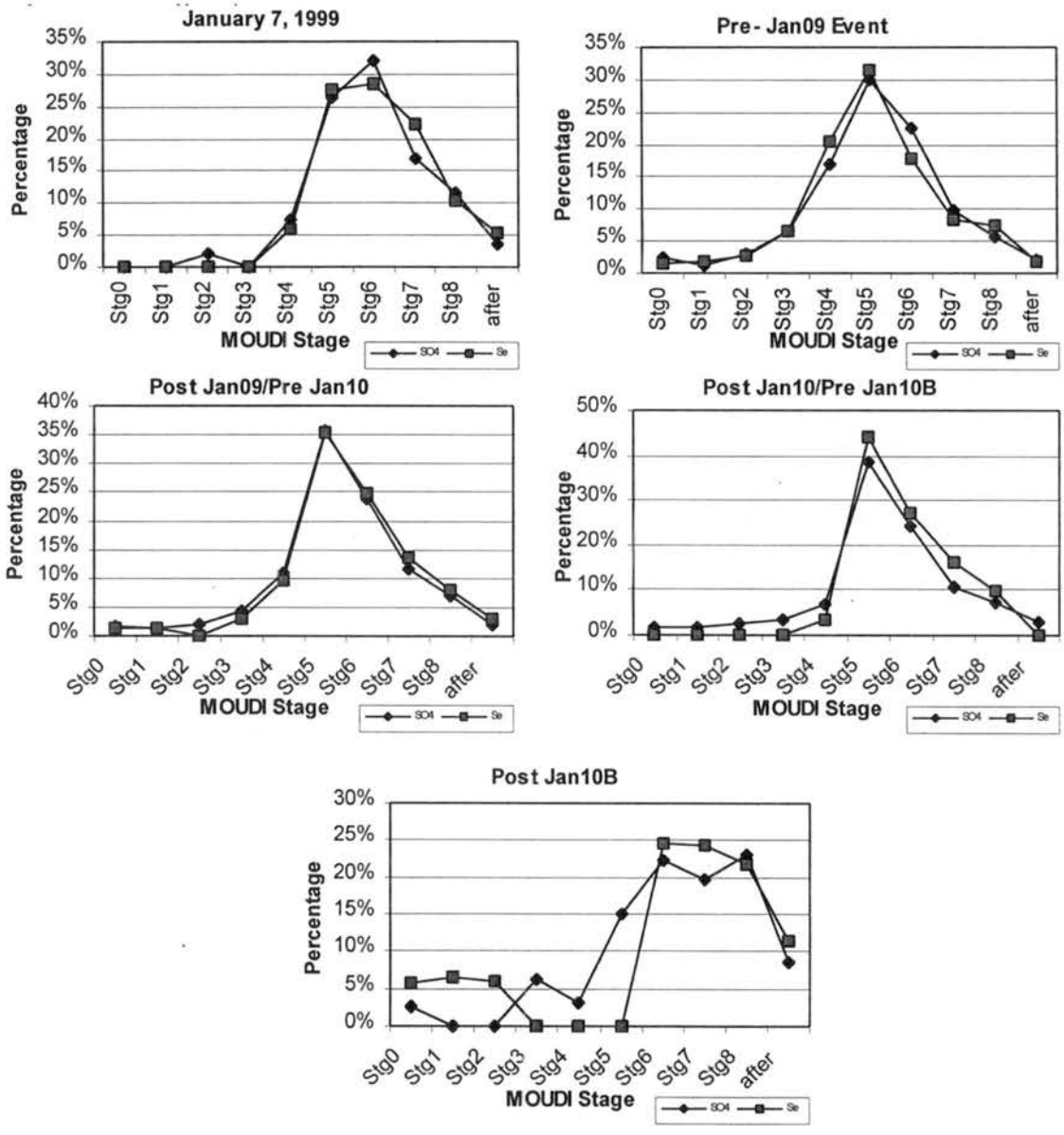

Figure 3.21: MOUDI data. These plots show the relationship of the size distributions of sulfate and selenium. The percentage of the each species in each stage is plotted. The 50% size cuts of the stages are: 20.5μm, 11.4μm, 6.4μm, 3.66μm, 2.06μm, 1.15μm, 0.65μm, 0.37μm, 0.22μm and the after filter.

3.3.2.1.2 Mass Transport Limitations

There is also the possibility that the discrepancy between the predicted ratios and the tracer determined ratios could stem from mass transport limitations for one or more reactants. These limitations may occur in the gas or aqueous phase, as well as at the drop/air interface. Under certain conditions these limitations can cause the large drop sulfate production rate to be reduced substantially from its predicted value.

The mass transport limitations become more important as the S(IV) oxidation rate inside the drop increases. The predicted ozone oxidation rates for the Davis samples are extremely fast, on the order of 10^{-6} **M**/s, while at Whiteface oxidation rates were on the order of 10^{-8} **M**/s. Larger drops also experience more severe mass transport limitations due to their decreased ratio of surface area to volume.

To investigate the role played by mass transport limitations the graphical analysis technique of Schwartz (1984,1986, 1988) was employed. This type of plot can be used to examine the possibility of all three types (gas phase, interfacial and aqueous phase) of mass transport limitations for a range of different temperatures, pH values, drop sizes and gas phase concentrations. Such a plot is shown in Figure 3.22 representing mass transport limitations for the S(IV) reaction with ozone.

This plot depicts the mass transport limitations for drops of three different diameters: 10, 20 and 30 μm. The area to the right of the vertical lines marked aqueous represents drops that will have an aqueous phase mass transport limitation to the oxidxation rate of greater than 10%. Where the y axis H (Henry's law constant) value is about 100 M/atm, these vertical lines become diagonal. This is the transition into the gas phase mass transport limitation regime. Again, the area to the right of these lines

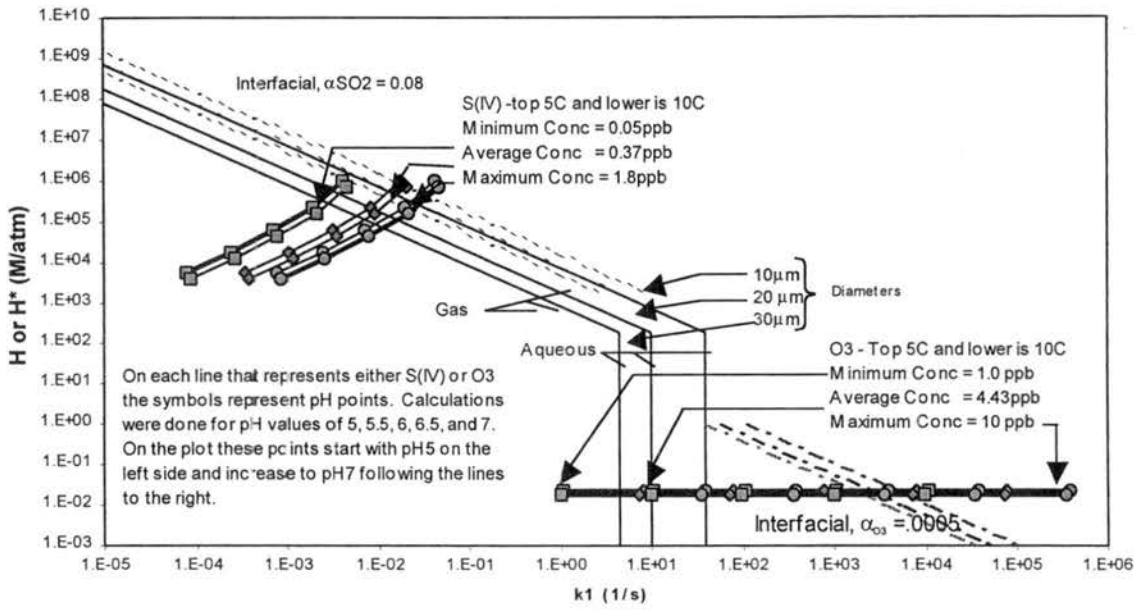

Figure 3.22: Mass transport limitations. This plot depicts the threshold values for mass transport limitations for the S(IV)-O_3 reaction.

represents drops with gas phase mass transport limitations to the oxidation rate greater than ten percent. The boundaries indicating ten percent interfacial mass transport limitations are marked by dashed lines. The lines on the bottom right of the diagram are for interfacial limitations for ozone transport, while the lines on the top left are for sulfur dioxide interfacial limitations.

These lines were calculated using inequalities expressed in Seinfeld and Pandis (1998). The aqueous phase mass transport limitation is described using

$$k_1 \leq \varepsilon \frac{\pi^2 D_{aq}}{R_p^2} \qquad (3.17)$$

Here D_{aq} is the aqueous phase diffusion coefficient, R_p is the drop radius and ε is an arbitrarily small constant. For these calculations, ε was chosen to be 0.1, representing a ten percent allowable mass transport limitation. The vertical lines seen on the plot were

obtained by setting the right and left hand sides of this equation equal to each other and solving for k_1, the first order rate constant.

Seinfeld and Pandis (1998) give the gas phase mass transport limitation relationship as

$$k_1 H_A \leq \varepsilon \frac{3D_g}{R_p^2 RT} \qquad (3.18)$$

R_p and ε are the same as in the aqueous phase calculations. D_g is the gas phase diffusion coefficient, R is the gas constant and T is temperature. Again the lines on the plot are generated by setting both sides of the equation equal to each other and solving for the left hand side.

The interfacial mass transport relationships are given by

$$k_1 H_A \leq \varepsilon \frac{3\alpha}{R_p (2\pi M_A RT)^{1/2}} \qquad (3.19)$$

The new variables α and M_A are the molecular accommodation coefficient and the molecular weight, respectively. The use of species specific accommodation coefficients and molecular weights create one set of interfacial limitation boundaries for ozone and another set for sulfur dioxide.

The lines marked with circles, squares and diamonds represent hypothetical sample values instead of the transport limitation thresholds. Calculations made using the minimum gas phase concentrations of sulfur dioxide and ozone found during the Davis events are denoted with squares. These concentrations did not occur during the same sample but are plotted together to show the most extreme case possible for the conditions that were found in Davis. The same is true for the maximum concentrations represented by circles.

The minimum SO_2 and O_3 concentrations are 0.05ppb and 1ppb respectively. Each square along the line represents a different pH value. The values range from 5 to 7 pH units and are marked in increments of one half pH unit. Note that there are a total of four lines marked by squares. The two on the top left of the diagram are for gas phase sulfur dioxide limitations and the two that are horizontal represent aqueous phase ozone limitations. Each of these pairs has one line for a temperature of 5 degrees C and another for 10 degrees C. These are typical temperatures for the fog events in Davis. In all cases the lower line of the two is representative of the 10 degree C temperature, while the slightly higher line represents the 5 degree C calculations.

Average gas concentration calculations are marked by diamonds and follow the same scheme for pH and temperature dependence. These values were arrived at by averaging the SO_2 and O_3 gas phase concentrations independently over all of the sampling events. Therefore these are average in-fog values. The concentrations used are SO_2 at 0.37 ppb and O_3 at 4.43 ppb. Circles mark the lines indicating calculations done at maximum gas phase concentrations of 1.8 ppb SO_2 and 10 ppb O_3. The case of maximum gas phase conditions should be the most severely limited by mass transport.

The plotted points are generated by calculating the first order rate constants (k_1) and the Henry's law constants for both species. Summarizing the reaction rate formula for the S(IV) – O_3 reaction gives

$$R=k_{O3}[O_3][S(IV)] \qquad (3.20)$$

In this abbreviated formula k_{O3} is the effective rate constant for the reaction and is dependent on temperature and pH. The psuedo-first-order rate constants for ozone and S(IV) can be calculated as follows

$$k_{1,O_3} = k_{O_3}[S(IV)] = k_{O_3} H^*_{S(IV)} p_{SO_2} \quad (3.21)$$

$$k_{1,S(IV)} = k_{O_3}[O_3] = k_{O_3} H_{O_3} p_{O_3} \quad (3.22)$$

These equations assume Henry's law equilibrium and that the partial pressures are given after phase equilibrium has been established (Seinfeld and Pandis, 1998).

The plot shows that there are many points to the right of the mass transport boundary lines, indicating limitations to the reaction rate exist. It also indicates that larger drops are more likely to experience limitations than smaller drops. The most severe cases of mass transport limitation appear to occur in the aqueous phase for ozone transport. A significant number of samples also experienced gas phase SO_2 mass transport limitations. For this single reaction plot it appears that aqueous phase limitations for S(IV) and gas phase limitations for ozone are unimportant. When more than just one reaction is acting as a sink for S(IV), aqueous phase limitations may become significant.

This graphical analysis also shows that it is possible for drops to experience more than just one type of limitation. In fact for the case where the gas phase concentrations are maximized and the pH value is given as seven, even drops of 10μm in diameter would experience all types of mass transport limitation. Thus it is apparent that many of the Davis samples will have at least one type of mass transport limitation.

Figure 3.23 depicts plots similar to the one in Figure 3.22 created for each event at Davis. For these plots the same markers for the limitations were used, but now each individual point represents an actual fog sample. These plots show that many of the Davis samples experience more than just one type of mass transport limitation. Again it is evident that the most severe limitation is for ozone in the aqueous phase.

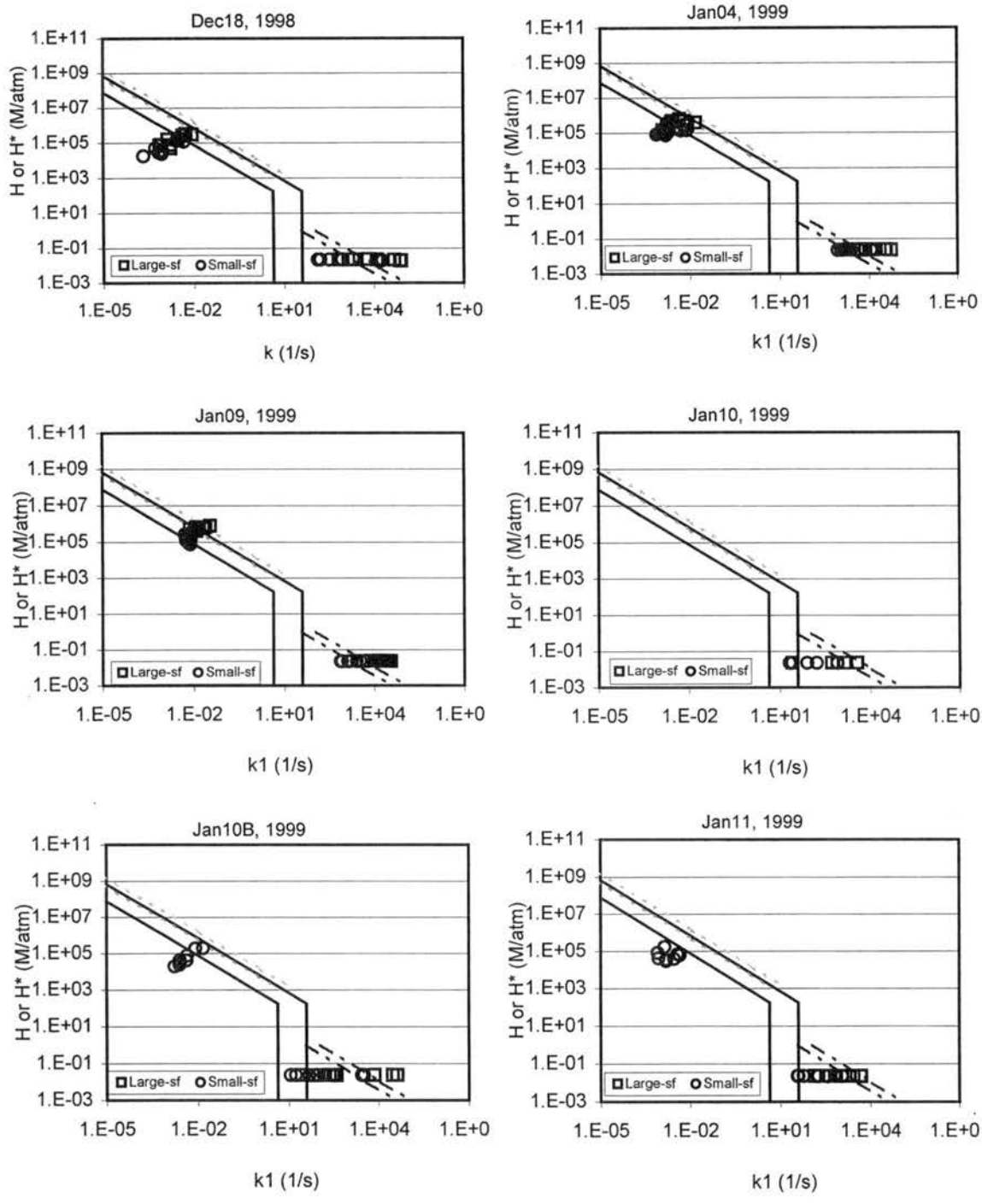

Figure 3.23: Mass transport limitation plots for Davis. These plots show the mass transport limitations experienced by each sf-CASCC sample during the Davis campaign. The squares represent large drop samples and the circles represent small drop samples. All other lines on the plots are the same as those in Figure 3.22.

It is useful to attempt to correct for these limitations in the rate calculations. Each sample was individually examined to determine which, if any, mass transport limitation was present. Several were found to have more than one, but the most prevalent limitation was the aqueous phase ozone transport, as seen in the diagram. To get an idea of the effects of mass transport limitations, aqueous phase limitations were incorporated into the sulfate production rate calculations.

This was done by adding a correction factor to the original production rate calculation. The reaction rate was scaled by a correction factor, Q. The original rate can be thought of as

$$R_{aq}=kC_s, \tag{3.23}$$

with the corrected rate given as

$$R_{aq}=QkC_s \tag{3.24}$$

For these equations R_{aq} represents the aqueous phase reaction rate, C_s is the concentration of the gas at the drop surface and k is the first order reaction rate. The correction factor is derived by using a differential equation for the concentration of species undergoing aqueous phase diffusion and irreversible reaction inside the drop. This equation is solved assuming a first order, steady state reaction. The solution is then integrated to get (Seinfeld and Pandis, 1998)

$$Q = 3\left(\frac{\coth q}{q} - \frac{1}{q^2}\right), \quad q = R_p\sqrt{\frac{k}{D_{aq}}} \tag{3.25, 26}$$

If it is assumed that there are no other mass transport limitations, the value for C_s can be given as

$$Cs=H_A p_A \tag{3.27}$$

Using these formulas, corrected rate calculations were done on a number of Davis samples, assuming other mass transport limitations to be insignificant when compared to the aqueous phase limitation. This allowed C_s to be defined as above. The results from these new calculations were promising. The addition of aqueous phase mass transport limitations resulted in much slower rates for the large drops. For the first few events the rates were reduced by about a factor of 10, but for the later events reductions by factors of 100 or greater are not uncommon.

In some cases the ratios of predicted large to small drop oxidation rates went down dramatically, by an order of magnitude or more. This decline led to sulfate production rate ratios (large:small) of near one for most samples. The corrected rate calculations are shown in Figure 3.24. Although, the predicted large to small drop

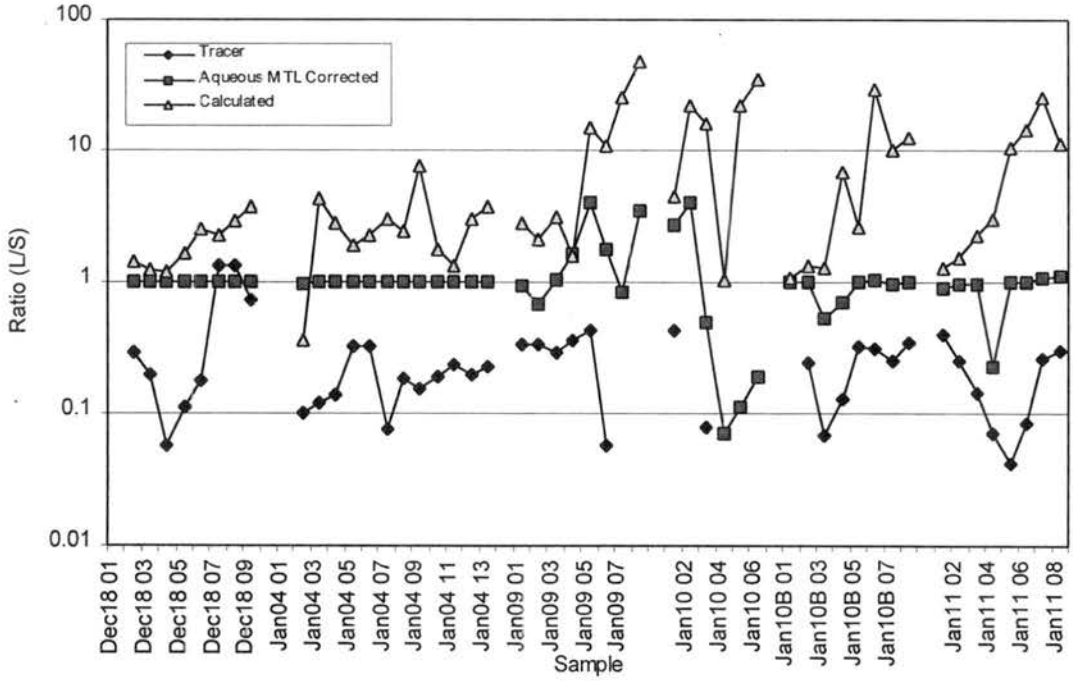

Figure 3.24: Aqueous phase mass transport corrected ratios. The corrected ratios are plotted with the tracer ratios and the originally calculated oxidation rate ratios for all available Davis samples.

oxidation ratios are now closer to the sulfate production ratios determined using the tracer technique, a significant difference still exists between the two results.

In order to further test the impact of the mass transport limitations on S(IV) oxidation it is necessary to examine the effects of gas phase transport limitations, interfacial limitations and combinations of the three. This is a difficult task due to the iterative nature of many of the calculations. To properly address this a more sophisticated drop chemistry model will be required.

3.3.2.1.3 Competing Reaction: HMS Formation

Another factor that may affect the amount of sulfate produced, especially in the larger drops is the complexation of S(IV) with formaldehyde. These two species can combine to form hydroxymethanesulfonate, HMS ($HOCH_2SO_3H$). Under certain circumstances the presence of formaldehyde in the cloud drop can provide an important sink for S(IV) and thereby limit the production of sulfate.

A significant amount of formaldehyde was found in the Davis samples. Formaldehyde in the atmosphere can be produced naturally by the reaction of the hydroxyl radical with methane, or it can also be a product of partial anthropogenic combustion of natural gas and can be formed by other volatile organic carbon oxidation mechanisms. The complexation of HCHO with S(IV) occurs in the aqueous phase. This complexation is not as straightforward as it may seem. Formaldehyde dissolves in water and undergoes hydrolysis to produce the gem-diol, methylene glycol,

$$HCHO(aq) + H_2O \leftrightarrow H_2C(OH)_2 \qquad (3.28)$$

In the gem-diol form, aqueous formaldehyde is unavailable to react with S(IV). The hydration constant of the above reaction is given by Seinfeld and Pandis(1998) as,

$$K_{HCHO} = [H_2C(OH)_2]/[\ HCHO(aq)] \qquad (3.29)$$

which has a value of 2530 at 298K. This indicates that nearly all the dissolved formaldehyde will exist in the unreactive gem-diol form. Therefore, only a small portion of the formaldehyde will be available for reaction with S(IV).

The kinetics and mechanism of the reaction between S(IV) and HCHO were studied in an acidic environment by Boyce and Hoffman (1984) in the early 1980's. They examined the reaction under psuedo-first-order conditions for both reactants (i.e. $[HCHO]_t >> [S(IV)]$ and $[S(IV)] >> [HCHO]_t$) at pH values ≤ 3. For the experiments of Boyce and Hoffman, $[HCHO]_t$ indicates both $[CH_2(OH)_2]$ and [HCHO]. A spectrophotometer was used to make the kinetic measurements.

The absorbance data generated from experiments using $[HCHO]_t >> [S(IV)]$ indicated that the rate of hydroxymethanesulfonate production was first order with respect to [S(IV)]. To confirm this result they then examined the dependence of the psuedo-first-order rate constant on the S(IV) concentration using formaldehyde as the limiting reagent. This relationship proved to be a straight line fit with $R^2 = 0.9937$, a slope of about 0.5 $M^{-1}s^{-1}$ and the y intercept close to zero (0.08 ± 1.00). Similar experiments were done testing the reaction rate as a function of formaldehyde concentration for $[HCHO]_t >> [S(IV)]$, the S(IV) limited case. Again a linear dependence was found, indicating that the reaction rate is also first order with respect to $[HCHO]_t$.

Boyce and Hoffman next examined the reaction rate dependence on pH by plotting the observed psuedo-second-order rate constant, $k_{obsd}/[HCHO]_t$, as a function of $[H^+]^{-1}$. The experimental data showed that the [S(IV)] concentration decreased more rapidly at higher pH values. They looked therefore at what happened to the rate over the pH range of 0 to 1, and the range 2.5 to 3.4, separately. The lower pH values yielded a straight line fit with R^2=0.9991, slope near 4.4 x 10^{-3} s^{-1}, and an intercept again close to zero (3.3 ±0.5 $M^{-1}s^{-1}$). They also found linear behavior for the higher pH range with R^2=0.9990, a slope of 7.68 x 10^{-4} s^{-1}, and an intercept of 0.348 ± 0.025 $M^{-1}s^{-1}$. These nonzero intercepts indicate the presence of two reaction pathways operating to produce hydroxymethanesulfonate.

From these experiments Boyce and Hoffman arrived at the following reaction mechanism for the production of HMS:

$$CH_2(OH)_2 \xleftrightarrow{k_d, k_{-d}} HCHO + H_2O \quad \text{(fast)} \tag{3.30}$$

$$SO_2 \bullet H_2O \xleftrightarrow{K_{a1}} H^+ + HSO_3^- \quad \text{(fast)} \tag{3.31}$$

$$HSO_3^- \xleftrightarrow{K_{a2}} H^+ + SO_3^{2-} \quad \text{(fast)} \tag{3.32}$$

$$HSO_3^- + HCHO \xleftrightarrow{k_1, k_{-1}} CH_2(OH)SO_3^- \quad \text{(slow)} \tag{3.33}$$

$$SO_3^{2-} + HCHO \xleftrightarrow{k_2, k_{-2}} CH_2(O^-)SO_3^- \quad \text{(slow)} \tag{3.34}$$

where for the values above the arrow, the positive number indicates the forward reaction and the negative number indicates the reverse reaction. For this mechanism there is nucleophilic addition of bisulfite and sulfite (two pathways) to the carbon atom in the carbonyl group of HCHO (Boyce and Hoffman, 1984). K_d can be defined as k_d/k_{-d} = 5.5 x 10^{-4} at 298K, indicating again that dissolved formaldehyde exists primarily in the gem-diol form.

The rate of HMS production can be given by,

$$d[HMS]/dt = k_1[HSO_3^-][HCHO] + k_2[SO_3^{2-}][HCHO] - k_{-1}[HMS] - k_{-2}[HMS] \quad (3.35)$$

Boyce and Hoffman indicate, however, that the above reactions that produce HMS have their equilibriums far enough to the right so that the terms involving the destruction of HMS can be dropped out of the tendency equation. Employing this assumption and substituting in as follows,

$$[HCHO] = (K_d[HCHO]_t)/(K_d + 1) \quad (3.36)$$

$$[HSO_3^-] = \alpha_1[S(IV)] \quad (3.37)$$

$$[SO_3^{2-}] = \alpha_2[S(IV)] \quad (3.38)$$

where α_1 and α_2 are both functions of K_{a1}, K_{a2} and $[H^+]$, the following rate equation can be obtained,

$$d[HMS]/dt = \{(K_d(k_1\alpha_1 + k_2\alpha_2))/(K_d + 1)\}[S(IV)][HCHO]_t \quad (3.39)$$

The two unknowns in the above equation are k_1 and k_2. Boyce and Hoffman examined the variation of $k_{obsd}/\alpha_1[HCHO]_t$ with pH in an attempt to refine the initial empirical estimates of k_1 and k_2. A temperature sensitivity analysis was also done at two different pH values. The kinetic values obtained from these analyses were then refined using a linear least squares regression. The results show the rate constant values are $k_1 = (7.9 \pm 0.32) \times 10^2\ M^{-1}s^{-1}$ and $k_2 = (2.48 \pm 0.24) \times 10^7\ M^{-1}s^{-1}$ (Boyce and Hoffman, 1984). Further work was done by Jacob in 1986 to compute the activation energy of this process. These values were estimated to be 9.7 kcal/mol for the bisulfite reaction and 3.6 for the sulfite reaction at a temperature of 298 K (Jacob, 1986).

The mechanism found by Boyce and Hoffman for hydroxymethanesulfonate production is almost identical to that found by Bell and Evans in the 1960's for HMS

formation in more neutral solutions, the major difference being that Bell and Evans believed the rate-limiting step to be the dehydration of the gem-diol. Boyce and Hoffman believe, however, that the rate-determining step for the formation of hydroxymethanesulfonate in an acidic solution is the nucleophilic addition of bisulfite and/or sulfite to the formaldehyde carbonyl group. Boyce and Hoffman concluded that the contributions of both bisulfite and sulfite to the reaction rate would be determined by the drop pH and the nucleophility of each species.

Early laboratory studies done by Boyce and Hoffman suggested that the presence of formaldehyde in aqueous solution "alters dramatically the kinetics of sulfur (IV) oxidation by hydrogen peroxide" (Boyce and Hoffman, 1984). They also found that at low pH values hydroxymethanesulfonate is resistant to oxidation by hydrogen peroxide when transition metal catalysts are not present.

In the mid-1990's research was done examining the complexation of formaldehyde and S(IV) in actual cloud and fog drops (Rao and Collett, 1995). The study done by Rao and Collett used samples collected at several different locations: Mt. Mitchell, NC, Whiteface Mountain, NY, Angora Peak, OR, and Bakersfield and La Jolla, CA. The variety of sites provided a wide variety of cloudwater pH ranges, and therefore different S(IV) oxidation mechanisms dominated at the different locations.

The results of this study indicate that in actual cloudwater with a pH of less than 4, the complexation of S(IV) with formaldehyde does not interfere with the rate of production of sulfate. This is because when compared to the timescale of sulfur (IV) oxidation by hydrogen peroxide, the time it takes for the production of HMS is too long. For pH values greater than about 5, however, both the complexation of S(IV) into HMS

and the oxidation of S(IV) by ozone become competitive with oxidation via the hydrogen peroxide pathway. Once there are pH values greater than 6 the ozone oxidation and the HMS production pathways dominate the depletion of S(IV). If the formaldehyde concentrations are great enough, the rate of hydroxymethanesulfonate production can be comparable to the rate of oxidation of S(IV) by ozone.

These results indicate that for the fog water samples collected during the Davis field campaign the complexation of S(IV) with formaldehyde should be a significant sink for S(IV), especially in higher pH samples from the large drop fraction of the sf-CASCC. This can be quantified by doing some rate calculations in order to examine if the complexation reaction rate is of the same order as the oxidation rate of S(IV) by ozone. The rate equation used is the one given above, with the concentrations of total HCHO being those measured in the fog water samples.

The calculations indicate that the complexation rate is on the order of 10^{-6} **M**/s, similar to the ozone oxidation rate. Therefore both reactions will be competing strongly for the available S(IV). Given the previously determined finite rate of mass transport of S(IV) in the large fog drops, this will lead to an overpredicted sulfate production rate, because not as much S(IV) will be available for reaction since it will be tied up with formaldehyde as HMS.

The complexation rate calculations also indicate that this reaction between HCHO and S(IV) takes place more rapidly for the larger drops than for the small. This can be seen in a ratio of the two rates. Figure 3.25 shows this ratio for each sample that had a measured value of HCHO. Not all samples were analyzed for formaldehyde so the data are somewhat incomplete. The plot clearly shows, however, that the ratio of HMS

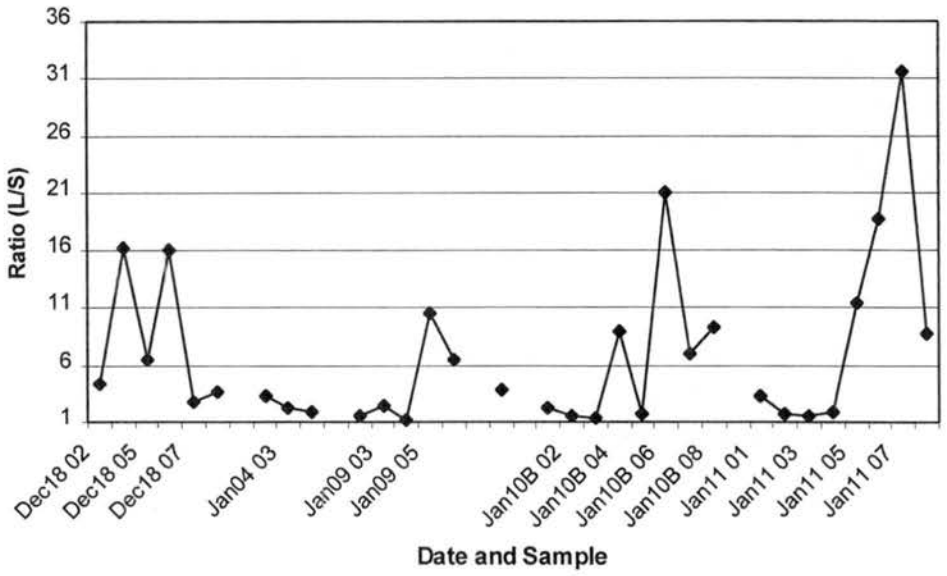

Figure 3.25: HMS complexation ratio. This is the large over small drop ratio of the rate of complexation of S(IV) with HCHO to form hydroxymethanesulfonate.

production in the large to the small drops is always greater than one, reaching a peak of 31.5.

These results suggest that the production of HMS may be responsible for depletion of free S(IV), especially in larger drops. The combined effects of HMS formation and mass transport limitations could, in theory, suppress sulfate formation rates in the large drops below those in small fog drops, consistent with the results provided by application of the tracer technique. Quantitative investigation of these phenomena is taken up below through the application of an aqueous phase chemistry model.

3.4.2.2 Aqueous Phase Chemistry Model

3.4.2.2.1 Model Overview

Many of the rate calculations for the Davis samples appear to be affected by both mass transport limitations and the competing complexation reaction with formaldehyde.

These two factors combine to make the actual sulfate production rates much less than those calculated using the S(IV) oxidation rate equations, especially in the larger drops. The interactions between all three types of mass transport limitations and the different S(IV) reaction pathways that are possible are extremely complex.

To quantify these interactions it is necessary to employ an aqueous phase chemistry model. The model chosen was aqchem, written by Sonia Kreidenweis and John Hobson in 1991. The existing aqchem model included several aqueous phase chemical reactions as well as subroutines designed to account for both gas phase and interfacial mass transport limitations for a single drop of any size.

The aqchem model was modified in order to make it particularly useful in the calculation of the rate of depletion of S(IV) for the Davis samples. This was done by eliminating any unnecessary reactions, such as those containing ammonia or nitric acid. This left the original model with only two reactions, the oxidation of S(IV) by H_2O_2 and the oxidation of S(IV) by ozone. The metals catalyzed pathway was neglected as the preliminary calculations done for the Davis samples indicate that the autooxidation pathway does not play a significant role in sulfate production for these samples. The reaction mechanism for HMS formation was added to the model. The complexation of S(IV) with HCHO provides another sink for S(IV) that makes it unavailable to react with either H_2O_2 or O_3 to form sulfate.

The aqueous phase mass transport limitation was added to the modified model as well. As seen from the mass transport studies mentioned above, for the ozone oxidation pathway the only species that experiences a significant limitation in the aqueous phase is ozone. Similarly for the hydrogen peroxide reaction with S(IV), H_2O_2 may be limited in

the aqueous phase. From the Schwartz-type diagrams it appears that there will be no aqueous phase limitation for S(IV). These diagrams, however, focus only on one reaction and therefore may not actually represent all the limitations that can occur when several reactions are taking place. Therefore it was also necessary to allow for the possibility of an aqueous phase mass transport limitation for S(IV) as well.

A guess and check type method was employed for this purpose. The method starts with a guess that all Q (recall that Q is the aqueous phase limitation rate correction factor) values are equal to one. The program then iterates, recalculating the rates and each one of the Q values. The iterations stop when the new Q value for S(IV) is the same as one form the previous iteration.

These reactions, along with the calculations of the three types of mass transport limitations enable the model to more accurately calculate the aqueous phase sulfate production rate.

3.4.2.2.2 Model Setup

The model was run for each sf-CASCC fog sampling period at Davis. Both the large and small drop fractions were simulated separately. The model input requires gas or aqueous phase values for hydrogen peroxide, ozone, sulfur dioxide and formaldehyde. Gas phase concentrations were used for hydrogen peroxide, ozone and sulfur dioxide, and were held constant over the model run. The specific value used was an average of the concentrations measured over the time the fog sample was being collected. Values for the formaldehyde input were taken from aqueous phase measurements made after the sample was preserved and taken to the lab, these values were also held constant. HCHO concentrations were not available for all samples. In the absence of an HCHO

measurement, it was necessary to make an estimate of the amount of formaldehyde in the sample in order to run the model successfully. When this type of estimated data is used it will be noted in the results. The model simulations were conducted while holding the drop pH fixed at the observed value for each sample.

Other parameters required for the model input were temperature (K), liquid water content (L water/L air), mean free path (cm), diffusivity constants (cm^2/s), pH, gas constant (L•atm/mol•K) and drop radius (cm). These are all straightforward except for selecting the drop radius. Due to an equipment problem, there were no drop size measurements available for the entire Davis campaign. Had there been drop size measurements, it would still be difficult to pick one drop radius to represent an entire drop size fraction that spans a broad range of drop sizes. Reasonable drop diameters were chosen to be 30μm for the large drop size fraction and 10 μm for the small drop fraction (sf-CASCC size cuts are 4 and 17 μm in diameter for the small and large drop size fractions).

Additional input parameters that are not specific to each sample are the number and length of each time step. The aqchem model recalculates all equations for each time step. For the purpose of this study it is necessary to allow the model to reach a steady state, where all the rates are stable. To accomplish this 120 time steps of 10 seconds each were used. These parameters allowed all calculated values to arrive at a steady state. The steady state rates can then be compared to the rates achieved using only the reaction mechanism equations. The oxidation rates found using the model should be less than those calculated previously because of the addition of the competing reaction as well as the presence of the mass transport limitations. The simulated small and large drop

oxidation rates can then be compared to the ratios of sulfate production in the small and large drops determined using the tracer technique.

3.4.2.2.3 Model Results

The results from the model appear very promising. In all cases the model predicts rates somewhat lower than those calculated previously using only the oxidation rate equations. The rate of HMS production was generally found to be very high. It was found to be anywhere from 2 to over 100 times as fast as the rate of S(IV) oxidation via the ozone pathway. The importance of this competing pathway is shown in the pie charts in Figure 3.26. The complexation of sulfur (IV) with formaldehyde acts as a sink for up to 84% of the available S(IV) according to model results. Also note that the hydrogen peroxide appears as the dominant oxidant for S(IV) in the small fraction. According to the model results, ozone remains the dominant pathway for S(IV) oxidation in the large fraction. The volume weighted averages for the S(IV) sinks and oxidation are almost identical to those of the large fraction. This is due to the fact that the drop size distributions in Davis heavily favored larger drops. Combined with the finite rate of

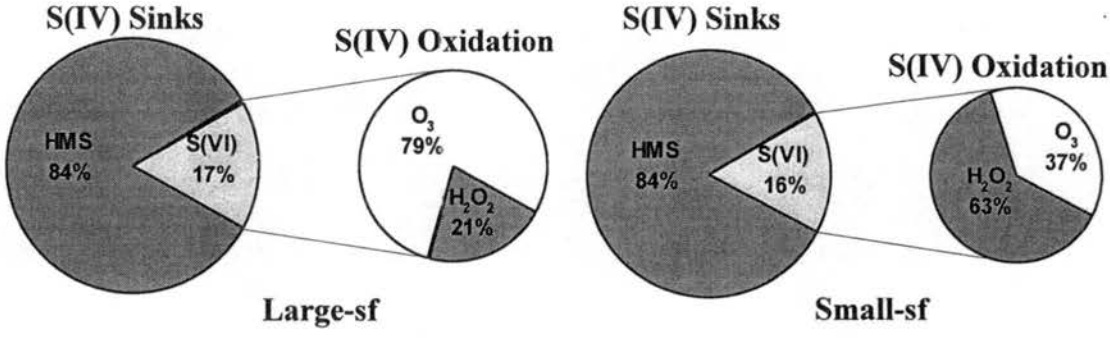

Figure 3.26: S(IV) sinks as calculated by the aqchem model for both the large and small fraction of the sf-CASCC.

mass transport, this reduces the overall sulfate production rate substantially from the original calculated value, especially in large drops.

The simulated large to small drop oxidation rate ratios for the model calculations were found to be much lower than those previously calculated. For the first three events all of the simulated large to small drop ratios are less than one. The final three events show a similar trend but each event includes at least one sample with a ratio larger than one. The largest ratio is from the final sample of the first January 10^{th} event, with a value of about 7.3.

These lower ratios are more consistent with SUNY's tracer results. While there still isn't an exact match between the two values, the differences between them are much reduced. An exact match between the values is highly unlikely given that they are measurements of two different quantities. The tracer study gives the amount of sulfate produced in the cloud or fog, while the model predicts the rate at which that production is taking place during a given time interval.

The improvement among the ratios can be seen in the plot in Figure 3.27. Here all samples for which there is at least some form of tracer data are shown. Samples for which formaldehyde was not measured are not included. It is apparent that the model calculations are much closer than the previously calculated oxidation ratios are to the tracer ratios.

Figure 3.28 shows the ratio comparisons for all the Davis events. Here the ratios from the model are compared to the ratios from the tracer determined method. For these plots samples without formaldehyde measurements are included. The values used for the

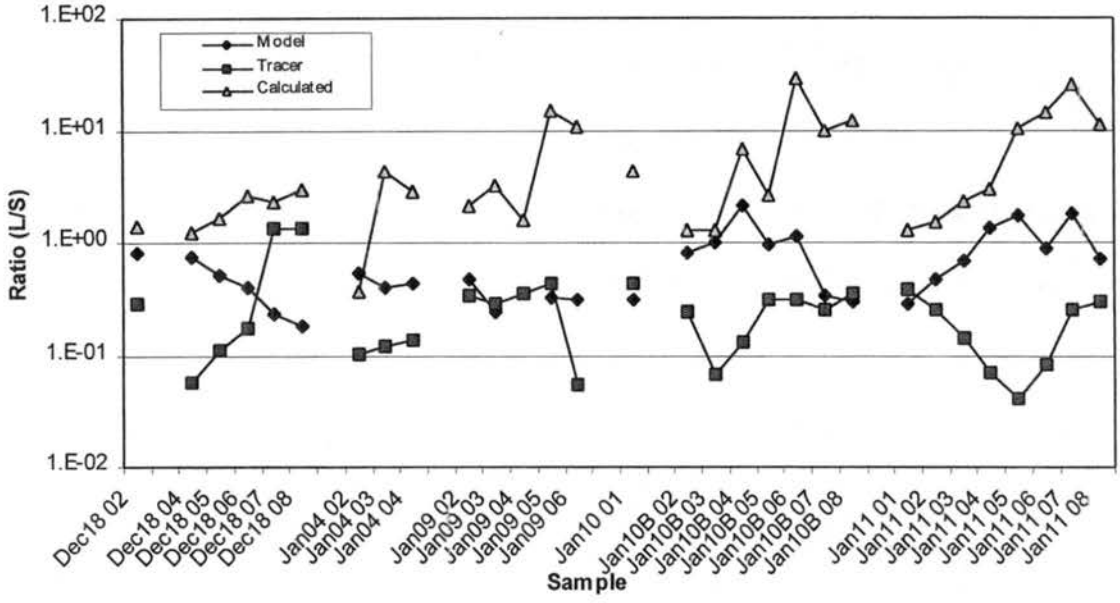

Figure 3.27: Model ratio comparison. The ratios obtained from the model results are plotted along with the ratios previously obtained from the tracer portion of the study and from the predicted oxidation rates. Only samples for which there were formaldehyde concentrations are shown.

formaldehyde concentrations were chosen to be reasonably close (within 1 to 5%) to the measured values found during the same event. In selecting the formaldehyde values the general trend of the HCHO concentration from any available values was considered. If the values were increasing a larger formaldehyde value was chosen, and if the values showed a negative trend, a smaller formaldehyde value was used.

For the December 18th event there appears to be good agreement in the trends of the two ratios for the first three comparable samples. After that the trends reverse, with the tracer ratio getting larger and the model ratio decreasing. By the seventh sample the tracer ratio has taken off, leaving a large difference between the two. For this event formaldehyde concentrations were unavailable for samples 1, 3 and 9. The best match for any of the fog episodes appears to occur for the January 4th event. Here the two ratios roughly track each other throughout the entire event. While the ratios still do not match,

the trend in the ratios appears similar for many samples. Formaldehyde measurements were missing for samples 1 and 5 through 13.

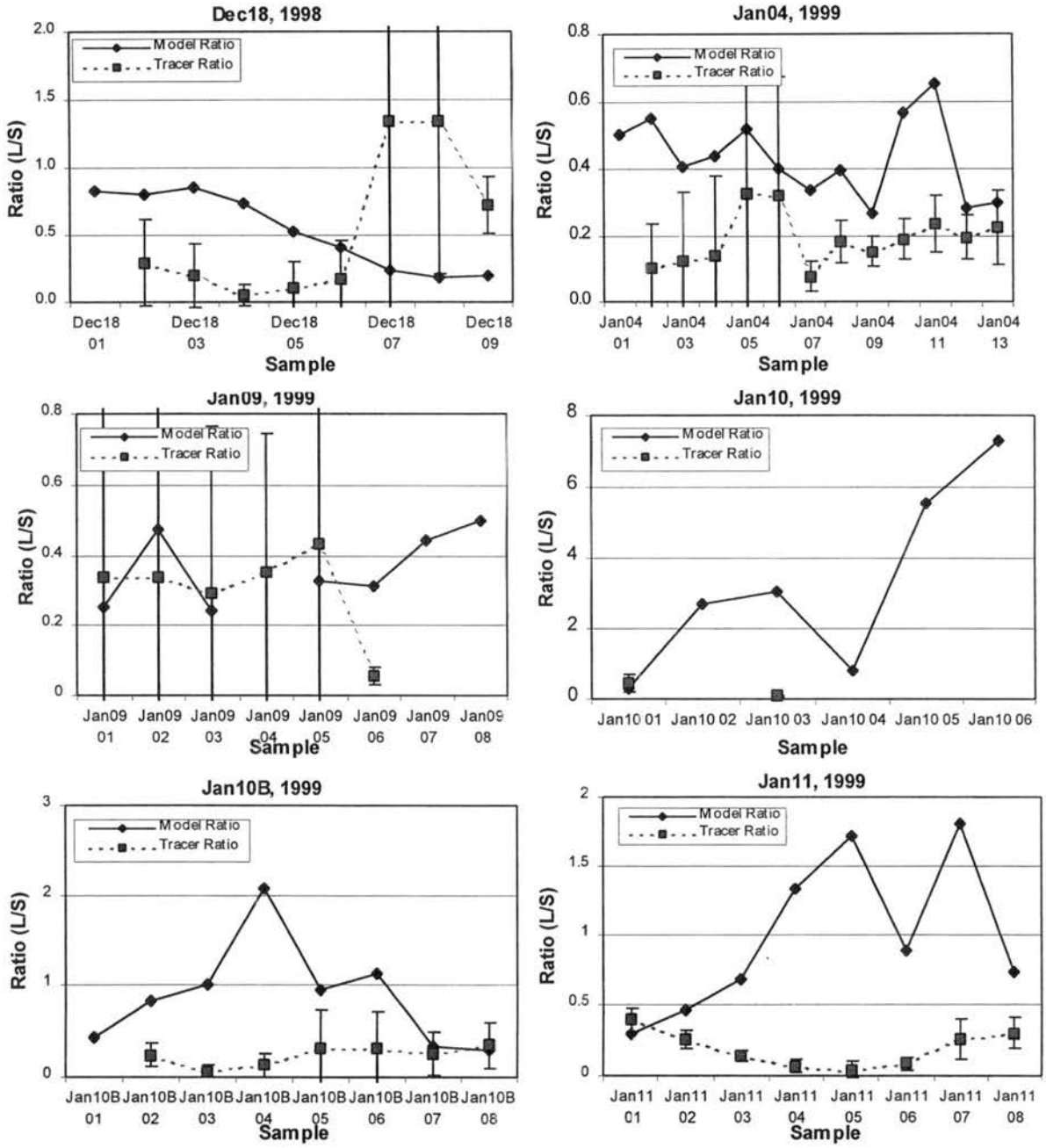

Figure 3.28: Ratio comparisons for Davis events. The above plots show comparisons of the ratios from the model to the ratios from the tracer technique. The tracer results have error bars.

The fourth plot in Figure 3.28 is from the first January 10th event. Here few data points are available; tracer data are available for only the first and third samples. The first sample matches very well: the two are within 30% of each other. The third sample shows far worse agreement, but this could be due to the fact that there was no formaldehyde measurement for this point. The only HCHO measurement taken for this event was for the first sample.

The plots in Figure 3.29 show the scatter associated with the comparisons of the model and tracer results, as well as the calculated and tracer results. The plots were created by graphing the ratios of the two methods being compared against each other. While neither plot shows a one to one relationship, the first one shows a better agreement between the results from the model and the results from the tracer technique. The second plot shows poor agreement between the calculated ratios (based on rate calculations made without consideration of mass transport limitations or HMS formation)and the tracer ratios.

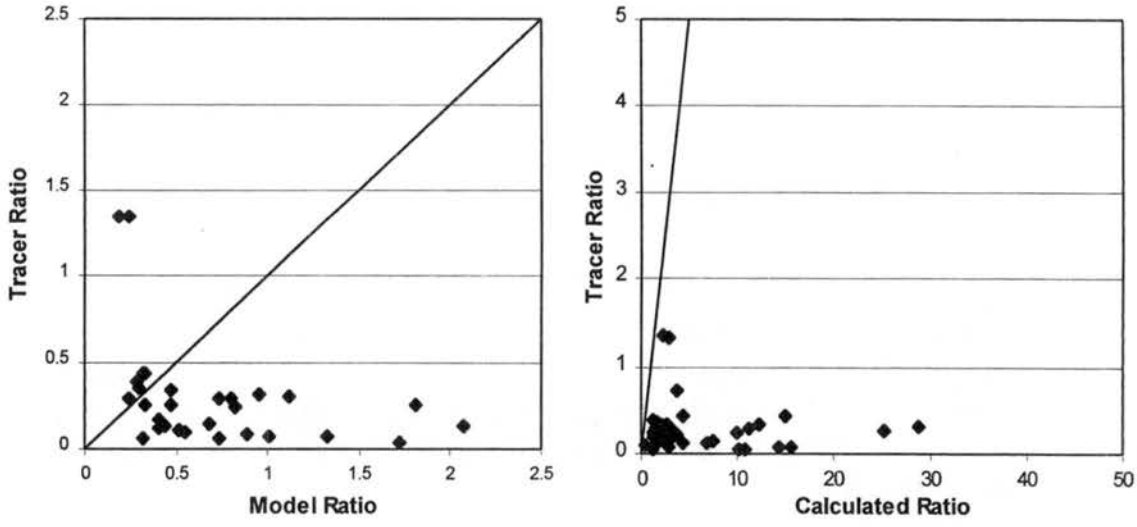

Figure 3.29: Scatter plots. The above are scatter plots of the tracer ratio vs. the model ratio and the calculated ratio, respectively.

3.4.2.2.4 Sensitivity Studies

Because there is some uncertainty in the model input, particularly for the drop radius, it is useful to examine what happens when different parameters are adjusted. Two types of sensitivity tests were done. The first type involved altering the ozone concentrations and the second involved changing the large drop size. These tests provide insight into how the model will behave under slightly different conditions than those originally used.

The ozone concentrations were considered highly uncertain because the measured values were so low. To test the sensitivity of the aqchem model to the gas phase

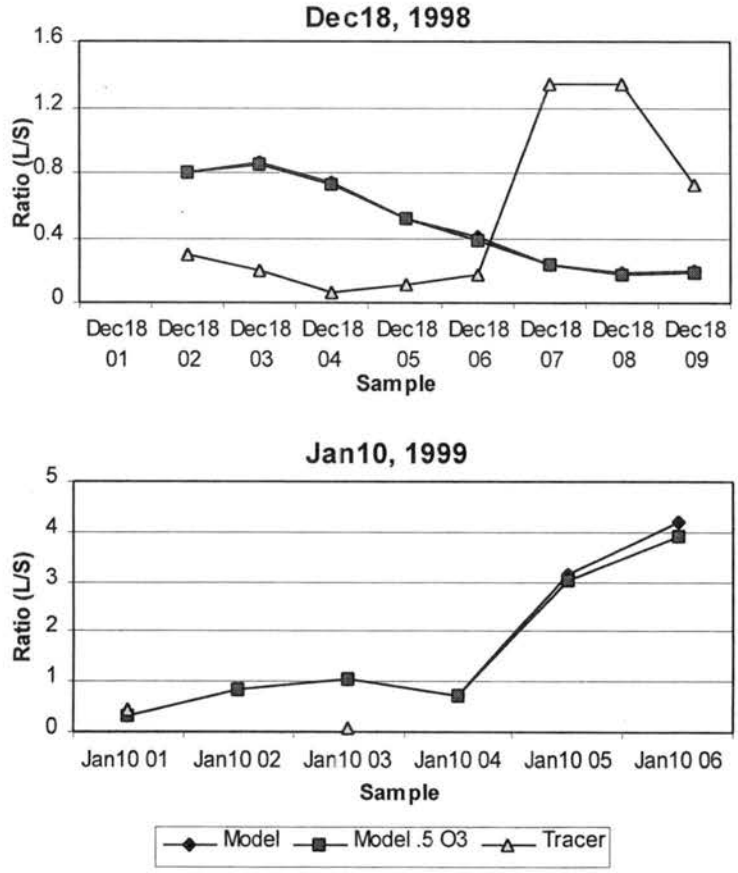

Figure 3.30: Ozone sensitivity plots. These plots show the impact that halving the ozone concentration has on the model ratios. The tracer data are shown without uncertainties.

concentration of ozone, the ozone concentrations were halved for two events. The events chosen were the December 18th event and the first event from the 10th of January. The model runs were redone keeping all other variables the same, but halving the ozone concentration. The results from this sensitivity study are shown in Figure 3.30. The plots show that the altered ozone concentration has little effect on the ratio of the rate of large to small sulfate production.

Table 3.11: Ozone sensitivity test values.

Sample	O_3 (ppb)	O_3 Rate	H_2O_2 Rate	Total S(VI)	½ O_3 O_3 (ppb)	1/2 O_3 O_3 Rate	1/2 O_3 H_2O_2 Rate	1/2 O_3 Total S(VI)
December 18, 1998								
Large-sf 01	1	4.02E-09	1.15E-07	1.19E-07	0.5	2.01E-09	1.15E-07	1.17E-07
Large-sf 02	2	9.46E-09	1.25E-07	1.34E-07	1	4.73E-09	1.25E-07	1.29E-07
Large-sf 03	3	8.11E-09	1.01E-07	1.09E-07	1.5	4.06E-09	1.01E-07	1.05E-07
Large-sf 04	1	4.75E-09	1.39E-07	1.44E-07	0.5	2.38E-09	1.39E-07	1.41E-07
Large-sf 05	1	6.79E-09	8.19E-08	8.86E-08	0.5	3.40E-09	8.20E-08	8.54E-08
Large-sf 06	2	1.62E-08	9.58E-08	1.12E-07	1	8.09E-09	9.60E-08	1.04E-07
Large-sf 07	2	2.21E-08	7.80E-08	1.00E-07	1	1.10E-08	7.81E-08	8.91E-08
Large-sf 08	2	2.14E-08	4.16E-08	6.30E-08	1	1.07E-08	4.17E-08	5.24E-08
Large-sf 09	3	3.23E-08	3.94E-08	7.17E-08	1.5	1.61E-08	3.95E-08	5.56E-08
Small-sf 01	1				0.5			
Small-sf 02	2	8.59E-09	1.59E-07	1.67E-07	1	4.29E-09	1.59E-07	1.63E-07
Small-sf 03	3	7.66E-09	1.20E-07	1.27E-07	1.5	3.83E-09	1.20E-07	1.23E-07
Small-sf 04	1	2.14E-09	1.93E-07	1.95E-07	0.5	1.07E-09	1.93E-07	1.94E-07
Small-sf 05	1	7.91E-09	1.63E-07	1.71E-07	0.5	3.96E-09	1.63E-07	1.67E-07
Small-sf 06	2	1.70E-08	2.62E-07	2.79E-07	1	8.51E-09	2.62E-07	2.70E-07
Small-sf 07	2	7.51E-08	3.47E-07	4.22E-07	1	3.76E-08	3.47E-07	3.85E-07
Small-sf 08	2	7.96E-08	2.62E-07	3.41E-07	1	3.98E-08	2.62E-07	3.02E-07
Small-sf 09	3	1.10E-07	2.52E-07	3.62E-07	1.5	5.51E-08	2.52E-07	3.07E-07
January 10, 1999								
Large-sf 01	5.8	1.36E-08	4.15E-11	1.37E-08	2.9	6.85E-09	4.20E-11	6.89E-09
Large-sf 02	6.9	1.57E-08	3.51E-11	1.57E-08	3.45	7.92E-09	3.57E-11	7.95E-09
Large-sf 03	8	1.19E-08	2.19E-11	1.19E-08	4	6.02E-09	2.24E-11	6.05E-09
Large-sf 04	7	2.57E-09	1.47E-10	2.72E-09	3.5	1.29E-09	1.48E-10	1.44E-09
Large-sf 05	8.5	1.28E-08	8.13E-11	1.29E-08	4.25	6.48E-09	8.28E-11	6.56E-09
Large-sf 06	8	1.53E-08	1.25E-10	1.54E-08	4	7.72E-09	1.26E-10	7.84E-09
Small-sf 01	5.8	4.28E-08	2.85E-10	4.30E-08	2.9	2.15E-08	2.87E-10	2.17E-08
Small-sf 02	6.9	1.82E-08	3.21E-10	1.85E-08	3.45	9.13E-09	3.21E-10	9.45E-09
Small-sf 03	8	1.12E-08	1.59E-10	1.13E-08	4	5.59E-09	1.60E-10	5.75E-09
Small-sf 04	7	3.56E-09	1.64E-10	3.72E-09	3.5	1.78E-09	1.64E-10	1.95E-09
Small-sf 05	8.5	3.88E-09	2.31E-10	4.11E-09	4.25	1.94E-09	2.32E-10	2.17E-09
Small-sf 06	8	3.31E-09	3.52E-10	3.67E-09	4	1.66E-09	3.52E-10	2.01E-09

The individual rates have been cut almost in half, but this is true for both the large and the small drop fraction, leaving the ratio practically the same as it was with the total amount of ozone. Table 3.11 shows the rates calculated by the model for both the original and halved ozone concentrations. Note that for the December 18th event the reduction in ozone has a very small effect even on the total production rates, especially for the first few samples. This is due to the dominance of the peroxide pathway for these samples. Total sulfate production values for the January 10th event are cut in half, due to the dominance of the ozone pathway during this event.

The second type of sensitivity study involved altering the radius input for the large drop fraction. This is a practical study in that there is a great deal of discretion in deciding what size drop radius to use. The fogs sampled at Davis tended to have their drop populations skewed towards larger drops. Since the mass transport limitations are more important for large drops it is likely that a change in the large drop size input would have a greater effect on the simulation results than a change in the small drop radius input.

The large drop radii were changed from an original value of 15μm, to 20 μm and then to 25μm. This was done for all events. The results from this indicate that a shift in the drop radius could have a substantial impact on the sulfate production rate. The drops with larger radii have slower sulfate production rates. A radius shift from 15 to 25 μm can cause the rate of sulfate production for the large drop fraction to be halved. The slower rates associated with the larger radii could be attributed to increased mass transport limitations.

The results from the radius sensitivity tests are shown in Figure 3.31. For most events the larger radii simply shift the ratio curves lower on the plot. The results from the January 9th event and the second event from January 10th show that increased radii change the shape of the ratio curves. The first few samples from the event on the 9th show a large change for radii of both 20 and 25μm. The 15μm radius ratio shows a peak at the second sample, while the other two plots show minima for the same sample. This indicates that the mass transport limitations have become very important even with only a 5μm change in radius. The second event on the 10th simply shows that the features of the ratio plot are flattened out at the largest drop radius. Again this is a mass transport effect.

The best results of the sensitivity test appear to occur for the event on January 4th. For this event it appears that a shift in drop population sizes could account for the difference between the tracer ratios and the model calculated ratios for most samples. The first sample, along with the tenth and eleventh, still appear different from the tracer ratios. The remainder of the tracer ratios, however, falls within a reasonable distance from the three model ratios, especially given the tracer ratio uncertainties.

On the whole, it appears that some of the best fits occur for the larger drop radii, suggesting that perhaps the actual drops collected in Davis had a mean radius value somewhat closer to 25μm than to 15μm. This is possible considering the abundance of large drops collected in Davis. It is also relevant to consider the volume mean size since the sulfate produced in the large size fraction is the SO_4^{2-} produced in each of the drops, weighted by their volumes. Again these measurements are not available for the Davis samples, but could provide further insight into sulfate production across the drop size

spectrum. Collett et al. (2000) have considered water sedimentation flux rates measured during these events and their results also suggest the presence of large drops.

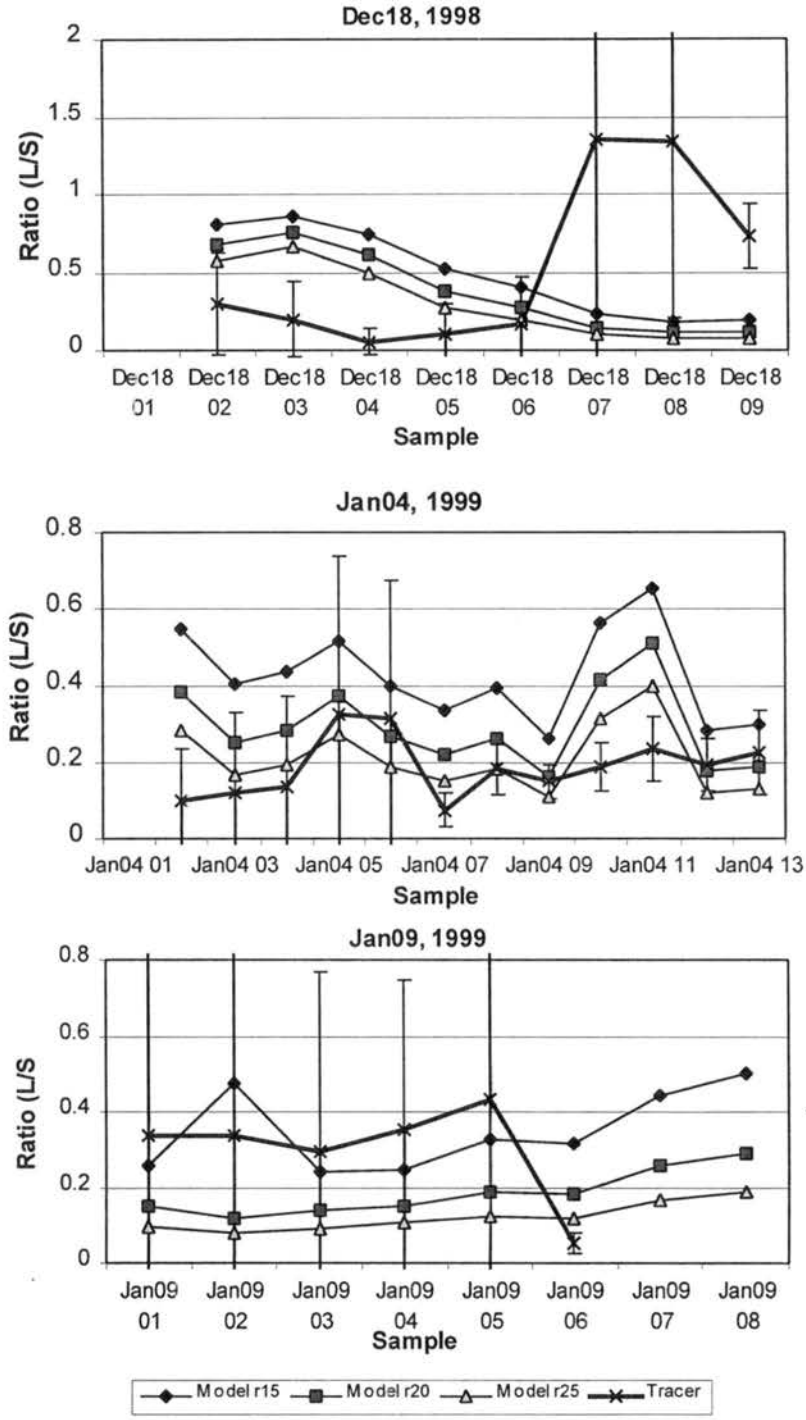

Figure 3.31: Radius sensitivity test. These plots compare the tracer ratios to the model results from the radius sensitivity tests.

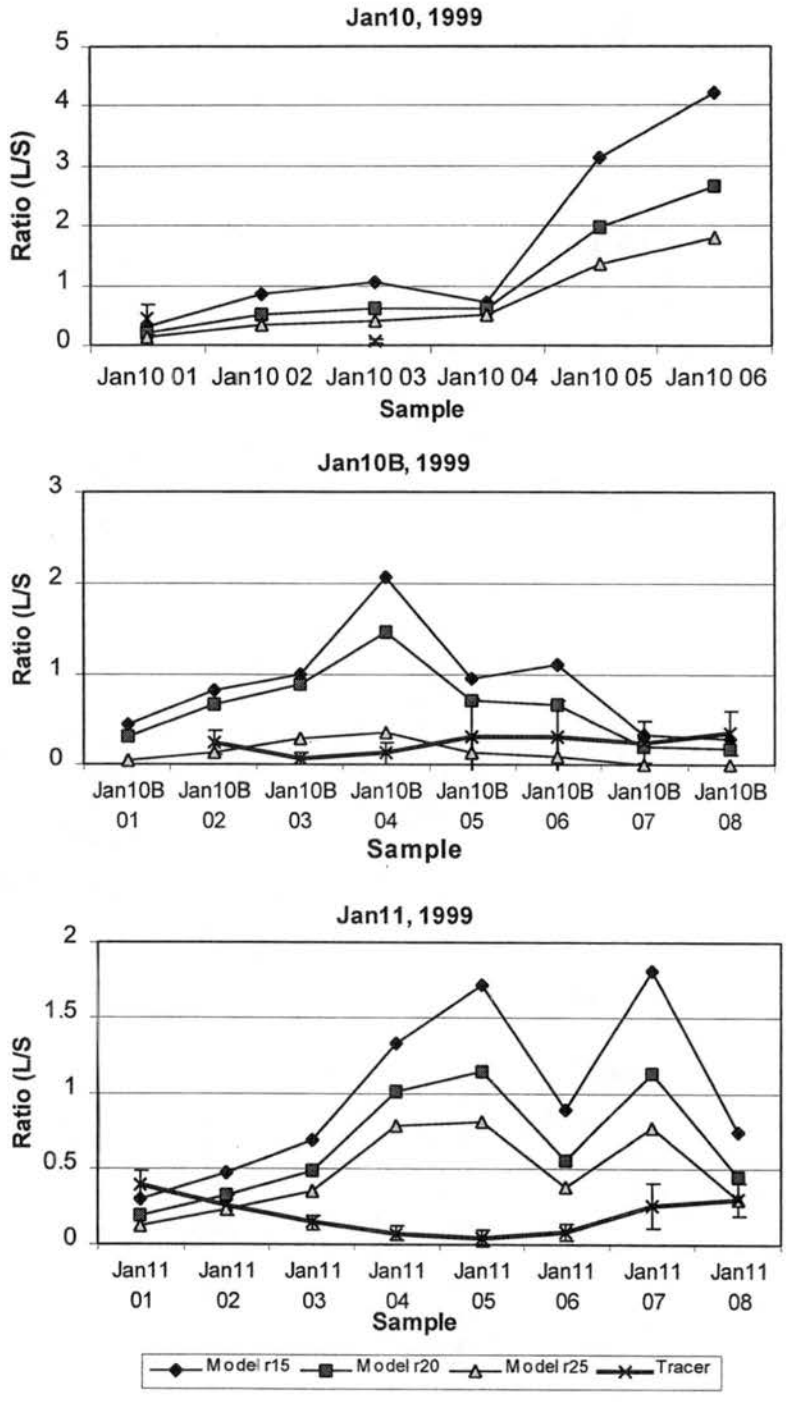

Figure 3.31 continued: Radius sensitivity test.

4. Conclusions

This study was successful in that it provided ample opportunity to compare the tracer technique with the aqueous phase S(IV) chemistry calculations. Because the results did not match exactly each method was examined. This examination resulted in the application of an aqueous phase chemistry model that indicates mass transfer effects to the calculation of the S(IV) oxidation rates. This should provide more accurate results for future studies.

The results from the two sampling sites chosen were as expected. The clouds at Whiteface Mountain had low pH values and sulfate was produced almost exclusively via the hydrogen peroxide pathway. There was little drop size related composition heterogeneity, and both large and small drops had similar oxidation rates. So, Whiteface Mountain acted as a good control environment.

Sulfate production at Davis, CA was dominated by the ozone oxidation pathway, as expected. There also existed significant chemical heterogeneity among the different drop sizes collected at this location. Higher pH values in large drops collected by the sf-CASCC yielded larger predicted oxidation rates for the large drops than for the small drop fraction.

Initial comparisons of the predicted and tracer derived ratios of large drop to small drop sulfate production showed relatively good agreement for the Whiteface data but poor agreement for the Davis data. The discrepancy between the ratios for the Davis data prompted an exploration of mass transport limitations and the competing S(IV) –

formaldehyde complexation reaction. Without this comparison to the tracer technique the importance of these sulfate production rate limiting factors may have been overlooked for some time.

From the study of mass transport limitations it can be concluded that for cloud or fog drops with high pH values in an environment dominated by S(IV) oxidation via the ozone pathway, there can be significant gas, interfacial and aqueous phase transport limitations. These limitations substantially reduce the sulfate production rates predicted from the aqueous phase S(IV) oxidation reactions. This is especially true of large drops, which typically have higher pH values and experience more severe mass transport limitations due to their larger size. Aqueous phase mass transport limitations alone can account for reductions in sulfate production rates by a factor of 100 or more.

The competing complexation of S(IV) with formaldehyde to form hydroxymethanesulfonate was also found to be important in reducing the amount of sulfate produced in the fog drops. The rate of this complexation was found to be competitive with the S(IV) oxidation rate by ozone, with both reactions occurring on the order of 10^{-6} **M**/s. This was particularly true again for large drops, due to their higher pH values. Ratios of large to small drop HMS formation were always found to be above one and frequently greater than five, indicating that this is an especially important reaction for large fog drops.

The aqchem model proved to be a useful tool in calculating the sulfate production rates in the drops in light of the complex mass transport limitations and competing reactions. The model showed that by incorporating both mass transport limitations and the competing complexation reaction, the small drop sulfate production rates could

actually be faster than those for the large drops. This brought the large to small drop S(IV) oxidation rate ratios closer to the SO_4in ratios determined using the tracer technique. While the model results did not match exactly with the results determined using the tracer technique, they are far more reasonable than those generated using only the S(IV) oxidation reactions. A true match between the tracer determined ratios and those generated using the model is not too likely. The tracer determined method measures the time integrated amount of sulfate produced in the cloud or fog drops, while the model is instead calculating the rates of S(IV) depletion. For the ratios of these two different quantities to be even within a factor of two is considered fairly good agreement. The application of the tracer technique succeeded in documenting the importance of considering the influence of chemical heterogeneity among cloud/fog drop populations on aqueous sulfur oxidation.

This study served to improve the methods used in the calculation of aqueous phase S(IV) oxidation rates. The importance of the mass transport limitations and competing reactions were brought to light, both of which greatly affect the overall rate of the production of sulfate. The addition of these factors to the S(IV) oxidation rate calculations should provide a more accurate view of the rate of sulfate production in cloud and fog drops.

5. Future Work

From this study several avenues of possible future work exist, the first being further development and use of the cloud chemistry model aqchem. This model proved to be extremely useful in providing a more accurate picture of the aqueous phase production of sulfate in clouds and fog. It should be employed in the future for any attempts at quantifying the rates of S(IV) oxidation.

The model can even be applied to the Whiteface Mountain data from this study in an attempt to get values that agree with the tracer ratios to a greater extent. While the two ratios agree rather well for most events, especially with the large error bars present for the tracer ratios, there are a few events for which further insight would be useful. This is true particularly for the July 16, 1998 event, where tracer and model ratios do not match well.

Another possible test to run using the aqchem model would be to check the effects of a time evolution of the drop pH. The model is capable of running this time evolution, but this feature has not yet been examined for this data. The use of this feature may provide a more accurate picture of how the rates of sulfate production are evolving in the drop.

For future cloud and fog collection studies, it will be important to realize the relevance of the formaldehyde measurement. This measurement is of particular importance for cloud or fog drops with high pH values due to the fast reaction rate of the S(IV)-HCHO complexation. This HMS complexation is a strong sink for S(IV) and

therefore affects the overall sulfate production rates. The formaldehyde measurement is also necessary when using the aqchem model; without it the model results are not well constrained.

Future work may also include further development of the tracer technique as a means of quantifying the amount of sulfate produced in clouds and fog. To make a more accurate comparison of the tracer technique and the S(IV) oxidation rate calculation method more data are needed. Different sampling sites could be used and a more complete data set should be obtained. Detailed measurement of drop size data appears to be very important in light of the model sensitivity studies. Having detailed drop size distribution data, as well as more formaldehyde concentration measurements would enable more accurate use of the aqchem model. The results from the model could then be compared to the tracer technique ratios as in the current study.

References

American Chemical Society. (1991) *Acid Rain Information Pamphlet*. ACS Department of Governmental Relations and Science Policy, Washington, DC.

Bator, A. and Collett, J.L. (1997) Cloud chemistry varies with drop size. *J. Geophys. Rev.* **102**, (D23), 28,071-28,078.

Bevington, P.R., and Robinson, D.K. (1992) *Data Reduction for the Physical Sciences*; McGraw-Hill, Inc.: New York.

Boyce, S. D. and Hoffman, M. R., (1984) Kinetics and mechanism of the formation of hydroxymethanesulfonic acid at low pH, *J. Phy. Chem.* **88**, 4740-4746.

Burkhard, E.G., Ghauri, B.M., Dutkiewicz, V.A., and Husain, L. (1995) A multielement tracer technique for the determination of SO2 oxidation in clouds. *J. Geophys. Res.-Atmos* **100**,(D12) 26,051-26,059.

Cahill, T.A. and Eldred, R.A. (1998) Particulate Selenium in the Atmosphere. *Environmental Chemistry of Selenium*. Edited by Frankenberger, W.T. and Engberg, R.A. Marcel Dekker, Inc.: New York. pp 613-632.

Calvert, J.G., Lazrus, A., Kok, G.L., Heikes, B.G., Walega, J.G., Lind, J. and Cantrell, C.A. (1985) Chemical mechanisms of aicd generation in the troposphere. *Nature* **317**, (5) 27-35.

Collett, J.L., Bator, A., Rao, X., and Demoz, B. (1994) Acidity variation across the cloud drop size spectrum and their influence on the rates of atmospheric sulfate production. *Geophys. Rev. Lett.* **21**, 2393-2396.

Collett, J.L., Hoag, K.J., Rao, X., and Pandis, S.N. (1999) Internal acid buffering in San Joaquin Valley fog drops and its influence on aerosol processing. *Atmos. Environ.* **33**, 4833-4847.

Collett, J.L., Sherman, D.E., Moore, K.F., Hannigan, M.P., and Lee, T. (2000) Aerosol particle processing and removal by fogs: observations in chemically heterogeneous central California radiation fogs. Submitted to *Water, Air and Soil Pollution*, 7/2000.

Dasgupta, P.K., DeCesare, K., and Ullrey, J.C. (1980) Determination of atmospheric sulfure dioxide without tetrachloromercurate(II) and the mechanism of the Schiff reaction. *Anal. Chem.* **52**, 1912-1922.

Demoz, B., Collett, J.L., and Daube B.C. Jr., (1996) On the Caltech Active Strand Cloudwater Collectors. *Atmos. Res.* **41**, 47-62.

Dong, S. and Dasgupta, P.K. (1987) Fast fluorometeric flow injection analysis of formaldehyde in atmospheric water. *Environ. Sci. Technol.* **21**, 581-588.

Dutkiewicz, V.A., Parekh, P.P. and Husain, L. (1987) An evaluation of regional elemental signatures relevant to the northeastern United States. *Atmos. Environ.* **21**: (5) 1033-1044.

Gurciullo, C.S. and Pandis, S.N. (1997) Effect of composition variations in cloud droplet populations on aqueous-phase chemistry. *J. Geophys. Res.-Atmos.* **102**, (D8) 9375-9385.

Hoffman, M.R., and Jacob, D.J. (1984) Kinetics and mechanism of the catalytic oxidation of dissolved sulfur dioxide in aqueous solution: an application to nighttime fog water chemistry. *SO2, NO, and NO2 Oxidation Mechanisms: Atmospheric Considerations*, edited by J.G. Calvert. Stoneham, MA.

Hoffman, M.R. and Calvert J.G. (1985) Chemical Transformation of Modules for Eulerian Acid Deposition Models, Volume II. The Aqueous Phase Chemistry. EPA/600/S3-85/036. June 1985.

Husain L., Webber J. S., Canelli E, Dutkiewicz V. A., and Halstead J. A. (1984) Mn/V ratio as a tracer of aerosol sulfate transport. *Atmos. Environ.*, **18**,1059 - 1071.

Husian, L. (1989) A technique for determining in-cloud formation of SO_4. *Geophys. Res. Lett.* **16**, 57-60.

Husain, L., Dutkiewicz, V.A., Hussain, M.M., Khwaja, H.A., and Burkhard, E.G. (1991) A study of heterogeneous oxidation of SO_2 in summer clouds. *J. Geophys. Res.-Atmos.* **96**, (D10) 18,789-18,805.

Ibusuki T. and Takeuchi K. (1987) Sulfur dioxide oxidation by oxygen catalyzed by mixtures of manganese (II) and iron (III) in aqueous solutions at environmental reaction conditions. *Atmos. Environ.* **21**, 1555-1560.

Jacob, D.J., (1986) Chemistry of OH in remote clouds and its role in the production of formic acid and peroxymonosulfate, *Journal of Geophysical Research,* **91**, 9807-9826.

Kelly, T.J., Schwartz, S.E., and Daum, P.H. (1989) Detectability of acid producing reactions in natural clouds. *Atmos. Environ.* **23**, 569-583.

Lazrus, A.L., Kok, G.L., Gitlin, S.N., and Lind, J.A. (1985) Automated flourometric method for hydrogen peroxide in atmospheric precipitation. *Anal. Chem.* **57**, 917-922.

Lelieveld, J., Heintzenberg, J., (1992) Sulfate cooling effect on climate through in-cloud oxidation of anthropogenic SO_2, *Science*, **258**, 117-120.

Martin, L.R. (1984) Kinetic studies of sulfite oxidation in aqueous solution. *SO2, NO, and NO2 Oxidation Mechanisms: Atmospheric Considerations*, edited by J.G. Calvert. Stoneham, MA.

Martin, L.R. and Good, T.W. (1991) Catalyzed oxidation of sulfur dioxide in solution: the iron and manganese synergism. *Atmos. Environ.* **25A**, 2395-2399.

McArdle, J.V., and Hoffman, M.R. (1984) Kinetics and mechanism of the oxidation of aquated sulfur dioxide by hydrogen peroxide at low pH, *J. Atmos. Chem.*, **87**, 5425-5429.

Mosher, B.W. and Duce, R.A. (1987) A global atmospheric selenium budget. *J. Geophys. Res.* **92**, 13,289-13,298.

Munger, J.W., Collett, J.L., Daube, B. Jr., and Hoffman, M.R. (1989) Fogwater chemistry in an atmosphere. *J. Geophys. Rev.* **88**, 5109-5121.

Rao, X., Collett, J.L. (1995) The behavior of S(IV) and formaldehyde in a chemically heterogeneous cloud, *Environ. Sci. Technol.*, **29**, 1023-1031.

Rao, X. and Collett, J.L. (1998) The drop size dependence of iron and manganese concentrations in clouds and fogs: implications for sulfate production. *J. Atmos. Chem.* **30**, 273-289.

Schwartz, S.E. (1984) Gas aqueous reactions of sulfur and nitrogen oxides in liquid water clouds. *SO2, NO, and NO2 Oxidation Mechanisms: Atmospheric Considerations*, edited by J.G. Calvert. Stoneham, MA.

Schwartz, S.E. (1986) Mass transport considerations pertinent to aqueous-phase reactions of gases in liquid-water clouds. *Chemistry of Multiphase Atmospheric Systems*, edited by W. Jaeschke. Springer-Verlag, Berlin, pp. 415-471.

Schwartz, S.E. (1988) Mass transport limitation to the rate of in-cloud oxidation of SO2: re-examination in light of new data, *Atmos. Environ.*, **22**, 2491-2499.

Seidl, W. (1989) Ionic concentrations and initial S(IV) oxidation rates in droplets during the condensational stage of cloud. *Tellus* **41B**, 32-50.

Sienfeld, J.H. and Pandis, S.N. (1998) *Atmospheric Chemistry and Physics: From Air Pollution to Climate Change;* Wiley-Interscience: New York.

Stockwell, W. R., Calvert, J.G., (1983) The mechanism of the HO-SO2 reaction, *Atmos. Environ.*, **17**, 2231-2235.

Twohy, C.H., Austin, P.H. and Charlson, R.J. (1989) Chemical consequences of the initial diffusional growth of cloud droplets: a clean marine case. *Tellus* **41B**, 51-60.

Wark, K., Warner, C.F., and Davis, W.T. (1998), *Air Pollution: Its Origin and Control.* Addison Wesley Longman, Inc., Menlo Park, CA.

Xu, G., Sherman, D.E., Andrews, E., Moore, K., Straub, D., Hoag, K. and Collett, J.L. (1999) The influence of chemical heterogeneity among cloud drop populations on processing of chemical species in winter clouds. *Atmos. Res.* **51**, 119-140.

APPENDIX A: Sample Compositions

Table A.1: Whiteface Mountain sample conditions for event 1. The gas concentrations given are from summit site. Note temperature, pressure and liquid water content data were not available for this event.

Whiteface Mountain: Event 1								
Sample	Date	Time	Temp (K)	Pres (mb)	LWC (mg/m^3)	SO_2 (ppb)	O_3 (ppb)	H_2O_2 (ppb)
July4 01	7/4/98	9:45-10:30PM				0.06	47.9	0.061
July4 02	7/4/98	10:30-11:00PM				0.07	47.6	0.051
July4 03	7/4/98	11:00PM-12:00AM				0.06	48.4	0.051
July4 04	7/5/98	12:00-1:00AM				0.11	47.7	0.036
July4 05	7/5/98	1:00-2:00AM				0.09	42.3	0.045
July4 06	7/5/98	2:00-3:00AM				0.13	38.4	0.031
July4 07	7/5/98	3:00-4:00AM				0.17	37.8	0.039
July4 08	7/5/98	4:00-5:00AM				0.32	39.4	0.041
July4 09	7/5/98	5:00-6:00AM				0.64	39.3	0.048
July4 10	7/5/98	6:00-7:00AM				0.74	38.6	0.060

Table A.2: Whiteface Mountain sample conditions for event 2.

Whiteface Mountain: Event 2								
Sample	Date	Time	Temp (K)	Pres (mb)	LWC (mg/m^3)	SO_2 (ppb)	O_3 (ppb)	H_2O_2 (ppb)
July7 01	7/7/98	12:30-1:00PM				0.68	43.9	0.186
July7 02	7/7/98	1:00-2:00PM	284.84	849.17	538.72	0.65	41.8	0.201
July7 03	7/7/98	2:00-3:00PM	285.00	855.35	555.12	0.55	37.9	0.160
July7 04	7/7/98	3:00-4:00PM	285.13	855.37	606.74	0.66	38.5	0.131
July7 05	7/7/98	4:00-4:30PM	285.09	855.26	501.41	0.73	39.6	0.122
July7 06	7/7/98	4:30-5:00PM	285.24	855.30	392.27	0.73	39.6	0.129
July7 07	7/7/98	5:00-5:30PM	285.39	855.17	520.07	0.70	39.9	0.124
July7 08	7/7/98	5:30-6:00PM	285.39	855.04	496.31	0.77	39.9	0.146
July7 09	7/7/98	6:00-6:30PM	285.46	855.09	497.89	0.72	37.4	0.135
July7 10	7/7/98	6:30-7:00PM	285.44	855.04	559.31	0.59	37.4	0.127
July7 11	7/7/98	7:00-7:30PM	285.48	850.20	538.04	0.58	34.7	
July7 12	7/7/98	7:30-8:00PM	285.29	855.04	342.89	0.60	34.7	0.093
July7 13	7/7/98	8:00-8:30PM	285.28	854.96	347.76	0.51	30.1	0.112
July7 14	7/7/98	8:30-9:00PM	285.15	854.91	193.56	0.39	30.1	0.083
July7 15	7/7/98	9:00-9:30PM	285.18	855.00	213.60	0.32	25.6	0.087
July7 16	7/7/98	9:30-10:00PM	285.38	855.00	427.46	0.29	25.6	0.056
July7 17	7/7/98	10:00-11:00PM	285.36	854.95	335.32	0.25	31.2	0.053
July7 18	7/7/98	11:00-12:00AM	285.30	854.88	405.98	0.32	37.4	0.060
July7 19	7/8/98	12:00-12:50AM	284.93	854.67	95.63	0.35	40.6	0.067

Table A.3: Whiteface Mountain sample conditions for event 3.

Whiteface Mountain: Event 3								
Sample	Date	Time	Temp (K)	Pres (mb)	LWC (mg/m^3)	SO_2 (ppb)	O_3 (ppb)	H_2O_2 (ppb)
July16 01	7/16/98	7:25-8:00AM	289.69	851.60	356.06	3.07	65.0	0.356
July16 02	7/16/98	8:00-8:30AM	289.91	853.51	533.27	3.09	63.0	0.179
July16 03	7/16/98	8:30-9:00AM	289.99	844.64	554.81	3.47	63.0	0.214
July16 04	7/16/98	9:00-9:30AM	290.22	853.14	357.96	3.18	73.5	0.287
July16 05	7/16/98	9:30-10:00AM	290.35	840.93	354.24	3.32	73.5	0.294
July16 06	7/16/98	10:00-10:30AM	290.41	853.01	318.87	2.91	74.4	0.263
July16 07	7/16/98	10:30-11:00AM	290.44	846.69	163.59	1.60	74.4	0.243
July16 08	7/16/98	11:00-11:30AM	290.71	853.06	20.93	1.75	76.2	0.404

Table A.4: Whiteface Mountain sample conditions for event 4.

Whiteface Mountain: Event 4								
Sample	Date	Time	Temp (K)	Pres (mb)	LWC (mg/m^3)	SO_2 (ppb)	O_3 (ppb)	H_2O_2 (ppb)
July17 01	7/17/98	1:30-2:00AM	288.95	849.63	294.67	1.59	65.3	
July17 02	7/17/98	2:00-3:00AM	289.14	849.63	380.80	2.49	76.1	0.193
July17 03	7/17/98	3:00-4:00AM	288.67	849.63	335.83	2.29	72.5	0.173
July17 04	7/17/98	4:00-5:00AM	288.11	849.59	419.47	1.34	72.6	0.180
July17 05	7/17/98	5:00-6:00AM	288.68	849.49	537.05	0.85	81.5	0.244
July17 06	7/17/98	6:00-7:00AM	288.70	849.43	545.62	0.56	77.5	0.231
July17 07	7/17/98	7:00-8:00AM	288.78	849.33	623.54	1.12	67.9	0.150
July17 08	7/17/98	8:00-9:00AM	288.95	849.29	744.15	2.29	60.7	0.125
July17 09	7/17/98	9:00-10:00AM	288.94	849.19	641.03	1.38	57.7	0.145
July17 10	7/17/98	10:00-11:00AM	288.86	849.19	587.17	0.58	62.6	0.200

Table A.5: Whiteface Mountain sample composition for event 5.

Whiteface Mountain: Event 5								
Sample	Date	Time	Temp (K)	Pres (mb)	LWC (mg/m^3)	SO_2 (ppb)	O_3 (ppb)	H_2O_2 (ppb)
July20 01	7/20/98	9:00-9:30AM	287.96	842.44	764.24	2.42	59.8	0.096
July20 02	7/20/98	9:30-10:00AM	288.02	846.93	690.07	2.53	59.8	0.115
July20 03	7/20/98	10:00-10:30AM	288.01	847.37	577.24	2.62	62.0	0.130
July20 04	7/20/98	10:30-11:00AM	288.08	847.29	529.11	3.05	62.0	0.146
July20 05	7/20/98	11:00-11:30AM	288.05	843.29	368.47	2.25	61.3	0.178
July20 06	7/20/98	11:30AM-12:00PM	288.09	843.24	288.49	1.55	61.3	0.158
July20 07	7/20/98	12:00-12:30PM	288.36	843.16	255.44	1.40	60.8	0.173
July20 08	7/20/98	12:30-1:00PM	288.54	843.11	158.34	1.21	60.8	0.027

Table A.6: Whiteface Mountain sample conditions for event 6.

Whiteface Mountain: Event 6								
Sample	Date	Time	Temp (K)	Pres (mb)	LWC (mg/m^3)	SO_2 (ppb)	O_3 (ppb)	H_2O_2 (ppb)
July22 01	7/22/98	2:00-2:30AM	289.99	847.73	146.57	2.48	65.8	0.523
July22 02	7/22/98	2:30-3:00AM	289.99	847.81	258.87	1.70	65.8	0.415
July22 03	7/22/98	3:00-3:30AM	289.92	847.86	370.40	1.15	65.9	0.367
July22 04	7/22/98	3:30-4:00AM	289.94	847.81	515.84	0.91	65.9	0.317

Table A.7: Davis, California sample conditions for event 1.

Davis, California: Event 1								
Sample	Date	Time	Temp (K)	Pres (mb)	LWC (mg/m^3)	SO_2 (ppb)	O_3 (ppb)	H_2O_2 (ppb)
Dec18 01	12/18/98	3:22-4:00AM	277.14	1013.99	67.95	0.571	1	0.491
Dec18 02	12/18/98	4:00-5:00AM	277.11	1013.68	177.71	0.646		0.494
Dec18 03	12/18/98	5:00-6:00AM	276.87	1013.50	246.02	0.475	3	0.494
Dec18 04	12/18/98	6:00-7:00AM	276.87	1013.73	218.30	0.696	1	0.543
Dec18 05	12/18/98	7:00-8:00AM	276.83	1013.98	188.03	0.620	1	0.522
Dec18 06	12/18/98	8:00-9:00AM	277.41	1014.23	249.89	1.033	2	0.529
Dec18 07	12/18/98	9:00-10:00AM	278.33	1014.50	243.30	1.769	2	0.538
Dec18 08	12/18/98	10:00-11:00AM	280.23	1014.03	113.05	1.640	2	0.540
Dec18 09	12/18/98	11:00-11:20AM	281.65	1013.28	53.04	1.715	3	0.540

Table A.8: Davis, California sample conditions for event 2. Note hydrogen peroxide data are unavailable.

Davis, California: Event 2								
Sample	Date	Time	Temp (K)	Pres (mb)	LWC (mg/m^3)	SO_2 (ppb)	O_3 (ppb)	H_2O_2 (ppb)
Jan04 01	1/4/99	8:08-9:00PM	277.20	1027.14	137.80	0.191	4	
Jan04 02	1/4/99	9:00-10:00PM	276.87	1027.28	116.77	0.321	2	
Jan04 03	1/4/99	10:00-11:00PM	276.52	1028.05	85.80	0.284	6	
Jan04 04	1/4/99	11:00-12:00AM	276.53	1028.15	72.63	0.159	4	
Jan04 05	1/5/99	12:00-1:00AM	276.00	1028.18	101.55	0.309	1	
Jan04 06	1/5/99	1:00-2:00AM	275.71	1027.99	89.68	0.254	1	
Jan04 07	1/5/99	2:00-3:00AM	275.53	1028.15	71.22	0.414	1	
Jan04 08	1/5/99	3:00-4:00AM	275.53	1027.50	65.78	0.392	1	
Jan04 09	1/5/99	4:00-5:00AM	275.64	1026.96	61.99	0.426		
Jan04 10	1/5/99	5:00-6:00AM	275.48	1027.10	78.56	0.473	2	
Jan04 11	1/5/99	6:00-7:00AM	275.50	1027.13	58.76	0.526	1	
Jan04 12	1/5/99	7:00-8:00AM	275.44	1027.29	50.76	0.679	1	
Jan04 13	1/5/99	8:00-10:00AM	275.92	1028.19	56.03	1.016	2.5	

Table A.9: Davis, California sample conditions for event 3.

Davis, California: Event 3								
Sample	Date	Time	Temp (K)	Pres (mb)	LWC (mg/m^3)	SO_2 (ppb)	O_3 (ppb)	H_2O_2 (ppb)
Jan09 01	1/9/99	3:00-4:00AM	274.90	1026.80	64.84	0.265		0.006
Jan09 02	1/9/99	4:00-5:00AM	275.77	1026.40	64.15	0.337	5	0.006
Jan09 03	1/9/99	5:00-6:00AM	276.07	1026.60	48.18	0.242	4	0.006
Jan09 04	1/9/99	6:00-7:00AM	276.23	1027.21	56.03	0.242	5	0.006
Jan09 05	1/9/99	7:00-8:00AM	276.19	1027.65	49.79	0.210	7	0.006
Jan09 06	1/9/99	8:00-9:00AM	276.23	1027.64	51.46	0.220	8	0.006
Jan09 07	1/9/99	9:00-10:00AM	276.38	1028.12	46.07	0.246	10	0.006
Jan09 08	1/9/99	10:00-10:36AM	276.71	1028.34	27.33	0.279	5.8	0.006

Table A.10: Davis, California sample conditions for event 4.

Davis, California: Event 4								
Sample	Date	Time	Temp (K)	Pres (mb)	LWC (mg/m^3)	SO_2 (ppb)	O_3 (ppb)	H_2O_2 (ppb)
Jan10 01	1/10/99	2:45-4:00AM	276.07	1023.05	56.85	0.109		0.006
Jan10 02	1/10/99	4:00-5:00AM	275.95	1023.11	56.84	0.102	8	0.006
Jan10 03	1/10/99	5:00-6:00AM	275.96	1023.53	55.42	0.051	7	0.006
Jan10 04	1/10/99	6:00-6:52AM	275.93	1023.85	46.29	0.050	8.5	0.006
Jan10 05	1/10/99	6:52-9:00AM	275.85	1023.91	44.68	0.070	8	0.006
Jan10 06	1/10/99	9:00-10:00AM	276.04	1024.05	34.68	0.105	5.714	0.006

Table A.11: Davis, California sample conditions for event 5.

Davis, California: Event 5								
Sample	Date	Time	Temp (K)	Pres (mb)	LWC (mg/m^3)	SO_2 (ppb)	O_3 (ppb)	H_2O_2 (ppb)
Jan10B 01	1/10/99	10:50-12:00AM	276.20	1020.11	45.02	0.130	7	0.136
Jan10B 02	1/11/99	12:00-1:00AM	276.04	1019.61	70.62	0.082	9.5	0.105
Jan10B 03	1/11/99	1:00-3:00AM	275.75	1019.80	51.87	0.060	8	0.116
Jan10B 04	1/11/99	3:00-5:00AM	275.55	1019.23	60.23	0.062	10	0.124
Jan10B 05	1/11/99	5:00-7:00AM	275.22	1018.44	67.61	0.114	6	0.121
Jan10B 06	1/11/99	7:00-8:00AM	274.91	1018.48	41.13	0.173	6	0.134
Jan10B 07	1/11/99	8:00-9:00AM	275.19	1018.75	71.47	0.244	10	0.138
Jan10B 08	1/11/99	9:00-9:42AM	275.52	1018.97	33.75	0.252	1	0.134

Table A.12: Davis, California sample conditions for event 6.

Davis, California: Event 6								
Sample	Date	Time	Temp (K)	Pres (mb)	LWC (mg/m^3)	SO_2 (ppb)	O_3 (ppb)	H_2O_2 (ppb)
Jan11 01	1/11/99	11:00-12:00AM	276.08	1019.03	69.36	0.104	1	0.033
Jan11 02	1/12/99	12:00-1:00AM	276.27	1019.08	71.83	0.114	5.5	0.057
Jan11 03	1/12/99	1:00-3:00AM	276.09	1019.39	54.71	0.077	7	0.077

Jan11 04	1/12/99	3:00-5:00AM	276.00	1019.56	70.26	0.050	4	0.058
Jan11 05	1/12/99	5:00-7:00AM	275.83	1020.15	51.45	0.063	2	0.079
Jan11 06	1/12/99	7:00-8:00AM	275.93	1020.55	56.73	0.226	5	0.046
Jan11 07	1/12/99	8:00-9:00AM	275.85	1020.88	56.79	0.145	7	0.063
Jan11 08	1/12/99	9:00-10:00AM	276.43	1021.05	43.30	0.209		0.063

Table A.13: Whiteface Mountain sample composition for event 1.

Whiteface Mountain: Event 1								
Sample	**Type**	**Mass (g)**	**pH**	**S(IV) (μM)**	**H_2O_2 (μM)**	**HCHO (μM)**	**Total Fe (μg/l)**	**Total Mn (μg/l)**
	CASCC2	68	4.61	0.039	8.403	3.826	6.78	0.44
July4 01	Small-sf	34.4	4.57	0.86	8.138	4.148	5.57	0.46
	Large-sf	251.7	4.67	0.45	8.417	3.274	6.14	0.46
	CASCC2	36.4	4.46				4.33	0.43
July4 02	Small-sf	25.4	4.43				6.22	0.47
	Large-sf	106.3	4.53				5.36	0.51
	CASCC2	60.5	4.28	0.72	14.217	4.510	4.44	0.61
July4 03	Small-sf	57.6	4.22	0		5.466	13.88	0.72
	Large-sf	179.5	4.22	0.45		4.561	6.61	0.57
	CASCC2	68.2	3.86	0.518	6.868	5.640	4.71	0.67
July4 04	Small-sf	74.9	3.84	0.45		4.676	10.66	0.68
	Large-sf	231.5	3.85	0.04		5.816	6.56	0.61
	CASCC2	85.9	4.28					
July4 05	Small-sf	67	4.07					
	Large-sf	341.7	4.23					
	CASCC2	85.7	4.45	0	1.488	3.380	9.1	0.75
July4 06	Small-sf	75.4	4.41				17.15	2.12
	Large-sf	243.2	4.45				5.01	0.53
	CASCC2	73.7	4.19	0.18			9.83	0.81
July4 07	Small-sf	71.9	4.21					
	Large-sf	243.1	4.18					
	CASCC2	71	4.22	0.72	10.337	3.757	6.2	0.47
July4 08	Small-sf	72.7	4.19	0.04		3.763	15.58	3.85
	Large-sf	237.8	4.22	0.45	9.583	3.588	7.98	0.57
	CASCC2	75.7	4.46	0.45	10.954	4.073	6.18	0.29
July4 09	Small-sf	64.3	4.41		9.614	3.597	12.64	0.94
	Large-sf	248.8	4.44		10.861	3.670	3.61	0.29
	CASCC2	85	4.59		12.305	2.269	6.49	0.29
July4 10	Small-sf	52	4.59			3.502	4.54	0.38
	Large-sf	283.2	4.58				4.28	0.21

Table A.14: Whiteface Mountain sample compositions for event 2.

Whiteface Mountain: Event 2								
Sample	Type	Mass (g)	pH	S(IV) (μM)	H_2O_2 (μM)	HCHO (μM)	Total Fe (μg/l)	Total Mn (μg/l)
	CASCC2	64.05	3.51	4.55	8.569	9.202	57.30	4.40
July7 01	Small-sf	70.8	3.59	2.36	7.851	11.809	30.04	1.18
	Large-sf	129.8	3.43	0.72	1.748	9.173	121.58	7.90
	CASCC2	94.55	3.55	1.54	11.490	8.694	50.70	3.30
July7 02	Small-sf	152	3.58	2.91	9.951	9.478	24.49	1.12
	Large-sf	342.1	3.48	2.77	11.396	9.004	72.31	4.78
	CASCC2	65.25	3.56	0.59	9.768	7.223	51.01	2.87
July7 03	Small-sf	140.9	3.58	1.82	9.170	8.263	15.24	1.01
	Large-sf	293.2	3.54	1.82	10.432	7.032	44.32	3.04
	CASCC2	101.05	3.55	1.27	5.415		33.09	2.02
July7 04	Small-sf	142.3	3.56	1.68	5.583		25.76	1.31
	Large-sf	305.7	3.55	2.64	6.397		40.72	2.40
	CASCC2	55.75	3.46				48.29	3.17
July7 05	Small-sf	72.9	3.45				25.23	1.41
	Large-sf	116	3.49				40.10	2.51
	CASCC2	46.55	3.33	2.09	16.582	6.042	45.76	3.10
July7 06	Small-sf	77	3.32	1.95	17.071	6.581	40.94	2.48
	Large-sf	70.7	3.31	2.77	15.983	4.470	113.00	4.96
	CASCC2	59.15	3.44				28.61	1.87
July7 07	Small-sf	70.6	3.39				40.11	3.00
	Large-sf	122.2	3.41				45.02	2.81
	CASCC2	57.75	3.45	0.72	9.649	5.802	28.57	2.05
July7 08	Small-sf	76.5	3.43	1.54	8.511	6.519	28.53	1.65
	Large-sf	114	3.47	2.64	9.021	5.993	36.59	2.17
	CASCC2	62.95	3.38				25.81	2.17
July7 09	Small-sf	80.6	3.39				25.17	1.54
	Large-sf	102.8	3.37				37.65	3.11
	CASCC2	62.05	3.44	2.23	9.037	5.698	40.22	2.36
July7 10	Small-sf	82.4	3.45	2.77	7.669	6.412	77.61	2.42
	Large-sf	130.5	3.41	3.18	7.830	5.808	38.04	3.26
	CASCC2	60.25	3.39				34.82	2.55
July7 11	Small-sf	73.2	3.83				24.31	1.55
	Large-sf	127.8	3.38				33.74	2.83
	CASCC2	34.15	3.2	3.05	14.893	5.968	54.08	4.08
July7 12	Small-sf	63.9	3.22	2.64	12.108	6.665	38.92	2.67
	Large-sf	56	3.34	2.77	6.317	5.513	39.16	3.16
	CASCC2	41.85	3.2				112.27	4.03
July7 13	Small-sf	66.4	3.13				47.22	3.35
	Large-sf	78	3.22				50.34	4.75

	CASCC2	18.85	2.95	0.18	18.596	7.507	73.15	6.02
July7 14	Small-sf	36.8	2.96	3.05	15.936	8.301	61.12	4.77
	Large-sf	20	3.23	2.50	8.606	5.865	40.96	3.55
	CASCC2	25.95	2.92				78.32	5.62
July7 15	Small-sf	55	2.92				73.54	4.98
	Large-sf	31.7	2.94				100.93	8.27
	CASCC2	50.05	3.28	0.31	7.394	4.292	37.13	2.27
July7 16	Small-sf	69.9	3.24	0.86		5.851	36.80	1.92
	Large-sf	89.3	3.17	2.77		5.425	44.72	3.81
	CASCC2	73.35	3.23	0.72	6.457	4.633	33.07	2.10
July7 17	Small-sf	120.2	3.22	2.91	6.015	10.182	32.03	1.72
	Large-sf	122.2	3.2	2.23	19.805	5.016	35.29	3.07
	CASCC2	92.15	3.33				20.68	1.19
July7 18	Small-sf	137.5	3.38				24.11	1.21
	Large-sf	172.1	3.32				40.68	1.92
	CASCC2	14.25	3.07	0	7.209	6.224	36.21	2.60
July7 19	Small-sf	30.7	3.46	1.54	6.801	6.716	33.66	1.76
	Large-sf	0	3.2	2.50	4.709	5.025	33.22	2.30

Table A. 15: Whiteface Mountain sample compositions for event 3.

Whiteface Mountain: Event 3								
Sample	Type	Mass (g)	pH	S(IV) (μM)	H_2O_2 (μM)	HCHO (μM)	Total Fe (μg/l)	Total Mn (μg/l)
	CASCC2	39.85	2.88				188.63	17.64
July16 01	Small-sf	74.9	2.79	0.18	67.480	13.940	150.64	12.60
	Large-sf	83.1	2.85	1.13	51.130	12.010	441.54	46.02
	CASCC2	60.95	3	1.00	13.591	12.972	173.89	14.47
July16 02	Small-sf	80.6	2.94	0.31	14.510	13.717	74.31	6.78
	Large-sf	123.3	3.04	0.04	14.150	12.808	414.04	28.00
	CASCC2	64.35	3.05	0	15.297	12.407	182.80	14.67
July16 03	Small-sf	80.1	2.99	0.45	14.207	16.001	57.69	5.99
	Large-sf	130.7	3.04	0.86	15.906	11.907	268.07	25.22
	CASCC2	40.65	2.98	0.59	49.826	12.015	291.48	26.46
July16 04	Small-sf	67	2.96	0.72	46.834	12.218	92.29	9.55
	Large-sf	60.6	3.04	0.04	46.450	11.387	471.02	48.30
	CASCC2	54.45	2.96	0.72	28.410	11.765	448.56	27.67
July16 05	Small-sf	78.5	2.93	0.86	29.190	12.242	101.11	9.21
	Large-sf	64.5	2.93	0.31	29.161	11.519	557.48	56.80
	CASCC2	36.65	2.95	1.54	33.791	10.813	428.10	33.74
July16 06	Small-sf	72	2.94				113.24	11.20
	Large-sf	49.4	2.96				646.25	77.08
	CASCC2	19.95	2.84				484.75	55.19
July16 07	Small-sf	38.8	2.84				174.07	15.64
	Large-sf	22.1	2.9				633.71	106.56

	CASCC2	0.35	2.77					
July16 08	Small-sf	1.2	2.74				467.15	28.13
	Large-sf	3.4	2.89				1159.18	169.62

Table A. 16: Whiteface Mountain sample compositions for event 4.

Whiteface Mountain: Event 4								
Sample	Type	Mass (g)	pH	S(IV) (μM)	H_2O_2 (μM)	HCHO (μM)	Total Fe (μg/l)	Total Mn (μg/l)
	CASCC2	40.9	3.01				208.47	17.58
July17 01	Small-sf	77.5	3.02				96.53	6.83
	Large-sf	41.1	2.97				508.06	47.98
	CASCC2	99	3.05	1.41	45.964	8.001	236.30	14.78
July17 02	Small-sf	190.1	3.06	0.59	48.340	8.316	67.94	4.88
	Large-sf	111.3	3.00	1.13	49.418	7.810	529.18	42.33
	CASCC2	83.1	3.09				188.67	12.87
July17 03	Small-sf	132.1	3.10				54.68	4.20
	Large-sf	114.7	3.06				413.79	29.64
	CASCC2							
July17 04	Small-sf	162.7	3.18	2.23		6.975	54.43	4.57
	Large-sf	179.1	3.16	1.00		5.386	244.94	17.22
	CASCC2	133	3.15				47.15	3.45
July17 05	Small-sf	169.8	3.17				148.08	10.48
	Large-sf	243.4	3.13				188.62	16.91
	CASCC2	130.2	3.18	1.13	43.856	8.095	135.76	10.00
July17 06	Small-sf	156.3	3.19				48.51	3.69
	Large-sf	322.1	3.16	0.45	44.950	6.325	185.43	15.41
	CASCC2	148.9	3.16				123.77	8.49
July17 07	Small-sf	164.2	3.17	1.27	45.478	8.258	74.75	5.05
	Large-sf	341.7	3.13				163.98	12.73
	CASCC2							
July17 08	Small-sf	185.3	3.27	0.72	4.136	7.170	39.42	2.44
	Large-sf	392.1	3.21	0.04	5.315	6.017	92.41	7.22
	CASCC2	151.3	3.27				79.33	5.50
July17 09	Small-sf	163.9	3.26				35.76	2.25
	Large-sf	341.7	3.25				90.89	7.04
	CASCC2	133.1	3.32	0	21.403	5.263	67.53	4.46
July17 10	Small-sf	215.8	3.29	2.64	19.771	6.172	34.18	2.18
	Large-sf	292.1	3.29	0.18	22.119	4.988	81.43	6.14

Table A.17: Whiteface Mountain sample compositions for event 5.

Whiteface Mountain: Event 5								
Sample	Type	Mass (g)	pH	S(IV) (μM)	H_2O_2 (μM)	HCHO (μM)	Total Fe (μg/l)	Total Mn (μg/l)
	CASCC2	93.6	3.61	0.16	0.466	7.754	44.86	2.38
July20 01	Small-sf	95.1	3.59	0.30	0.154	9.360	22.28	1.24
	Large-sf	209.6	3.58	1.36	0.196	8.550	103.28	4.91
	CASCC2	90	3.5	0.65	1.921	7.846	44.76	3.45
July20 02	Small-sf	95.5	3.5	0.94	0.865	8.211	37.95	1.88
	Large-sf	201.4	3.51	1.58	0.945	9.162	53.11	4.62
	CASCC2	74	3.37	1.79	3.368	10.807	50.27	3.50
July20 03	Small-sf	87.4	3.36	0.94	2.174	7.478	23.82	1.49
	Large-sf	137.6	3.33	0.37	2.715	6.264	62.52	5.03
	CASCC2	71.2	3.36	0.16	12.265	9.922	77.92	5.76
July20 04	Small-sf	82.6	3.3	0.87	9.345	7.085	31.27	1.92
	Large-sf	135.8	3.34	0.30	9.974	6.164	65.55	5.98
	CASCC2	45.4	3.16	0.54	18.868	11.001	58.76	4.46
July20 05	Small-sf	75.1	3.17	0.23	14.726	6.897	40.48	2.70
	Large-sf	63.7	3.17	1.51	13.282	6.563	96.24	9.22
	CASCC2	38.2	3.1	0.61	22.244	10.912	76.53	6.09
July20 06	Small-sf	62.6	3.09	0.65	20.701	7.292	39.37	3.15
	Large-sf	43.1	3.07	0.51	17.534	7.388	95.14	11.65
	CASCC2	31.8	3.05	0.99	29.656	11.678	76.58	7.30
July20 07	Small-sf	58.8	3.04	1.08	28.756	7.580	46.74	3.31
	Large-sf	34.6	3.04	1.22	25.049	7.159	111.97	13.94
	CASCC2	20.1	2.96				106.59	10.56
July20 08	Small-sf	45.9	2.98				51.80	4.12
	Large-sf	23.7	2.994				165.21	15.70

Table A.18: Whiteface Mountain sample compositions for event 6.

Whiteface Mountain: Event 6								
Sample	Type	Mass (g)	pH	S(IV) (μM)	H_2O_2 (μM)	HCHO (μM)	Total Fe (μg/l)	Total Mn (μg/l)
	CASCC2	19.8	3.32	0.39	77.723	16.695	259.57	17.40
July22 01	Small-sf	40.4	3.41	0.24	71.714	19.455	112.73	9.77
	Large-sf	16.2	3.41	0.39	61.536	15.851	464.45	68.98
	CASCC2	36.3	3.48	0.99	59.398	14.788	225.36	15.59
July22 02	Small-sf	61.5	3.39	0.69	57.902	17.063	102.92	7.60
	Large-sf	32.3	3.48	0.84	57.848	18.621	578.96	76.71
	CASCC2	48	3.68	0.99	31.400	11.363	110.74	8.76
July22 03	Small-sf	79	3.6	0.39	33.490	14.044	74.92	4.46
	Large-sf	66.8	3.63	0.69	33.039	13.337	278.77	25.76
	CASCC2	63.7	3.78	0.69	25.102	10.303	96.07	7.07
July22 04	Small-sf	92.7	3.77	1.88	24.683	12.876	52.14	4.08
	Large-sf	135.3	3.76	0.39	11.100	10.667	195.72	

Table A.19: Davis, CA sample compositions event 1. Note pH for small-sf sample 1 is not available due to small volume collected.

Davis, California: Event 1								
Sample	Type	Mass (g)	pH	S(IV) (μM)	H_2O_2 (μM)	HCHO (μM)	Total Fe (μg/l)	Total Mn (μg/l)
	CASCC2	5.4	5.52					
Dec18 01	Small-sf	0.18	N/a					
	Large-sf	18.2	6.03					
	CASCC2	41.7	5.9	6.06	1.52	20.94	189.15	9.85
Dec18 02	Small-sf	7.2	5.68			29.15		
	Large-sf	161	6.08	8.27	1.57	20.15	189.20	10.42
	CASCC2	72.3	5.78	4.44		21.17	105.01	4.69
Dec18 03	Small-sf	14.8	5.6					
	Large-sf	244	5.9	0.02				
	CASCC2	60.3	5.9	3.14		29.16	108.63	4.90
Dec18 04	Small-sf	11.8	5.47			31.44		
	Large-sf	207	6.08			30.84		
	CASCC2	65.9	6.18	3.51	1.52	31.02	104.82	6.26
Dec18 05	Small-sf	16.5	5.88			37.64		
	Large-sf	206	6.34			29.69		
	CASCC2	71.1	6.26	4.44	3.55	42.77	119.85	5.50
Dec18 06	Small-sf	20.2	5.8			40.69		
	Large-sf	238	6.38			45.33		
	CASCC2	56.9	6.48	7.92	5.90	13.90	139.54	5.70
Dec18 07	Small-sf	21.2	6.31			61.64		
	Large-sf	187	6.56			54.15		
	CASCC2	36.4	6.4	4.32	10.52	41.91	273.19	9.59
Dec18 08	Small-sf	11.9	6.39			59.42		
	Large-sf	127	6.68			55.89		
	CASCC2	6.2	6.42					
Dec18 09	Small-sf	2.48	6.36					
	Large-sf	14.7	6.69					

Table A.20: Davis, CA sample compositions event 2.

Davis, CA: Event 2								
Sample	Type	Mass (g)	pH	S(IV) (μM)	H_2O_2 (μM)	HCHO (μM)	Total Fe (μg/l)	Total Mn (μg/l)
	CASCC2	37.3	6.45	1.96		22.28	85.24	3.14
Jan04 01	Small-sf	0						
	Large-sf	151	6.55	0.02	11.74	22.53	116.49	3.13
	CASCC2	45.5	6.4	3.56	6.88	22.71	93.51	3.05
Jan04 02	Small-sf	5.6	6.45	6.34	8.36	36.38	335.91	5.85
	Large-sf	178	6.05	1.42	6.29	19.14	114.18	3.31
	CASCC2	35.4	6.63	1.90	4.64	20.88	56.95	2.57
Jan04 03	Small-sf	11	6.31	7.15	5.59	42.04	145.53	4.64
	Large-sf	131	6.66		3.92	18.69	84.80	3.14
	CASCC2	34.7	6.48	1.42	3.67	19.51	55.27	2.74
Jan04 04	Small-sf	12	6.29		4.51	25.51	120.12	4.47
	Large-sf	125	6.56	1.32	4.39	18.16	57.68	2.43
	CASCC2	41.5	6.5	2.11	2.50	18.49	67.34	2.28
Jan04 05	Small-sf	12	6.11				111.10	4.13
	Large-sf	156	6.45				101.33	2.75
	CASCC2	41.7	6.6	1.88	2.49	17.29	72.60	2.35
Jan04 06	Small-sf	10.1	6.24					
	Large-sf	165	6.57					
	CASCC2	37.6	6.59	2.46	2.66	23.71	78.20	2.67
Jan04 07	Small-sf	6.58	6.21				129.47	5.04
	Large-sf	146	6.64				97.63	3.02
	CASCC2	38.2	6.53	5.37	3.50	27.44	89.35	3.05
Jan04 08	Small-sf	6.9	6.2				151.14	6.28
	Large-sf	146	6.57				101.54	2.90
	CASCC2	36.3	6.4					
Jan04 09	Small-sf	7.68	6.13					
	Large-sf	135	6.79					
	CASCC2	35.5	6.32	4.09	5.14	39.33	100.97	3.79
Jan04 10	Small-sf	16.8	6.15					
	Large-sf	128	6.37					
	CASCC2	33.6	6.32					
Jan04 11	Small-sf	9.08	6.05					
	Large-sf	123	6.28					
	CASCC2	32.1	6.54	3.97	4.19	52.13	64.27	3.20
Jan04 12	Small-sf	9.6	6.34					
	Large-sf	84.3	6.7					
	CASCC2	46.9	6.55					
Jan04 13	Small-sf	16.6	6.36					
	Large-sf	165	6.7					

Table A.21: Davis, CA sample composition event 3.

Davis, CA: Event 3								
Sample	Type	Mass (g)	pH	S(IV) (μM)	H_2O_2 (μM)	HCHO (μM)	Total Fe (μg/l)	Total Mn (μg/l)
	CASCC2	35.4	6.7	2.96	10.27	38.97	34.44	3.02
Jan09 01	Small-sf	2.18	6.48	12.80				
	Large-sf	114	6.7	3.63		37.07	42.28	3.29
	CASCC2	37.7	6.7	2.46		49.55	55.00	4.44
Jan09 02	Small-sf	12.3	6.64	9.43		62.79	89.89	6.88
	Large-sf	115	6.8	7.11		44.37	58.13	3.79
	CASCC2	23.8	6.66	4.20		82.14	94.63	7.85
Jan09 03	Small-sf	14.3	6.41	14.31		90.52	147.07	9.44
	Large-sf	59.1	6.66	2.81		70.59	164.71	9.07
	CASCC2	15.8	6.65	6.41	26.99	106.39	198.70	13.26
Jan09 04	Small-sf	10.4	6.35	13.08		112.86	127.49	10.98
	Large-sf	39.9	6.45	2.23		79.37	278.89	15.39
	CASCC2	13.7	6.59	8.29	29.01	101.46	191.56	21.02
Jan09 05	Small-sf	7.78	6.23	13.49		130.86	203.61	15.76
	Large-sf	15.8	6.82	2.23		91.60	234.65	21.02
	CASCC2	14.2	6.57	8.58	29.16	124.19	272.20	26.86
Jan09 06	Small-sf	3.6	6.26			153.28	277.88	15.50
	Large-sf	36.7	6.78	2.00		91.43	222.67	25.07
	CASCC2	12.9	6.75	6.95	38.78	107.84	284.17	16.70
Jan09 07	Small-sf	1.28	6.1				514.66	22.11
	Large-sf	37.7	6.82	2.11		98.25	230.05	21.50
	CASCC2	4.9	6.68					
Jan09 08	Small-sf	0.7	6.05					
	Large-sf	15	6.89					

Table A.22: Davis, CA sample compositions event 4.

Davis, CA: Event 4								
Sample	Type	Mass (g)	pH	S(IV) (μM)	H_2O_2 (μM)	HCHO (μM)	Total Fe (μg/l)	Total Mn (μg/l)
	CASCC2	25.9	6.51	7.92	35.49	105.49	185.66	17.17
Jan10 01	Small-sf	7.78	6.27			84.34	127.45	12.19
	Large-sf	76	6.59	1.77		73.58	190.60	16.43
	CASCC2	16.7	6.55	5.54	20.08	115.98	193.95	14.67
Jan10 02	Small-sf	0.6	5.94					
	Large-sf	46.6	6.61			87.61	163.56	11.80
	CASCC2	11.8	6.5	7.42	33.70	134.02	327.40	13.13
Jan10 03	Small-sf	1.38	5.93				373.51	14.93
	Large-sf	34	6.55			108.00	140.08	11.96
	CASCC2	8.2	5.64	11.60	25.03	121.13	286.51	15.81

Jan10 04	Small-sf	0.6	5.69					
	Large-sf	1.4	5.69			104.15	238.11	9.75
	CASCC2	19.1	5.94	7.96	26.62	127.84	219.08	11.65
Jan10 05	Small-sf	0.78	5.59					
	Large-sf	44.9	6.27			97.57	178.49	8.13
	CASCC2	9	5.94	7.69	26.00	126.98	225.79	11.12
Jan10 06	Small-sf	0.5	5.48	5.41				
	Large-sf	27.1	6.27			104.04	182.56	8.51

Table A.23: Davis, CA sample compositions for event 5.

Davis, CA: Event 5								
Sample	**Type**	**Mass (g)**	**pH**	**S(IV) (μM)**	**H_2O_2 (μM)**	**HCHO (μM)**	**Total Fe (μg/l)**	**Total Mn (μg/l)**
	CASCC2	31.9	5.98	1.10	20.33	82.48	112.64	5.82
Jan10B 01	Small-sf	4.78	6.05	6.06		30.47		
	Large-sf	116	6.07	0.18	22.83	60.38	131.01	6.07
	CASCC2	25.3	5.65	3.71	18.40	78.94	97.09	5.28
Jan10B 02	Small-sf	6.3	5.72	2.66		61.81	95.48	6.57
	Large-sf	86.9	5.81	0.44		62.78	87.02	4.44
	CASCC2	30.1	5.51	1.49	15.28	66.44	87.40	4.79
Jan10B 03	Small-sf	7.48	5.56	4.10		71.55	122.87	8.66
	Large-sf	100	5.66	0.70		57.26	93.28	4.60
	CASCC2	35	5.76	1.81	11.02	57.96	82.37	4.84
Jan10B 04	Small-sf	11	5.47	2.14		100.75	171.16	9.68
	Large-sf	105	6.12	1.49		45.36	94.89	5.10
	CASCC2	40.9	5.84	5.01	8.69	36.72	52.27	3.30
Jan10B 05	Small-sf	12.2	5.78	7.60		64.50	102.81	7.27
	Large-sf	129	6.04	0.69		34.26	51.38	3.33
	CASCC2	20.5	6.38	2.27	8.42	30.16	183.04	3.78
Jan10B 06	Small-sf	6.8	5.79	2.40		62.94	135.63	8.42
	Large-sf	63	6.64	1.36		26.31	60.98	2.25
	CASCC2	17.8	6.68	4.19	8.45	30.46	96.68	3.86
Jan10B 07	Small-sf	8.38	6.36	4.04		41.97	217.91	23.28
	Large-sf	58	6.87	1.75		28.09	107.42	3.71
	CASCC2	4	6.69	2.96	11.37	43.88	136.21	5.33
Jan10B 08	Small-sf	2.6	6.39	3.23		50.67	189.18	12.37
	Large-sf	15.5	6.94	3.10		37.25	171.38	6.66

Table A.24: Davis, CA sample compositions for event 6.

Davis, CA: Event 6								
Sample	Type	Mass (g)	pH	S(IV) (μM)	H_2O_2 (μM)	HCHO (μM)	Total Fe (μg/l)	Total Mn (μg/l)
	CASCC2	38.1	6.06	3.84	4.82	40.99	76.50	4.15
Jan11 01	Small-sf	4.08	6.35	6.61		15.27	83.71	5.17
	Large-sf	125	6.41	1.23		37.98	84.30	3.44
	CASCC2	39	6.2	4.88	11.99	55.45	96.77	5.32
Jan11 02	Small-sf	9.3	6.08	8.50	3.74	62.18	113.19	7.58
	Large-sf	116	6.21	0.03	12.49	61.30	102.12	4.80
	CASCC2	65.7	6.31	2.22	10.19	44.24	55.09	3.60
Jan11 03	Small-sf	12.3	6	11.94		59.43	114.95	7.42
	Large-sf	202	6.2	0.31		34.31	66.04	2.90
	CASCC2	42.7	6.07	2.27	10.74	33.61	85.87	4.33
Jan11 04	Small-sf	9.5	5.77	10.24		51.70	178.75	10.03
	Large-sf	127	6.05	0		26.97	81.27	4.12
	CASCC2	57.7	6.18	0.83	7.16	29.12	61.68	2.96
Jan11 05	Small-sf	11.1	5.73	7.55		43.15	103.24	6.97
	Large-sf	171	6.36	0.18		27.19	93.45	2.80
	CASCC2	29.2	6.44	2.40	7.64	38.43	116.46	6.10
Jan11 06	Small-sf	6	5.79	7.42		52.67	97.17	6.37
	Large-sf	92.6	6.49	1.23		39.15	134.24	5.15
	CASCC2	18	6.3	2.92	10.81	42.07	141.98	6.88
Jan11 07	Small-sf	6.68	5.64	7.15	4.15	48.80	96.42	5.20
	Large-sf	57.3	6.47	2.01	10.07	33.64	196.94	7.18
	CASCC2	12.5	6.38	2.79	16.68	44.59	145.17	7.04
Jan11 08	Small-sf	4.7	5.97			58.63	90.14	7.32
	Large-sf	32	6.52	0.57		40.96	219.49	10.43

Table A.25: Whiteface Mountain inorganic ion data for CASCC2 samples

CASCC2										
Sample	**Time**	**pH**	**Cl^-**	**NO_3^-**	**SO_4^{2-}**	**Na^+**	**NH_4^+**	**K^+**	**Mg^{2+}**	**Ca^{2+}**
July4 01	9:45-10:30PM	4.61	2.09	10.67	20.97	1.68	15.83	1.65	2.51	9.58
July4 02	10:30-11PM	4.46	1.99	13.69	26.63	1.44	17.11	1.53	2.53	8.63
July4 03	11PM-12AM	4.28	1.94	24.37	41.98	1.79	22.16	1.75	2.96	15.81
July4 04	12-1AM	3.86	4.24	82.58	69.59	4.13	29.54	2.53	3.74	17.42
July4 05	1-2AM	4.28	0.00	27.91	28.85	0.85	15.41	1.18	2.80	10.27
July4 06	2-3AM	4.45	4.40	15.95	22.73	4.57	9.97	2.47	2.80	9.52
July4 01	3-4AM	4.19	2.25	25.81	47.33	1.91	17.21	1.56	3.08	13.72
July4 07	4-5AM	4.22	0.00	17.52	40.56	1.09	15.06	1.26	2.85	10.16
July4 08	5-6AM	4.46	0.00	9.71	23.16	0.75	12.18	1.04	2.28	5.57
July4 09	6-7AM	4.59	0.00	6.45	15.98	0.70	8.49	0.96	2.19	4.24
July7 01	12:30-1PM	3.51	12.14	149.12	237.86	0.94	148.05	4.83	6.11	31.31
July7 02	1-2PM	3.55	12.80	143.62	230.36	1.08	146.10	2.64	5.26	23.92
July7 03	2-3PM	3.56	9.24	130.44	235.75	0.73	133.27	2.17	5.94	17.53
July7 04	3-4PM	3.55	12.78	89.50	241.12	5.81	104.53	4.59	4.14	16.19
July7 05	4-4:30PM	3.46	11.43	125.31	294.64	2.59	125.03	4.77	4.39	14.35
July7 06	4:30-5PM	3.33	14.42	147.60	410.77	4.26	160.02	7.21	4.57	16.62
July7 07	5-5:30PM	3.44	9.10	92.91	290.86	3.27	118.32	4.92	4.11	17.77
July7 08	5:30-6PM	3.45	9.34	90.46	322.99	2.58	116.94	4.38	7.87	35.77
July7 09	6-6:30PM	3.37	7.14	86.52	369.23	1.69	127.36	3.51	3.97	14.66
July7 10	6:30-7PM	3.44	7.38	76.23	328.30	2.55	114.39	4.27	4.02	13.25
July7 11	7-7:30PM	3.39	8.15	80.32	389.69	3.25	125.95	4.91	3.95	17.58
July7 12	7:30-8PM	3.20	9.27	142.00	614.81	2.64	182.26	5.53	4.84	18.24
July7 13	8-8:30PM	3.20	9.07	138.89	615.13	2.16	176.30	4.86	4.59	16.74
July7 14	8:30-9PM	2.95	13.78	208.40	1254.21	3.91	301.51	8.97	7.48	24.32
July7 15	9-9:30PM	2.92	11.39	209.52	1319.69	3.67	317.11	7.98	10.63	30.15
July7 16	9:30-10PM	3.28	6.81	85.37	470.28	1.84	141.97	4.25	3.81	14.63
July7 17	10-11PM	3.23	8.41	95.30	591.56	2.55	159.27	3.56	3.25	11.14
July7 18	11PM-12AM	3.33	7.62	76.71	420.62	1.24	125.08	2.71	2.94	10.05
July7 19	12-12:50AM	3.07	14.57	161.66	896.76	4.73	244.69	7.11	4.06	17.49
July16 01	7:25-8AM	2.88	29.75	399.99	987.84	3.02	503.22	5.93	28.08	78.38
July16 02	8-8:30AM	3.00	25.46	353.94	852.85	2.40	458.68	4.97	23.00	68.01
July16 03	8:30-9AM	3.05	26.60	343.60	782.10	2.73	393.10	3.67	22.56	69.64
July16 04	9-9:30AM	2.98	34.74	580.48	1069.70	3.66	541.58	2.92	36.17	129.31
July16 05	9:30-10AM	2.96	39.54	588.38	1081.93	4.18	560.11	6.55	42.49	141.59
July16 06	10-10:30AM	2.95	44.08	679.09	1146.86	4.47	596.23	6.80	46.98	179.23
July16 07	10:30-11AM	2.84	58.50	974.64	773.75	6.83	894.50	10.38	68.74	307.12

July17 01	1:30-2AM	3.01	25.22	468.42	1247.98	5.03	576.17	6.72	34.59	96.04
July17 02	2-3AM	3.05	18.72	383.23	1010.46	4.37	441.89	4.46	25.02	74.51
July17 03	3-4AM	3.09	17.94	307.45	924.39	3.56	381.53	4.56	22.71	68.85
July17 04	4-5AM									
July17 05	5-6AM	3.17	18.00	290.76	610.75	3.58	275.94	3.86	19.84	50.28
July17 06	6-7AM	3.18	15.48	322.60	580.51	3.79	306.51	3.94	18.22	47.91
July17 07	7-8AM	3.16	15.60	286.86	590.47	2.66	252.04	2.79	14.80	49.03
July17 08	8-9AM	3.27	12.72	190.79	505.61	2.26	215.78	3.04	10.67	31.34
July17 09	9-10AM									
July17 10	10-11AM	3.32	9.69	158.90	468.71	3.99	218.24	2.25	11.71	35.49
July20 01	9-9:30AM	3.61	9.52	82.01	243.23	1.42	150.19	2.73	6.43	26.63
July20 02	9:30-10AM	3.50	9.45	120.19	281.58	2.10	163.13	2.99	7.06	28.56
July20 03	10-10:30AM	3.37	12.02	154.56	375.33	0.27	167.13	2.60	7.31	26.21
July20 04	10:30-11AM	3.36	15.80	174.12	447.47	1.57	201.52	2.99	8.52	32.60
July20 05	11-11:30AM	3.16	19.03	231.06	681.73	1.99	282.05	3.85	10.17	37.79
July20 06	11:30AM-12PM	3.10	16.56	248.29	800.03	2.17	338.81	5.10	11.27	38.58
July20 07	12-12:30PM	3.05	19.19	268.85	928.53	5.01	391.88	8.76	14.16	42.95
July20 08	12:30-1PM	2.96	21.79	297.73	1174.99	3.07	509.76	7.41	16.70	49.45
July22 01	2-2:30AM	3.32	33.70	366.49	749.51	9.65	650.68	11.66	37.35	127.04
July22 02	2:30-3AM	3.48	23.51	219.25	517.01	8.47	471.48	10.41	25.81	82.02
July22 03	3-3:30AM	3.68	11.55	128.96	348.28	4.94	296.84	6.24	15.48	51.03
July22 04	3:30-4AM	3.78	8.55	81.75	225.61	3.53	182.87	5.77	11.23	43.04

Table A.26: Whiteface Mountain inorganic ions for the Large-sf.

Large-sf Sample	Time	pH	Cl^-	NO_3^-	SO_4^{2-}	Na^+	NH_4^+	K^+	Mg^{2+}	Ca^{2+}
July4 01	9:45-10:30PM	4.66	0.00	9.22	20.11	0.87	13.71	1.02	2.68	14.00
July4 02	10:30-11PM	4.53	0.00	11.96	22.81	1.08	16.41	1.29	2.37	11.51
July4 03	11PM-12AM	4.22	0.00	22.96	37.78	1.17	19.85	1.44	2.56	18.17
July4 04	12-1AM	3.84	2.64	78.60	61.79	1.99	26.87	1.62	2.77	20.53
July4 05	1-2AM	4.22	0.00	30.86	26.48	0.78	15.62	1.03	2.38	7.21
July4 06	2-3AM	4.45	3.60	15.64	20.96	2.92	14.29	1.99	2.44	8.26
July4 01	3-4AM	4.18	2.90	24.29	40.79	2.08	18.64	1.73	2.90	11.22
July4 07	4-5AM	4.22	1.93	18.04	36.20	0.99	15.44	1.22	9.29	24.15
July4 08	5-6AM	4.44	0.00	9.23	22.70	0.61	12.14	0.88	2.85	5.25
July4 09	6-7AM	4.58	0.00	5.44	14.27	0.52	8.69	0.78	2.34	2.91
July7 01	12:30-1PM	3.48	16.97	161.87	294.51	0.92	159.55	4.87	10.84	49.70
July7 02	1-2PM	3.54	13.50	153.92	259.38	0.40	152.88	3.66	7.77	35.78
July7 03	2-3PM	3.55	11.15	136.20	239.22	0.58	135.73	3.26	5.34	23.05
July7 04	3-4PM	3.49	8.33	93.53	233.02	1.54	109.82	3.08	4.23	15.93
July7 05	4-4:30PM	3.31	7.49	94.96	256.17	1.10	107.25	2.68	3.92	14.44
July7 06	4:30-5PM	3.41	13.08	149.74	413.58	2.63	156.92	4.25	4.86	30.23

July7 07	5-5:30PM	3.47	8.15	93.79	294.86	1.84	113.90	3.77	3.79	13.99
July7 08	5:30-6PM	3.37	6.88	81.81	279.29	1.14	103.16	2.83	3.57	11.87
July7 09	6-6:30PM	3.41	7.78	94.18	380.03	1.93	126.90	4.12	4.06	13.80
July7 10	6:30-7PM	3.38	6.71	77.22	342.74	1.68	113.90	3.54	3.78	12.77
July7 11	7-7:30PM	3.34	6.56	81.09	373.20	1.73	115.50	2.99	3.80	12.02
July7 12	7:30-8PM	3.22	7.72	88.74	421.75	2.32	127.57	3.68	4.11	12.46
July7 13	8-8:30PM	3.23	8.35	132.04	576.61	1.94	162.16	4.64	5.17	19.31
July7 14	8:30-9PM	2.94	7.70	121.59	505.98	1.54	147.93	3.98	4.90	14.23
July7 15	9-9:30PM	3.17	11.08	193.69	1219.96	2.76	293.98	7.64	6.88	25.29
July7 16	9:30-10PM	3.20	8.04	124.99	628.88	1.73	173.22	4.68	4.68	14.99
July7 17	10-11PM	3.32	8.80	95.11	587.90	2.18	166.75	5.43	4.37	11.42
July7 18	11PM-12AM	3.20	9.76	80.30	463.41	3.72	143.88	6.87	10.61	14.74
July7 19	12-12:50AM	2.85	13.15	127.23	631.64	5.81	188.21	7.71	4.51	17.56
July16 01	7:25-8AM	3.04	38.02	535.30	974.12	5.47	515.30	7.97	58.83	217.98
July16 02	8-8:30AM	3.04	29.68	370.88	731.86	3.68	375.49	5.72	37.44	121.24
July16 03	8:30-9AM	3.04	26.31	345.02	682.32	3.51	368.37	5.06	37.39	122.23
July16 04	9-9:30AM	2.93	39.17	607.13	924.04	6.64	476.34	8.70	58.27	235.07
July16 05	9:30-10AM	2.96	46.46	701.26	1008.74	8.18	556.23	9.73	71.44	293.44
July16 06	10-10:30AM	2.90	52.14	931.64	1142.31	8.33	594.50	10.52	98.27	414.94
July16 07	10:30-11AM	2.89	63.99	1246.23	1333.27	11.70	715.76	14.49	140.02	629.07
July17 01	1:30-2AM	2.97	38.00	658.28	1486.77	10.38	642.31	9.66	91.24	348.06
July17 02	2-3AM	3.00	28.32	569.16	1273.32	8.33	533.64	8.35	80.18	268.28
July17 03	3-4AM	3.05	25.02	402.58	1055.40	6.50	419.23	6.67	52.26	174.00
July17 04	4-5AM	3.16	17.71	246.11	793.06	4.76	304.27	4.87	35.18	93.92
July17 05	5-6AM	3.13	20.93	327.27	649.49	4.10	279.07	3.78	37.84	83.82
July17 06	6-7AM	3.16	17.88	344.00	592.40	3.65	295.85	3.46	31.42	71.58
July17 07	7-8AM	3.13	18.10	309.67	602.84	2.74	245.62	2.11	25.02	57.92
July17 08	8-9AM	3.21	16.37	220.66	499.39	5.23	206.55	3.39	15.60	44.18
July17 09	9-10AM	3.25	12.98	196.67	505.06	2.36	209.52	1.60	13.65	44.14
July17 10	10-11AM	3.30	10.01	165.50	469.85	2.61	217.59	2.88	15.62	38.44
July20 01	9-9:30AM	3.58	9.84	85.49	229.91	0.37	133.70	2.17	7.26	37.75
July20 02	9:30-10AM	3.51	9.36	118.62	259.27	0.28	133.59	2.33	7.54	35.95
July20 03	10-10:30AM	3.33	13.63	161.84	394.74	0.37	168.09	2.80	10.13	40.50
July20 04	10:30-11AM	3.34	14.59	167.40	414.33	0.29	172.12	2.77	11.51	42.20
July20 05	11-11:30AM	3.17	17.16	215.13	595.61	0.97	228.76	3.87	14.85	49.50
July20 06	11:30AM-12PM	3.07	18.73	252.02	790.18	1.77	290.73	4.08	17.87	54.55
July20 07	12-12:30PM	3.04	20.57	294.26	958.64	2.47	360.03	5.85	23.84	66.01
July20 08	12:30-1PM	2.99	23.52	311.67	1101.33	2.98	411.73	8.10	27.70	78.31
July22 01	2-2:30AM	3.41	39.48	458.80	813.77	21.46	672.80	18.48	85.00	370.35
July22 02	2:30-3AM	3.48	36.11	416.51	796.82	22.85	664.33	17.86	88.71	367.32
July22 03	3-3:30AM	3.63	16.49	182.19	444.62	10.12	367.03	9.56	43.65	146.42
July22 04	3:30-4AM	3.76	9.16	122.27	269.00	4.36	217.54	5.33	26.04	71.50

Table A.27: Whiteface Mountain inorganic ions for the Small-sf.

Sample	Small-sf Time	pH	Cl^-	NO_3^-	SO_4^{2-}	Na^+	NH_4^+	K^+	Mg^{2+}	Ca^{2+}
July4 01	9:45-10:30PM	4.57	0.00	9.38	27.80	1.09	19.33	10.63	2.99	5.55
July4 02	10:30-11PM	4.43	0.00	11.40	33.74	1.19	22.88	6.03	3.07	7.16
July4 03	11PM-12AM	4.22	2.39	20.89	46.99	2.10	29.66	5.16	3.29	12.86
July4 04	12-1AM	3.84	0.00	68.79	80.99	1.08	33.20	4.26	3.09	13.31
July4 05	1-2AM	4.07	2.77	44.65	52.69	2.59	25.58	3.24	3.36	24.25
July4 06	2-3AM	4.41	5.01	22.18	36.33	5.04	16.90	3.68	3.89	24.23
July4 01	3-4AM	4.21	4.24	25.12	53.71	6.58	20.22	3.50	6.42	25.36
July4 07	4-5AM	4.19	3.34	22.97	60.21	7.21	20.58	3.77	5.35	27.11
July4 08	5-6AM	4.41	2.56	13.26	37.65	3.50	16.64	2.41	3.52	14.99
July4 09	6-7AM	4.59	2.35	8.67	23.75	1.99	12.89	1.57	2.37	4.26
July7 01	12:30-1PM	3.58	10.64	133.02	180.55	0.66	132.57	1.91	3.63	8.39
July7 02	1-2PM	3.58	13.09	131.98	197.74	3.21	138.56	3.70	3.65	8.15
July7 03	2-3PM	3.56	12.40	124.40	219.10	3.79	134.27	3.55	3.67	7.76
July7 04	3-4PM	3.45	7.93	86.81	243.85	2.03	119.21	2.98	5.92	15.66
July7 05	4-4:30PM	3.320	9.60	121.32	292.01	1.62	127.44	2.84	3.61	9.00
July7 06	4:30-5PM	3.39	17.21	146.98	395.05	7.33	158.06	5.68	3.98	9.27
July7 07	5-5:30PM	3.43	11.39	98.70	319.70	4.05	126.63	3.85	3.80	10.35
July7 08	5:30-6PM	3.39	11.01	90.27	327.37	5.11	129.54	5.39	3.69	9.23
July7 09	6-6:30PM	3.45	8.39	81.64	359.19	1.61	128.17	2.76	3.54	8.25
July7 10	6:30-7PM	3.38	8.31	69.66	303.74	2.66	108.79	2.98	3.58	7.43
July7 11	7-7:30PM	3.22	7.61	74.87	368.09	2.38	122.71	3.84	3.69	8.29
July7 12	7:30-8PM	3.13	7.74	133.16	573.75	1.33	172.50	3.57	3.91	8.25
July7 13	8-8:30PM	2.960	8.54	151.06	709.80	1.72	206.05	4.01	4.26	9.27
July7 14	8:30-9PM	2.92	10.71	198.55	1161.51	2.46	300.11	6.10	13.86	33.64
July7 15	9-9:30PM	3.24	12.01	210.90	1310.38	3.89	317.60	6.31	5.50	15.65
July7 16	9:30-10PM	3.22	7.09	96.13	523.76	1.21	149.47	2.69	3.86	8.96
July7 17	10-11PM	3.38	7.22	95.20	562.53	1.36	158.12	3.27	3.69	9.22
July7 18	11PM-12AM	3.15	8.73	75.37	390.61	1.75	119.03	3.22	3.55	9.22
July7 19	12-12:50AM	2.79	11.64	151.24	787.39	3.15	221.30	5.51	3.99	8.91
July16 01	7:25-8AM	2.94	36.70	473.69	1349.32	3.15	720.95	6.75	10.86	45.02
July16 02	8-8:30AM	2.99	28.89	364.27	1045.73	2.24	531.39	5.60	7.30	24.15
July16 03	8:30-9AM	2.96	24.17	335.16	898.06	1.35	464.82	4.18	4.84	17.82
July16 04	9-9:30AM	2.93	36.51	500.67	1107.48	13.31	599.07	6.17	6.52	28.15
July16 05	9:30-10AM	2.940	31.48	500.12	1139.49	2.61	579.45	6.07	8.96	25.71
July16 06	10-10:30AM	2.84	35.66	520.97	1151.07	2.18	583.67	4.86	6.99	27.00
July16 07	10:30-11AM	2.73	39.53	662.45	1549.93	3.74	819.10	8.49	15.24	44.80
July17 01	1:30-2AM	3.02	25.27	392.14	1151.63	2.63	540.85	6.07	7.93	39.23
July17 02	2-3AM	3.06	20.09	325.00	928.06	2.15	409.61	3.50	4.36	29.05
July17 03	3-4AM	3.1	16.41	259.03	827.30	2.54	347.55	3.39	4.00	35.95
July17 04	4-5AM	3.18	19.13	195.44	779.67	7.56	322.11	7.16	5.08	48.63
July17 05	5-6AM	3.19	17.82	245.73	568.32	4.95	259.09	4.98	4.60	36.92

July17 06 6-7AM	3.17	15.25	296.48	587.98	3.90	305.40	4.18	4.38	24.96
July17 07 7-8AM	3.15	13.34	266.00	609.44	2.80	265.33	2.96	3.90	19.05
July17 08 8-9AM	3.27	11.44	177.64	428.95	1.63	172.44	1.59	6.75	23.84
July17 09 9-10AM	3.26	13.18	179.82	490.66	2.19	212.37	2.23	3.72	13.96
July17 10 10-11AM	3.29	9.69	161.39	482.52	1.25	223.69	2.18	2.86	9.86
July20 01 9-9:30AM	3.59	9.44	66.31	237.04	1.30	127.24	2.09	2.95	17.14
July20 02 9:30-10AM	3.5	7.72	85.85	274.92	-0.30	141.26	1.72	2.74	13.67
July20 03 10-10:30AM	3.36	11.95	147.22	375.89	-0.12	158.17	1.54	3.19	14.17
July20 04 10:30-11AM	3.3	14.22	177.11	471.56	-0.11	190.59	2.01	3.43	14.57
July20 05 11-11:30AM	3.17	17.90	214.25	638.01	-3.42	266.95	3.72	4.59	18.55
July20 06 11:30AM-12PM	3.09	16.53	230.46	748.08	0.46	282.05	3.00	4.20	15.15
July20 07 12-12:30PM	3.04	16.97	264.44	913.89	0.73	353.76	3.55	4.80	18.45
July20 08 12:30-1PM	2.98	20.13	286.53	1131.54	0.92	441.20	6.07	8.54	24.12
July22 01 2-2:30AM	3.28	28.30	301.39	691.00	6.13	596.03	10.48	15.31	48.60
July22 02 2:30-3AM	3.39	21.06	224.09	564.00	4.88	441.95	7.55	13.94	36.82
July22 03 3-3:30AM	3.6	14.41	124.87	339.89	5.10	273.43	6.28	7.93	27.73
July22 04 3:30-4AM	3.77	19.20	78.55	240.86	12.13	160.03	11.00	10.01	32.34

Table A.28: Davis, CA inorganic ion concentrations for the CASCC2

CASCC Name	Time	pH	Cl^-	NO_3^-	SO_4^{2-}	Na^+	NH_4^+	K^+	Mg^{2+}	Ca^{2+}
Dec18 01	3:22-4AM	5.52	11.39	1019.62	90.86	20.09	1285.40	25.40	23.68	82.50
Dec18 02	4-5AM	5.9	6.88	529.53	38.12	11.14	618.33	9.02	3.58	11.31
Dec18 03	5-6AM	5.78	6.36	297.98	23.88	2.84	378.53	5.04	3.68	6.12
Dec18 04	6-7AM	5.9	6.46	275.18	18.23	2.49	386.91	6.07	3.69	6.05
Dec18 05	7-8AM	6.18	6.47	320.78	24.53	3.77	475.90	6.34	3.92	5.93
Dec18 06	8-9AM	6.26	5.88	280.60	25.31	2.73	467.15	4.48	3.62	5.66
Dec18 07	9-10AM	6.48	6.89	297.72	40.84	2.57	505.32	4.49	1.02	5.66
Dec18 08	10-11AM	6.4	7.07	446.43	66.75	3.76	803.94	7.09	4.19	8.62
Dec18 09	11-11:20AM	6.42	15.16	752.56	155.22	6.87	1285.20	12.60	8.56	29.37
Jan04 01	8:08-9PM	6.45	5.55	182.09	29.41	2.31	360.94	2.83	3.84	5.10
Jan04 02	9-10PM	6.4	5.30	217.59	31.41	2.55	382.36	2.87	3.71	5.03
Jan04 03	10-11PM	6.63	5.08	280.36	31.09	1.39	433.14	2.97	3.76	5.95
Jan04 04	11-12AM	6.48	5.43	330.01	35.42	0.26	479.54	2.76	-0.02	9.73
Jan04 05	12-1AM	6.5	4.26	175.91	25.80	0.15	327.95	2.13	0.51	4.03
Jan04 06	1-2AM	6.6	3.72	96.52	18.15	0.01	277.58	1.66	0.61	4.13
Jan04 07	2-3AM	6.59	4.48	97.65	18.27	1.40	312.10	2.68	0.94	5.57
Jan04 08	3-4AM	6.53	5.06	123.01	22.79	1.11	311.23	1.77	0.82	5.62
Jan04 09	4-5AM	6.4	5.11	154.26	27.71	1.58	379.90	2.68	1.36	8.52
Jan04 10	5-6AM	6.32	4.80	228.65	36.59	0.37	438.30	2.52	0.25	7.46
Jan04 11	6-7AM	6.32	4.55	204.31	32.62	0.30	407.25	2.72	1.22	4.96
Jan04 12	7-8AM	6.54	5.60	214.03	36.80	1.80	469.73	2.95	1.30	2.34

Jan04 13	8-10AM	6.55	9.87	264.52	55.95	1.77	538.64	4.07	1.48	5.09
Jan09 01	3-4AM	6.7	7.71	668.63	81.66	2.91	1007.51	6.72	2.55	5.84
Jan09 02	4-5AM	6.7	14.19	1122.23	136.23	5.44	1546.87	8.07	2.48	8.43
Jan09 03	5-6AM	6.66	26.72	2034.46	267.31	8.42	2757.65	11.88	2.16	11.74
Jan09 04	6-7AM	6.65	43.21	3120.94	425.76	16.53	4178.39	15.56	4.50	17.65
Jan09 05	7-8AM	6.59	53.46	3659.72	491.11	18.61	4925.60	24.89	7.82	17.55
Jan09 06	8-9AM	6.57	47.95	3647.63	507.57	18.08	4412.03	34.24	5.28	19.13
Jan09 07	9-10AM	6.75	49.03	3502.75	490.16	18.38	4271.27	17.59	5.85	31.16
Jan09 08	10-10:36AM	6.68	70.60	4539.57	644.11	22.52	5937.41	21.85	10.21	34.48
Jan10 01	2:45-4AM	6.51	41.17	2937.51	352.37	8.85	3910.76	22.81	4.47	14.66
Jan10 02	4-5AM	6.55	47.80	3113.51	338.53	8.11	4247.13	30.48	2.26	11.21
Jan10 03	5-6AM	6.5	70.28	3662.89	373.21	8.20	4835.58	27.90	3.92	9.49
Jan10 04	6-6:52AM	5.64	135.19	4843.86	510.63	15.02	6562.56	28.29	2.14	13.14
Jan10 05	6:52-9AM	5.94	77.25	4308.67	368.43	8.47	5165.55	21.77	4.12	12.29
Jan10 06	9-10AM	5.94	54.74	3649.93	296.82	12.21	4385.49	25.50	2.78	14.43
Jan10B 01	10:50-12AM	5.98	20.37	1054.69	80.18	3.86	1371.88	12.08	1.72	12.17
Jan10B 02	12-1AM	5.65	18.14	1176.19	82.43	2.92	1449.24	13.98	2.65	8.66
Jan10B 03	1-3AM	5.51	16.80	1319.62	73.60	4.56	1448.93	12.83	1.40	10.78
Jan10B 04	3-5AM	5.76	22.88	1203.61	79.66	3.12	1324.72	12.70	2.67	11.05
Jan10B 05	5-7AM	5.84	26.25	770.08	63.69	2.61	895.26	9.50	1.06	9.25
Jan10B 06	7-8AM	6.38	17.89	611.80	56.31	2.50	746.64	7.82	-0.39	3.96
Jan10B 07	8-9AM	6.68	10.68	523.42	46.01	2.07	710.13	6.41	2.04	7.89
Jan10B 08	9-9:42AM	6.69	23.02	715.52	72.10	10.01	1147.52	14.49	3.45	19.13
Jan11 01	11-12AM	6.06	13.19	246.85	38.21	2.50	502.22	7.63	1.84	5.77
Jan11 02	12-1:00AM	6.2	19.24	346.44	57.88	5.02	670.83	16.95	2.40	6.83
Jan11 03	1-3AM	6.31	19.61	508.89	64.04	2.86	680.68	9.58	1.88	7.33
Jan11 04	3-5AM	6.07	16.21	822.80	63.59	2.60	906.99	7.14	2.89	8.62
Jan11 05	5-7AM	6.18	8.19	526.27	34.43	2.58	624.78	5.72	2.24	5.31
Jan11 06	7-8AM	6.44	10.69	494.86	37.28	5.54	641.43	7.37	4.15	31.62
Jan11 07	8-9AM	6.3	13.10	538.36	47.38	8.79	691.21	11.66	3.58	36.04
Jan11 08	9-10AM	6.38	12.90	572.54	62.23	5.73	766.87	9.68	2.38	16.86

Table A.29: Davis, CA inorganic ion concentrations for the Large-sf.

Large-sf Name	Time	pH	Cl^-	NO_3^-	SO_4^{2-}	Na^+	NH_4^+	K^+	Mg^{2+}	Ca^{2+}
Dec18 01	3:22-4AM	6.03	10.12	563.81	63.16	15.72	757.39	25.41	16.99	69.89
Dec18 02	4-5AM	6.08	5.13	298.92	24.95	4.77	453.30	7.49	5.15	16.56
Dec18 03	5-6AM	5.9	4.01	173.91	16.14	2.44	251.90	3.38	3.64	7.15
Dec18 04	6-7AM	6.08	3.19	124.26	10.80	2.54	231.67	3.90	3.52	5.77
Dec18 05	7-8AM	6.34	3.36	160.23	14.61	2.53	320.24	3.32	3.61	5.96
Dec18 06	8-9AM	6.38	3.46	160.48	19.55	2.68	328.04	3.37	1.52	4.93
Dec18 07	9-10AM	6.56	4.11	181.68	34.83	2.55	429.37	2.80	3.51	6.48
Dec18 08	10-11AM	6.68	4.93	243.37	49.53	2.91	561.29	3.96	4.20	8.00
Dec18 09	11-11:20AM	6.69	6.09	280.45	77.85	6.98	874.28	7.22	6.43	18.20
Jan04 01	8:08-9PM	6.55	3.88	113.19	18.59	1.74	273.52	2.33	3.70	5.09
Jan04 02	9-10PM	6.45	4.10	120.91	18.43	1.64	249.62	1.83	1.36	3.92
Jan04 03	10-11PM	6.66	3.94	155.46	20.02	1.14	292.65	2.06	3.78	5.85
Jan04 04	11-12AM	6.5	3.74	171.13	21.02	0.03	305.41	1.43	0.04	7.46
Jan04 05	12-1AM	6.45	3.12	102.96	14.76	0.28	240.75	1.39	0.29	2.05
Jan04 06	1-2AM	6.57	2.83	61.23	12.05	-0.24	209.62	0.94	-0.48	3.11
Jan04 07	2-3AM	6.64	3.00	56.08	11.59	0.77	254.28	1.91	0.76	6.31
Jan04 08	3-4AM	6.57	3.10	70.55	14.28	-0.17	246.43	0.95	-0.57	5.15
Jan04 09	4-5AM	6.79	3.86	90.18	19.05	0.02	279.99	1.55	1.87	8.50
Jan04 10	5-6AM	6.37	4.07	151.39	26.11	1.12	316.75	2.37	3.62	5.05
Jan04 11	6-7AM	6.28	3.43	137.93	23.49	0.26	329.57	2.17	0.49	1.31
Jan04 12	7-8AM	6.7	3.69	125.48	24.49	1.19	329.55	2.48	3.58	4.53
Jan04 13	8-10AM	6.7	6.25	137.31	32.09	1.15	414.04	2.97	0.98	5.17
Jan09 01	3-4AM	6.7	6.26	330.09	48.61	2.18	635.65	5.79	1.53	5.31
Jan09 02	4-5AM	6.8	9.59	533.47	82.28	3.17	904.55	5.48	1.60	5.65
Jan09 03	5-6AM	6.66	17.22	928.86	155.48	6.78	1504.26	10.04	3.54	12.42
Jan09 04	6-7AM	6.45	28.10	1345.80	226.80	10.16	1851.62	11.72	1.64	10.85
Jan09 05	7-8AM	6.82	29.01	1368.01	227.14	10.98	2039.94	16.15	6.17	18.89
Jan09 06	8-9AM	6.78	21.48	1408.46	233.94	9.80	2128.78	11.13	4.35	19.07
Jan09 07	9-10AM	6.82	26.61	1334.80	218.35	8.37	1824.49	8.59	3.24	11.40
Jan09 08	10-10:36AM	6.89	28.01	1530.52	249.58	10.48	2473.60	17.85	4.23	19.47
Jan10 01	2:45-4AM	6.59	20.74	1207.41	167.32	5.14	1828.22	12.18	5.83	19.61
Jan10 02	4-5AM	6.61	19.50	1327.90	163.41	4.64	2022.33	13.84	5.61	17.28
Jan10 03	5-6AM	6.55	25.79	1479.83	175.99	4.57	2147.12	10.90	2.23	10.75
Jan10 04	6-6:52AM	6.4	36.99	1613.85	191.38	5.64	2231.30	10.45	3.80	15.34
Jan10 05	6:52-9AM	6.27	34.22	1459.91	149.72	5.46	1887.63	11.03	2.40	16.69
Jan10 06	9-10AM	5.59	27.11	1353.69	126.63	8.52	1785.78	11.18	2.76	15.54

Jan10B 01	10:50-12AM	6.07	8.91	476.16	39.22	2.45	764.45	6.98	2.44	14.80
Jan10B 02	12-1AM	5.81	7.40	495.08	38.25	1.69	658.35	5.61	1.47	6.89
Jan10B 03	1-3AM	5.66	8.36	496.48	31.44	3.77	603.26	6.38	0.83	8.36
Jan10B 04	3-5AM	6.12	11.81	496.54	39.84	2.14	614.75	6.42	2.08	7.11
Jan10B 05	5-7AM	6.04	16.23	365.53	37.26	1.52	470.27	4.16	1.38	5.51
Jan10B 06	7-8AM	6.64	11.37	300.94	31.31	0.70	449.50	4.41	0.27	5.09
Jan10B 07	8-9AM	6.87	6.38	248.50	25.03	1.19	422.66	3.74	3.24	5.45
Jan10B 08	9-9:42AM	6.94	8.24	314.05	36.40	2.12	645.22	6.07	1.28	7.63
Jan11 01	11-12AM	6.41	7.39	128.69	20.39	1.07	330.50	4.39	2.51	4.94
Jan11 02	12-1:00AM	6.21	8.78	180.37	31.22	0.98	447.47	7.02	1.23	2.35
Jan11 03	1-3AM	6.2	10.07	219.71	29.88	1.04	372.24	4.58	1.42	2.38
Jan11 04	3-5AM	6.05	8.48	314.07	28.29	2.00	409.47	4.47	2.67	6.79
Jan11 05	5-7AM	6.36	4.43	242.47	17.43	1.43	335.73	3.08	1.71	3.30
Jan11 06	7-8AM	6.49	4.77	211.30	19.00	2.18	322.50	3.43	3.03	19.77
Jan11 07	8-9AM	6.47	5.77	214.18	25.23	2.74	321.38	4.53	1.90	29.96
Jan11 08	9-10AM	6.52	6.28	165.96	31.00	3.37	355.75	3.92	2.20	11.70

Table A.30: Davis, CA inorganic ion concentrations for the Small-sf.

	Small-sf									
Name	Time	pH	Cl^-	NO_3^-	SO_4^{2-}	Na^+	NH_4^+	K^+	Mg^{2+}	Ca^{2+}
Dec18 01	3:22-4AM									
Dec18 02	4-5AM	5.68	28.67	2557.17	185.51	24.93	2901.84	24.89	11.23	44.57
Dec18 03	5-6AM	5.6	19.07	1778.68	130.20	11.85	2041.77	17.68	6.86	17.35
Dec18 04	6-7AM	5.47	19.16	1740.60	126.84	9.19	1945.85	16.24	5.42	11.52
Dec18 05	7-8AM	5.88	23.02	1937.58	132.65	10.07	2227.52	17.23	5.16	9.66
Dec18 06	8-9AM	5.8	22.72	1691.10	119.00	8.32	1945.17	16.39	4.74	8.51
Dec18 07	9-10AM	6.31	17.44	1301.37	101.29	7.35	1636.43	13.12	4.79	10.32
Dec18 08	10-11AM	6.39	21.68	1553.25	133.60	8.11	2028.42	15.65	4.85	12.11
Dec18 09	11-11:20AM	6.36	30.80	2235.01	190.89	11.18	2755.06	20.42	9.80	24.77
Jan04 01	8:08-9PM									
Jan04 02	9-10PM	6.45	28.08	1305.57	166.77	9.49	1718.63	13.13	2.77	10.96
Jan04 03	10-11PM	6.31	22.57	1452.62	165.49	7.79	1826.64	14.28	3.97	6.36
Jan04 04	11-12AM	6.29	22.27	1497.38	152.68	6.01	1807.70	12.06	0.18	13.54
Jan04 05	12-1AM	6.11	18.77	1342.77	138.86	4.71	1614.18	12.95	1.86	8.47
Jan04 06	1-2AM	6.24	21.24	1134.83	131.14	6.10	1366.24	13.31	0.73	8.98
Jan04 07	2-3AM	6.21	26.30	1096.37	134.38	10.46	1428.63	15.14	1.75	10.21
Jan04 08	3-4AM	6.2	26.10	1021.70	139.15	9.05	1327.08	18.52	2.82	12.69
Jan04 09	4-5AM	6.13	31.22	1083.16	161.56	12.35	1243.15	14.47	3.01	11.80
Jan04 10	5-6AM	6.15	33.21	1036.70	149.91	17.58	1363.14	16.33	4.74	10.71
Jan04 11	6-7AM	6.05	23.74	935.48	122.87	8.69	1177.87	12.30	2.36	10.69
Jan04 12	7-8AM	6.34	29.21	1189.58	158.11	10.36	1496.70	15.10	4.39	8.66
Jan04 13	8-10AM	6.36	34.32	1329.29	188.96	9.83	1677.36	14.87	3.61	11.67

Jan09 01	3-4AM	6.48	13.55	1321.83	144.32	5.38	1709.08	9.57	2.37	7.64
Jan09 02	4-5AM	6.64	30.28	3088.68	325.10	9.84	3601.05	19.49	2.89	12.49
Jan09 03	5-6AM	6.41	44.35	4187.64	471.33	15.76	5150.84	19.33	0.18	7.74
Jan09 04	6-7AM	6.35	63.60	5817.48	731.79	23.21	7273.90	38.69	1.22	11.33
Jan09 05	7-8AM	6.23	83.72	7553.77	940.69	31.43	9447.00	28.64	0.79	17.95
Jan09 06	8-9AM	6.26	106.36	9570.79	1215.55	39.87	11754.23	47.92	6.92	19.63
Jan09 07	9-10AM	6.1	121.59	11498.50	1511.72	49.02	14249.25	61.19	6.93	19.90
Jan09 08	10-10:36AM	6.05	176.93	14047.80	1746.63	68.08	18119.40	55.52	14.06	47.88
Jan10 01	2:45-4AM	6.27	60.78	3926.70	463.10	16.53	5019.61	23.89	2.79	14.59
Jan10 02	4-5AM	5.94	69.66	4670.31	529.02	15.85	7097.77	33.18	10.10	19.98
Jan10 03	5-6AM	5.93	113.99	7358.88	817.66	17.20	9286.69	64.14	4.84	20.12
Jan10 04	6-6:52AM	5.69	136.81	7361.51	784.60	19.77	9437.03	37.50	8.70	40.64
Jan10 05	6:52-9AM	5.59	302.99	12970.90	1276.34	46.31	15799.10	86.27	-3.30	27.60
Jan10 06	9-10AM	5.48	241.84	12633.80	1185.66	23.07	15008.00	64.71	16.82	57.47
Jan10B 01	10:50-12AM	6.05	25.68	841.85	66.37	9.10	976.51	15.96	5.59	35.42
Jan10B 02	12-1AM	5.72	47.24	2263.03	168.56	4.86	2808.32	25.87	5.45	37.29
Jan10B 03	1-3AM	5.56	67.06	4032.85	256.48	5.61	4746.83	43.27	10.11	40.96
Jan10B 04	3-5AM	5.47	73.28	5219.84	315.49	6.63	5552.25	54.43	6.01	39.33
Jan10B 05	5-7AM	5.78	85.79	4516.63	280.03	4.91	5133.28	41.69	3.83	34.98
Jan10B 06	7-8AM	5.79	78.67	3543.15	234.43	7.55	4096.14	31.68	2.48	32.06
Jan10B 07	8-9AM	6.36	59.98	1953.23	147.74	24.74	2295.22	32.17	16.20	40.01
Jan10B 08	9-9:42AM	6.39	52.21	2084.05	161.31	16.76	2526.93	30.04	10.49	36.05
Jan11 01	11-12AM	6.35	21.34	204.01	35.55	12.10	346.17	11.50	4.08	15.63
Jan11 02	12-1:00AM	6.08	37.74	880.56	135.17	5.44	1260.94	23.07	4.31	17.19
Jan11 03	1-3AM	6	49.84	1367.25	188.19	5.63	1812.75	33.66	5.01	17.27
Jan11 04	3-5AM	5.77	71.61	2622.27	268.92	5.66	3138.03	30.78	4.89	16.02
Jan11 05	5-7AM	5.73	48.62	2701.46	226.82	6.75	3307.25	32.90	5.62	14.98
Jan11 06	7-8AM	5.79	43.03	2624.09	215.78	8.39	3303.43	29.31	5.21	29.89
Jan11 07	8-9AM	5.64	36.95	2268.27	182.24	8.26	2723.27	26.98	6.35	30.74
Jan11 08	9-10AM	5.97	43.18	2738.07	226.88	11.22	3395.68	31.17	8.56	35.01

APPENDIX B: S(IV) Oxidation Rate Formulas.

1. Excel Macro for S(IV) oxidation via the hydrogen peroxide pathway

```
'The following codes define the function "pergaspath"
'The function "pergaspath" will calculate & output the S(IV) oxidation rate
'by H2O2 pathway scaled by [SO2.H2O], i.e., -d[S(IV)]/dt*(1/[SO2.H2O]) w/H2O2
'Units of Inputs: tempK~K, perconc~ppbv, pres~mb
'perconc--H2O2 (gas) Concentration; pres--air pressure
'Unit of Output: second^(-1)
Option Explicit

Function pergaspath(tempK, perconc, pres, pH)

'Define Rate Constants

Dim Ka1

   Ka1 = 0.0129 * Exp(-(-16300 / 8.3145) * (1 / tempK - 1 / 298))

Dim k8

   k8 = 74500000 * Exp(-(39500 / 8.3145) * (1 / tempK - 1 / 298))

Dim Hper
'Henry's Constant for H2O2 (M/Atm):
   Hper = 74500 * Exp(-(-55000 / 8.3145) * (1 / tempK - 1 / 298))

'air pressure conversion to "atm" unit and H2O2 pressure in gas phase

Dim peratm
Dim pres1
'Unit for both ~ Atm
   pres1 = pres / 1013.25
   peratm = perconc * (10 ^ (-9)) * pres1

Dim Hion
'H ion concentration
   Hion = 10 ^ (-pH)

'S(IV) oxidation rate by H2O2
```

```
   pergaspath = k8 * Ka1 * (Hper * peratm) / (1 + 13 * Hion)

End Function
```

2. Excel Macro for S(IV) oxidation via the ozone pathway

```
'The following codes define the function "ooopath"
'The function "ooopath" will calculate & output the S(IV) oxidation rate
'by O3 pathway scaled by [SO2.H2O], i.e., -d[S(IV)]/dt*(1/[SO2.H2O]) w/O3
'Units of Inputs: tempK~K, pres~mb, ooo~ppb
'Unit of Output: second^(-1)
'pres -- air pressure, O3 (gas) concentration is assumed to be 30 ppb
Option Explicit

Function ooopath(tempK, pres, pH, ooo)

'Define Rate Constants

Dim Ka1

   Ka1 = 0.0129 * Exp(-(-16300 / 8.3145) * (1 / tempK - 1 / 298))

Dim Ka2

   Ka2 = 0.000000064 * Exp(-(-11900 / 8.3145) * (1 / tempK - 1 / 298))

Dim k9

   k9 = 24000 * Exp(-(0 / 8.3145) * (1 / tempK - 1 / 298))

Dim k10

   k10 = 370000 * Exp(-(46000 / 8.3145) * (1 / tempK - 1 / 298))

Dim k11

   k11 = 1500000000 * Exp(-(43900 / 8.3145) * (1 / tempK - 1 / 298))

Dim Hooo
'Henry's Constant for O3:
   Hooo = 0.011 * Exp(-(-21300 / 8.3145) * (1 / tempK - 1 / 298))

'air pressure conversion to "atm" unit and O3 pressure in gas phase

Dim oooatm
```

```
Dim pres1

   pres1 = pres / 1013.25
   oooatm = ooo * (10 ^ (-9)) * pres1

'H ion Concentration (M)
Dim Hion

   Hion = 10 ^ (-pH)

'S(IV) oxidation rate by O3

   ooopath = (k9 + k10 * Ka1 / Hion + k11 * Ka1 * Ka2 / (Hion ^ 2)) * Hooo * oooatm

End Function
```

3. Excel Macro for S(IV) oxidation via the autooxidation pathway

```
'
'The following codes define the function "meltalspath"
'The function "metalspath" will calculate & output the S(IV) oxidation rate
'by O2/(Fe(III)&Mn(II)) pathway scaled by [SO2.H2O], i.e.,
'-d[S(IV)]/dt*(1/[SO2.H2O]) w/O2/(Fe(III)&Mn(II))
'Units of Inputs: tempK~K, iron~µg/l, manganese~µg/l,
'Unit of Output: second^(-1)
Option Explicit

Function metalspath(tempK, iron, manganese, pH)

'Define Rate Constants and calculate [H+]

Dim Ka1

   Ka1 = 0.0129 * Exp(-(-16300 / 8.3145) * (1 / tempK - 1 / 298))

Dim Ka2

   Ka2 = 0.000000064 * Exp(-(-11900 / 8.3145) * (1 / tempK - 1 / 298))

Dim Hion
'H ion concentration
   Hion = 10 ^ (-pH)

'Metals' Cncentrations
```

```
Dim Fethree
' using 25% of iron as Fe(III) and conversion to M units
   Fethree = (10 ^ (-6) * 0.25 * iron) / 55.847

Dim Mntwo
' using all manganese as Mn(II) and conversion to M units
   Mntwo = (10 ^ (-6) * manganese) / 54.938

'S(IV) oxidation rate by O2/Fe(III)&Mn(II)) (Ibusuki & Takeuchi (1987))

'for pH > 4.2

If pH >= 4.2 Then

Dim kx

   kx = 25100000000000# * Exp(-(70100 / 8.3145) * (1 / tempK - 1 / 298))

   metalspath = kx * (1 + Ka1 / Hion + Ka1 * Ka2 / (Hion ^ 2)) * Fethree * Mntwo *
(Hion ^ 0.67)

End If

'for pH < 4.2

If pH < 4.2 Then

Dim ky

   ky = 37200000# * Exp(-(70100 / 8.3145) * (1 / tempK - 1 / 298))

   metalspath = ky * (1 + Ka1 / Hion + Ka1 * Ka2 / (Hion ^ 2)) * Fethree * Mntwo *
(Hion ^ (-0.74))

End If

End Function
```

APPENDIX C: Modifications to the Aqchem Model

In order to use the Aqchem model for the Davis, CA samples several modifications were made to the code. These modifications allowed for the use of the available data, incorporated the aqueous phase mass transport limitation and added the competing complexation reaction of S(IV) with formaldehyde. The changes to the code are outlined here.

1.Simplification:

The Aqchem model originally included not only SO_2, O_3 and H_2O_2, but also NH_3, HNO_3 and HCHO. The first step in simplifying the model was to eliminate all species not directly involved in the production of sulfate. This involved zeroing out all reactions containing ammonia, nitric acid and formaldehyde. All input values for these species were set to zero.

The remaining reactions were only the oxidation of S(IV) via the ozone and hydrogen peroxide pathways. The model gives the rate of production of S(VI) by reactions 1 and 2 (r1 and r2), and the oxidation of S(IV) by ozone and hydrogen peroxide respectively.

r1=ya(7)*((xk1*so2)+(xk2*hso3)+(xk3*so3))

r2=xk4*h*ya(8)*hso3/(1+(13*h))

In these equations, xk_ represents the rate constant for each reaction, ya(_) is the aqueous concentration of the species (7 is for O_3 and 8 is for H_2O_2); the other variables represent the species concentrations. These equations are similar to Equations 3.10 for ozone and 3.8 for hydrogen peroxide in the text. The total rate of sulfate production could then be acquired by the addition of r1 and r2.

2. Addition of the aqueous mass transport limitation:

The Aqchem model already includes rate modifications based on gas phase and interfacial limitations, but the aqueous phase limitations had been omitted. The aqueous phase mass transport limitations are based on the drop radius, the diffusivity of the species being transported and the first order rate constant of the reaction in question. Using these parameters, a scaling factor labeled Q is generated. This Q-value is then multiplied by the reaction rate (r1 or r2) to produce a new, smaller rate that reflects the effects of the aqueous phase mass transport limitation.

The model first checks to make sure that there is in fact some concentration of the species for which it is creating a Q-value. It then calculates the first order reaction constant for the species. This is done by creating a new rate constant variable by dividing the reaction rate by the species concentration

$$xkO3 = r1/ya(7)$$

This is more conventionally written

$$k'_{O_3} = r1/[O_3] = (k_1 * [SO_2] + k_2 * [HSO_3] + k_3 * [SO_3])$$

The first order rate constant is then used to calculate a variable known as q. This is then used to calculate Q. The equations used in the code for this purpose are as follows

$$qO3 = rad*(xkO3/diffO3)^(0.5)$$

$$bigQO3 = 3 * (((1/tanh(qO3))/qO3)-(1/(qO3^2)))$$

Here, rad indicates drop radius and diff__ is for the diffusivity of the species. These are the same as Equations 3.25 and 3.26 in the text. Using this Q-value, r_ is modified. For ozone this equation looks like

$$r1 = r1 * bigQO3$$

The reaction rate is simply redefined using the scaling factor. The calculation of *bigQ* was done only for ozone and hydrogen peroxide. This is because in using the first order approximation it appears unlikely that S(IV) will undergo any aqueous phase mass transport limitations.

3. Addition of the competing reaction:

Preliminary calculations indicate that the formation of hydroxymethanesulfonate may be a large sink for available S(IV). Therefore the complexation reaction between S(IV) and formaldehyde responsible for the production of HMS should be included in the model. Unlike O_3 and H_2O_2, HCHO was not measured in the gas phase, but instead was measured in the aqueous phase in many of the Davis samples. The model was already equipped to handle either gas or aqueous phase input so no modifications for this were necessary.

The HMS formation reaction was added in the form

$$r4 = hcho*((xk5*hso3)+(xk6*so3))$$

The same naming conventions apply to this equation. The concentration of formaldehyde is corrected for the amount of HCHO present in the gem-diol form. This reaction acts as

a sink for S(IV), so the total amount of S(VI) produced can still be obtained through the addition of r1 and r2.

4. Addition of aqueous phase mass transport limitation to S(IV):

The reaction rate of the formation of HMS is comparable to that of the reaction rate of S(IV) and ozone for the Davis samples. Due to this large aqueous phase sink for S(IV) it is now possible for there to exist some mass transport limitations for this species in the aqueous phase. This will affect all of the calculations of the Q-values because the reactions can no longer be treated strictly as psuedo-first order. The scaling of the reactions will now be based on two different Q-values. The aqueous phase mass transport limitations of S(IV) will affect all three of the possible reactions.

Therefore the model was modified in such a way that the Q-value for S(IV) was calculated in an iterative manner, with the iterations stopping once the value from the previous iteration was within 0.1% of the new value. This was done by initially setting all Q-values to one.

$$Q_{S(IV)} = 1$$

$$Q_{O3} = 1$$

$$Q_{H2O2} = 1$$

The rates are then calculated as before, but are all multiplied by the Q-values pertaining to the species involved in the reaction. A simplified version of these reaction rates is

$$r1 = (O3\ oxidation\ rate) * Q_{S(IV)} * Q_{O3}$$

$$r2 = (H2O2\ oxidation\ rate) * Q_{S(IV)} * Q_{H2O2}$$

$$r4 = (HMS\ production\ rate) * Q_{S(IV)}$$

$$r3 = r1 + r2 + r4$$

Then a first order reaction rate is calculated for ozone, hydrogen peroxide and S(IV). These first order reaction rates are then used to calculate new Q-values. The logic is as follows

$$k'_{O3} = r1/([O_3] * Q_{O3})$$

$$\text{calculate } Q_{O3}\text{new based on } k'_{O3}$$

$$\text{then } r1 = r1 * (Q_{O3}\text{new}/ Q_{O3})$$

$$k'_{H2O2} = r2/([H_2O_2] * Q_{H2O2})$$

$$\text{calculate } Q_{H2O2}\text{new based on } k'_{H2O2}$$

$$\text{then } r2 = r2 * (Q_{H2O2}\text{new}/ Q_{H2O2})$$

$$k'_{S(IV)} = (r1 + r2 + r4)/([S(IV)] * Q_{S(IV)})$$

$$\text{calculate } Q_{S(IV)}\text{new based on } k'_{S(IV)}$$

$$\text{then } r3 = r3 * (Q_{S(IV)}\text{new}/ Q_{S(IV)})$$

Note that in the new calculation of the rates (r_) in each case the equation calls for division by the old Q-value. This is necessary because the rates have already been multiplied by the old Q-values and without dividing by them the code would just be compounding the Q-values. The calculations for Q are carried out in the same manner outlined above in step 2.

The next step is to check for the convergence of the new Q-value for S(IV) with the old value. If the values converge within 0.1% then the iterative process is done and

these are the Q-values used to scale the rates. If there is not convergence then the iterations will continue. The loop starts again by recalculating the r_ values and then repeating the process of calculating the new Q-values. The loop will stop once the Q-values for S(IV) converge or the iterations exceed the number of loops allowed by the model.

These are the major modifications done to the model. Some other smaller things were done, such as adding a pH input, fixing the pH and gas concentrations, and adding a temperature dependence to the Henry's law constants. These additions to the Aqchem model allowed for a more accurate calculation of the rate of sulfate produced in the cloud or fog drops.